Vibration Control of Wave Energy Point Absorbers for Optimal Power Take-off

Sun, Tao

Publication date:
2019

Document Version
Publisher's PDF, also known as Version of record

VIBRATION CONTROL OF WAVE ENERGY POINT ABSORBERS FOR OPTIMAL POWER TAKE-OFF

BY
TAO SUN

DISSERTATION SUBMITTED 2019

AALBORG UNIVERSITY
DENMARK

Vibration Control of Wave Energy Point Absorbers for Optimal Power Take-off

Ph.D. Dissertation
Tao Sun

Dissertation submitted November 2019

Dissertation submitted: November 2019

PhD supervisor: Prof. Søren R.K. Nielsen
Aalborg University

PhD committee: Professor John Dalsgaard Sørensen (chairman)
Aalborg University

Professor Jianbing Chen
Tongji University

Professor Steen Krenk
Technical University of Denmark

PhD Series: Faculty of Engineering and Science, Aalborg University

Department: Department of Civil Engineering

ISSN (online): 2446-1636
ISBN (online): 978-87-7210-479-9

Published by:
Aalborg University Press
Langagervej 2
DK – 9220 Aalborg Ø
Phone: +45 99407140
aauf@forlag.aau.dk
forlag.aau.dk

Printed in Denmark by Rosendahls, 2019

Contents

Preface

The present thesis "Vibration Control of Wave Energy Point Absorbers for Optimal Power Take-Off" is the outcome of a Ph.D. study within the period September 2016 to August 2019 at the Department of Civil Engineering, Aalborg University, Aalborg, Denmark. The thesis is presented as a collection of peer-reviewed journal articles published within this period.

I would like to show grateful thanks to Prof. Søren R.K. Nielsen for the impressive and fruitful supervision in this PhD project. I sincerely appreciate his persistent support and guidance throughout my study, which enables me to overcome all obstacles and keep on progressing. The constructive ideas, invaluable discussions and patient corrections for each paper greatly contribute to this work. I benefit a lot from his unique insights, rigorous logic and meticulous attitude, profound knowledge, which improve my ability of academic researching, self-discipline, time management and plan execution. Further, he makes me realize the importance of innovative thinking and pursuit of excellence, which brings a major influence on my academic career.

I would like to greatly thank Prof. Biswajit Basu of Trinity College Dublin (TCD), Ireland, for his important contributions and constructive suggestions for a joint paper. Moreover, I wish to thank Mr. William Dick, the director of Swirl Generators Limited in TCD, for his important contributions to the industrial placement. Considering the confidential property, the work related to Swirl will not be included in this thesis.

I appreciate the ICONN (European Industrial DoCtorate on Offshore WiNd and Wave ENergy) project funded by the Marie Sklodowska-Curie Innovative Training Network initiative under the European Commission's Horizon 2020 programme. My thanks also go to all colleagues I have worked with, in Aalborg and Dublin, for all help that they have provided. Special thanks are given to all my friends for pleasant conversations, moral support and encouragement, and help in life during the extraordinary three years.

Finally but foremost, I would like to thank my family for giving me enough support to make me keep going. Even though they do not exactualy know what kind of things I'm doing, they indeed believe I'm enjoying what I'm doing now.

Tao Sun
Aalborg University, November 1, 2019

Curriculum Vitae

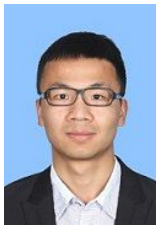

Tao Sun

E-mail: tsu@civil.aau.dk; tj_suntao@126.com
Date of birth: August 15, 1989
Place of place: Anhui, China

Education Background

06/2016	Master of Engineering in Structural Engineering Tongji University, Shanghai, China
06/2013	Bachelor of Engineering in Civil Engineering Sichuan University, Chengdu, China

Professional Experiences

09/2016 - 09/2019	PhD fellow at Department of Civil Engineering, Aalborg University
04/2018 - 08/2019	Visiting PhD researcher at Department of Civil, Structural and Environmental Engineering, Trinity College Dublin, Ireland
04/2018 - 08/2019	Visiting Industrial researcher, Swirl generators Ltd, Dublin, Ireland

Honors and Awards

2016 - 2019	Marie Skłodowska-Curie Fellowship, Aalborg University
2013 - 2016	Class A Scholarship, Tongji University
2010	Monomial Scholarship, Sichuan University

Research Interests

Structural dynamics, Vibration control, Modeling and control of wave energy convertors, Hydrodynamics, Control theory

Academic Memberships

Member of Danish Center for Applied Mathematics and Mechanics (DCAMM)

List of papers

This thesis is complied from the work presented in the following five papers:

- Sun, T., Nielsen, S.R.K. (2019). Stochastic Control of Wave Energy Converters for Optimal Power Absorption with Constrained Control Force. Applied Ocean Research, 87, 130-141.
- Sun, T., Nielsen, S.R.K., Basu, B. (2019). Stochastic Control of Wave Energy Converters with Constrained Displacements for Optimal Power Absorption. Applied Ocean Research, 89, 1-11.
- Sun, T., Nielsen, S.R.K. (2018). Stochastic Optimal Control of a Heave Point Wave Energy Converter Based on a Modified LQG Approach. Ocean Engineering, 154, 357-366.
- Sun, T., Nielsen, S.R.K. (2019). Semi-Active Feedforward Control of a Floating OWC Point Absorber for Optimal Power Take-Off. IEEE Transaction on Sustainable Energy. Published online.

Abstract

As a consequence of increasing demand of energy and corresponding environmental impact the interest in renewable energy sources has increased correspondingly. Among these wave energy energy makes up a promising contributor due to its higher energy in unit volume, higher availability and good prediction. Although many principles have been designed and tested, the technology is still immature compared with solar and wind energy due to the inefficient energy extraction. A key issue for improving the competition capacity is to improve the absorbed energy from the waves by the use of improved vibration control of wave energy absorbers. Hence, there is a need to improve and develop optimal control strategies for this purpose. Further, in reality there are some physical displacement and control force constraints present, which restricts the efficiency of wave energy converters because there exist threshold stroke and saturation in the actuator system. Hence, it is necessary to investigate control strategies considering physical constraints.

This PhD thesis has looked into optimal vibration control strategies of wave energy converters for absorbed energy under the physical constraints, mainly dealing with heave point absorbers and oscillating water column devices.

Due to the limited observability and predictability of the surrounding irregular sea state, the indicated control problem is essentially stochastic. Assuming linear wave theory, the semi-analytical solutions at optimal control considering the control force and the vertical displacement constraints respectively are indicated. The optimal control law for the optimization problem with the control force constraints has feedback from the motion of the absorber. The analytical solution for the constrained displacement problem at optimal control is composed of a closed loop during unconstrained states and an open loop during constraints-activated states. Further, the control force during the constraints-activated states is dependent on the present wave load, which needs to be estimated based on the prediction of the future surface elevations. Algorithms are presented for the purpose of estimating the wave load and predicting future velocities based on simultaneous online measurement of the vertical accelerator of the absorber, and the sea-surface

elevation near the absorber. The prediction and estimation algorithms rely on the narrow-bandedness of the involved stochastic processes in combination to a van der Pol transformation. The derived control laws have been verified by comparison with the nonlinear programming based numerical solutions.

Further, a modified LQG control has been put forward to control the point absorber motion. The vertical displacement and control force constraints are introduced for the consideration of the energy loss due to the aforementioned constraints in the quadratic objective functional. According to the rational approximations to the corresponding frequency response functions, the wave excitation force and radiation force are replaced, and the integrated dynamic system is then represented by a Gaussian white noise driven linear stochastic differential equation. It turns out that there is a linear relationship between the obtained LQG based control force and the integrated state vector. The integrated state vector needs to be estimated due to the partial observation of the state vector. This can be achieved by the Kalman filter. The proposed LQG controller can successfully optimize the absorbed energy from waves whilst it can keep both the control force and the displacement small. Further, with proper gain parameters the averaged absorbed power from the proposed LQG controller is merely a little less than the nonlinear programming based optimum.

Further, a semi-active control strategy for a floating oscillating wave column point absorber has been devised in order to maximize power take-off. The piston model and Wells turbine were introduced. The control of the pressure is regulated by a valve, which is assumed to be either fully opened or fully closed. At optimal control, the interval lengths of the opened and the closed state of the valve vary randomly due to the irregular sea state. In the paper the closing interval of the valve has been suggested as a constant proportion relative to the peak period associated with waves. Compared to the nonlinear programming based optimal solution, the optimal proportion parameter was obtained. The proposed control is dependent on the wave loads estimation, which was achieved by predicting the future surface elevation based on a Kalman-Bucy filter. The reduced performance, in terms of the absorbed energy for the proposed controller, is mainly dependent on the estimation error of wave loads.

Resumé

Som følge af stadig voksende efterspørgsel efter energi og den herat følgende miljøbelastning, er interessen for vedvarende energikilder øget tilsvarende. Blandt disse er bølgeenergi en potentiel bidragsyder. Skønt mange principper for bølgeenergi absorbtion er blevent testet, er teknologien stadig ikke fuldt udviket i sammenlingning med sol-og vindenergi pågrund af ineffektiv energiudvinding. Derfor er maksimering af den absorberede energi fra bølger et centralt emne, der bestemmer anvendeligheden af bølgeenergi sammenlignet med andre alternative energikilder som sol-og vindenergi. Som velkendt kan korrekt vibration af kontrolstrategier for bøleabsorber væsentligt forøge den absorberede energi fra bølger. Der er derfor et behov for at forbedre og udvikle optimale kontrolstrategier til dette formål. Yderligere er der i virkeligheden nogle fysiske begrænsninger for at begrænse effektiviteten af bølgeenergikonverter. Derfor er det nødvendigt at undersøge kontrolstrategier i betragtning af fysiske begrænsninger.

Denne ph.d.-afhandling har som emne at tilvejebringe optimale vibrationsstyrings strategier for bølgeenergikonvertere, hovedsageligt med henblik på point absorbere og oscillating water column absorbers, under iagttagelse af de fysiske begrænsninger.

På grund af begrænset observerbarhed og den uregelmæssige søtilstand, er kontrolproblemet væsentligt stokastisk. Under forudsætning af lineær bølgeteori er semi-analytiske løsninger til optimal kontrol udviklet for en heave absorber under hensyntages til restriktioner på kontrolkraften. Den optimale kontrol lov har feed-back fra nuværende bevægelse. I tidsintervaller hvor flytnings constraints er inaktive er den optimale kontrol af lukket løkke typen med feedback fra den øjeblikkelige flytning og acceleration og fra fremtidige hastigheder af absorberen. I intervaller, hvor flytningsconstraints er aktiv, har den optimale kontrolkraften åben løkke afhængighed af den øjeblikkelige bølgekraft på absorberen, som derfor må estimeres baseret på prediktion af fremtidige overflade elevationer. Algoritmer er formuleret til estimering af bølgelasten på absorberen og prediktionen af det fremtidige hastighedsrespons baseret på online-måling af den vertikale flytnings-, hastigheds- og accelerationsrespons af absorberen, tillige med elevationen af middel havover-

fladen. Prediktions og estimerings algoritmerne er baseret på en antagelse om smalbåndethed af de involverede stochastiske processer i kombination med en van der Pol transformation. Kvaliteten af de udviklede kontrol love er verificeret ved sammenligning med numeriske løsninger opnået ved ikke-lineær programmering.

Endvidere er foreslået en modificeret LQG kontroller til at styre bevægelsen af en absorber med constraint på både flytning og kontrolkraft. Constraints på flytning og aktuatorkraft er approksimativt taget i betragting ved reduktion af den absorberede effekt ved kvadratiske led i flytning og kontrolkraft i objekt funktionalen. Baseret på rationale approksimationer til radiationskraften og bølgelasten, kan det integrerede dynamiske system reformuleres som en lineær stokastisk differentialligning, drevet af en unit intensity Gaussisk hvid støj. Den optimale LQG kontrolkraft bliver en lineær funktion af tilstandsvektoren af det integrerede system. Kalman-Bucy filter teknik er anvendt til at estimere den kombinerede tilstandsvektor under forudsætning af partiel observation af tilstandsvektoren. Den foreslåede LQG kontroller absorberer maximal effekt samtidig med at flytningen af absorberen og kontrolkraften holdes begrænset. Det effervises, at med passende kalibreret gain parametre opnås en energiabsorption med den foreslåede kontroller, der er ubetydelig mindre end ved optimal kontrol baseret på ikke-lineær programmering.

Endvidere er udviklet en semi-aktiv kontrol strategi for en oscillating water column punkt absorber med henblik på optimal power take-off, hvor den såkaldt piston-model og Wells turbinen introduceres. Styringen af trykket reguleres af en ventil, som antages at være enten helt åben eller helt lukket. Ved optimal styring varierer intervallængderne af den åbnede og den lukkede tilstand af ventilen tilfældigt som følge af den uregelmæssige søtilstand. Som en approksimtion antages lukningsintervallerne af ventilen at udgøre en konstant relativ lille brøkdel af peak bølgeperioden. Den optimale værdi af den nævnte brøkdel er bestemt ved sammenligning med den optimale opløsning opnået ved ikke-lineær programmering. Den beskrevne kontrolstrategi forudsætter et estimat af bølgebelastningen på flyderen og vandsøjlen, hvilket er tilvejebragt ved prediktion af fremtidige overflade elevationer ved hjælp af et Kalman-Bucy filter. Den reducerede effekt af den udviklede kontroller skyldes primært bølgelast estimationen, og i mindre grad den beskrevne styring af ventilen mellem trykkammeret og turbinen.

Chapter 1

Introduction

This chapter gives the background, motivation and organization of this work. The hydrodynamic and model for wave energy converters (WECs), different control strategies widely used for WECs are presented. Based on this literature survey, the objectives and structure of this thesis are outlined.

1.1 Background and motivation

As an important renewable energy source, much attention is paid to wave energy. Although wave energy conversion techniques are immature compared with the utilisation of other renewable energy resources, wave energy has promising potential due to its huge reserve, wide distribution and high availability. Further, wave energy conversion devices have a less environmental impact.

The primary goal for developing renewable energy technologies is to reduce the cost of unit delivered energy. There are still severe challenges for commercial utilization of WECs. As well known, the power generation of WECs can be significantly improved by proper active or passive vibration control strategies. This has led to the necessity and urgency of exploring and developing control strategies of WECs to enhance wave energy extraction and to reduce the cost of energy, so as to eventually increase its market competition in comparison to alternative renewable energy sources. In this respect, the thesis presents some active vibration control algorithms for point absorber and oscillating water column absorbers, which turn out to be close to optimal.

1.2 Control of WECs

1.2.1 Modelling of WECs

A variety of WECs have been developed to harvest wave energy based on different principles (Sheng, 2019a). Falcao (2010) suggested that wave energy devices may be roughly divided into three styles, including oscillating bodies, oscillating water columns (OWCs) and overtopping devices, see Fig 1.1. According to the types of power take-off, the more specific classification can be given as the direct drives or hydraulic systems for oscillating bodies (Eriksson et al., 2005; Gao et al., 2016; Gaspar et al., 2018; Henderson, 2006), the air turbines for OWCs (Brito-Melo et al., 2002; Falcao et al., 2014; Hashem et al., 2018; Setoguchi et al., 2001), and the water turbines for overtopping devices (Kofoed et al., 2006; Margheritini et al., 2009). This work only considers two types of WECs of oscillating bodies and OWCs.

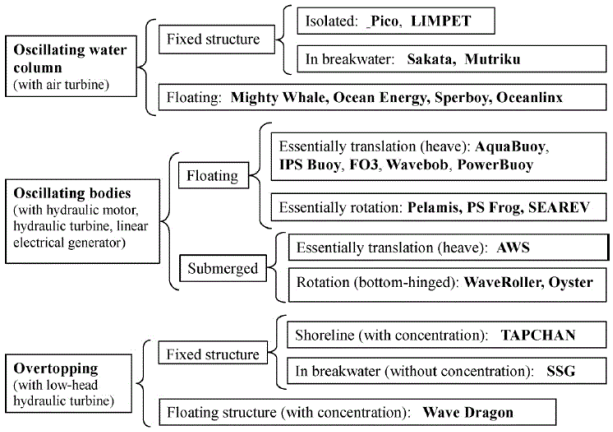

Fig. 1.1: Categories of wave energy converters (Falcao, 2010).

Point-absorbing WECs, as a kind of floating oscillating bodies, have attracted much attention due to their small size, low cost and simple construction (Beatty et al., 2015, 2019; Nielsen et al., 2013; Pastor and Liu, 2014). Point absorbers are designed with significantly smaller horizontal dimensions in comparison to the dominating wavelength in order to capture wave energy in arbitrary directions. Among them, there are a kind of heave point absorbers, which are constrained to merely move in the vertical direction, and which extract wave energy from the float motion relative to a sea-bed or a submerged oscillating body.

Numerical modelling of WECs is needed to clarify the wave-structure interaction. The WECs can move excited by waves, indicating that mechanical

energy has been transferred to the absorber. At the same time, the motion of the absorber produces waves radiating away from the absorber, where some of the absorbed energy is dissipated (Falnes, 1980).

For the wave-structure interaction, it is actually to consider the fluid dynamic pressure acting on the structures. Generally, two approaches can be applied. One approach is the potential flow theory. It can be easily solved with a boundary element method (BEM), which is applied to calculate the radiation and diffraction velocity potentials using a discrete number of sources or dipoles on the surfaces of submerged bodies so as to fulfil all boundary conditions. The other approach is related to the Reynolds-averaged Navier-Stokes (RANS) equations. This approach can provide more advantages in handling strong nonlinearity, complex viscous, and turbulence etc. in comparison to the potential flow theory. However, its computational efficiency is low.

In fact, the potential flow theory, especially linear potential theory, is the most useful and most popular numerical tool for modelling wave energy converters, although some studies have used computational fluid dynamics (CFD) (Elhanafi et al., 2017; Ransley et al., 2017). The approach of linear potential theory for WECs has been justified throughout the operational regime (Falnes, 2002). Evans applied potential flow theory for regular waves to analytically study the hydrodynamics of oscillating body WECs (Evans, 1976) and piston model based OWC WECs (Evans, 1978), respectively. BEM numerical approximations to the Green function corresponding to the free surface were introduced for the purpose of estimating the hydrodynamics for offshore structures with complex geometries. Several additional studies were made using BEM based potential flow algorithms to model the other types of oscillating body devices. Similar analyses were performed by Bhinder et al. (2015); Pizer (1992) for pitching WECs, and by Ruellan et al. (2010), Hansen et al. (2011), Li et al. (2018) and Kim et al. (2019) for floating oscillating-body devices.

Similarly, potential flow methods have been used to model the oscillating water column devices. Unlike oscillating bodies, the essential is to model the inner free surface for the oscillating water column device. There are typically two different methods to analyzing the interaction between the buoy and the OWC. One method is the piston model (Evans, 1978), see Fig. 1.2(a). The piston model presumes that the top fluid particles of the water column are constrained to having the identical motion, which behaves like a rigid body motion. In principle, the approximation can only be justified on the condition that the horizontal dimension of the pressure chamber should be smaller compared to the incident wavelengths (Falnes, 1999; Robinson, 1982). The other method is the uniform pressure distribution model (Evans, 1982), see Fig. 1.2(b), in which the air flow rate and the dynamic air pressure are introduced to the governing equations. This is different from the piston model

employing the forces and velocities to model WECs. Further, the interaction between waves and WECs in the piston model can be simplified by an equivalent reduced 2-DOF model owing to the assumption that the inner water column is regarded as a massless or limited mass rigid body, (Evans, 1978; Falnes, 2002). This is the reason why the piston model is often preferred in favour of the more correct surface pressure distribution approach. Falcao et al. (2012) computed the frequency-dependent hydrodynamic coefficients of the Spar buoy OWC wave energy converter using potential flow theory in combination with a weightless piston model. Bingham et al. (2015) analysed a kind of OWC WEC device numerically based on linearized potential flow theory using a a high-order panel method to consider wave-body interactions. Sheng et al. (2019b) applied the potential flow theory based BEM to obtain the hydrodynamic parameters for the floater and the internal water column for a OWC device. Further, Falnes and Kurniawan (2015) presented the summary for applying the potential flow theory to WECs.

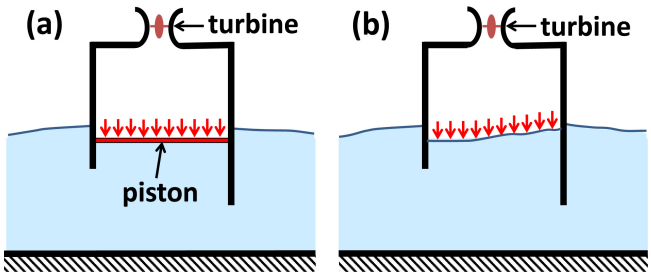

Fig. 1.2: Schematic representation of OWC modelling: (a) piston model; (b) free-surface uniform pressure model (Falcao and Henriques, 2016).

The power take-off (PTO) system is applied for the purpose of converting mechanical energy into electricity. For this reason, the PTO system influences the motion of WECs because the removed power is equivalent to a damping of the motion. For oscillating body WECs, the PTO can be a system with hydraulic components and an electric generator (Kim et al., 2019; Negahdari et al., 2018), or a direct drive system (Temiz et al., 2018). The PTO in an OWC device is an air turbine, for example Wells turbine (Scuotto and Falcao, 2005). The PTO is commonly assumed to behave as a linear damper system corresponding to a passive derivative controller (Clement and Babarit, 2012). Additionally, feedback effects from inertia and spring effects may be included in the control strategy. It has been demonstrated that negative control inertia and stiffness can improve the performance of the PTO (Antonio, 2017).

Assuming small body motions in combination to a linear PTO control force, the numerical modeling of WECs in the frequency domain can be performed using linear potential flow theory. Bosma et al. (2012) used the frequency domain approach to analyse the power output for a two-body

heave point absorber. Similar analyses were performed by Pastor and Liu (2014) and Cheng et al. (2014) for a heaving point absorber WEC system. Ye and Chen (2017) established a frequency domain model of a 3-DOF (heave, pitch and surge) point absorber so as to predict the power production and the eigenfrequencies of the 3-DOF systems. Wei et al. (2019) applied the frequency domain analysis to an ensemble of heave point absorbers. The involved hydrodynamic parameters were obtained by BEM. Gomes et al. (2012) used a piston model to model a floating OWC WEC device installed with a Wells turbine in the frequency domain. Further, a linearized model was applied for the air compressibility.

Although the frequency domain analysis is simple, it cannot handle nonlinearities in the structural response, and from nonlinear control and wave forces. Generally, feedback control strategies applied to WECs are highly nonlinear. Further, a linear equivalent PTO force can not reflect the realistic system. It is necessary to consider the time domain method. Even though the time domain modelling is computationally demanding, it can deal with nonlinearities from the vibration control forces, non-linear wave excitation forces, mooring forces, etc. The equation of motion for marine structures was first proposed by Cummins (1962) using linear potential flow theory, which contains a causal convolution integral containing the memory effect of the radiation damping. The indicated radiation convolution term makes numerical calculations somewhat cumbersome but this can be circumvented applying an approximation to the radiation convolution term (Taghipour et al., 2008) or to the radiation frequency response function (Perez and Fossen, 2008). This changes the integro-differential equation to a ordinary differential system, at the expense of introducing lots of additional state variables. The extra state variables carry over the memory of previous velocities of the absorber.

Approximations to the convolution term have been applied extensively to analyse the dynamic responses for WECs (Jefferys, 1984; Nielsen et al., 2014; Perez and Fossen, 2008; Taghipour et al., 2008). Ricci et al. (2008) and Kurniawan et al. (2013) compared the approximations to the radiation convolution term in the frequency domain and the time domain with direct convolution integration, respectively. Zurkinden et al. (2014) used the state-vector approach to approximate the radiation force in the time domain. The results were positively verified by the experimental measurement result. Penalba et al. (2017) studied the impact from the non-linear Froude-Krylov (FK) force to the dynamic response and power output of cylindrical and spherical point absorbers in regular waves. The nonlinear FK force slightly influences WEC devices of constant cross-sectional areas, while significantly influences WEC devices of varying cross-sectional area. Sheng et al. (2014) applied the piston model to analyze the hydrodynamics of a fixed OWC device in the frequency domain and time domain. It was demonstrated that the impact of the piston length on the absorber motion for different frequencies can be ignored in the

frequency domain analysis, while it is significant in the time domain analysis. The motion response in the time domain is consistent with the result in the frequency domain when the piston is long enough. Comprehensive reviews of numerical modelling of WECs have been given by Babarit et al. (2012); Evans (1981a); Folley (2016); Sheng (2019a).

1.2.2 Control strategies of wave energy converters

Generally, WECs perform better if they are tuned so their dominating eigenfrequencies approach the dominating wave frequency. In theory, optimal power output can be obtained through so-called reactive control, which means the system is regulated into resonance with the incoming waves (Falnes, 2002). However, this can hardly be achieved for broad-banded sea states. Thus, alternative control strategies have been put forward.

Latching control proposed by Falnes (1978) and French (1979) may be qualified as a kind of open-loop control strategy. Further, it is the simplest and the most investigated control strategy (Henriques et al., 2016; Sheng et al., 2015; Wu et al., 2017). For latching control, its working principle is to latch the absorber motion when its velocity is zero, and release it when the phases of the velocity and the wave load are identical so mechanical energy is supplied to the absorber, see Fig. 1.3. The challenge of the strategy is to determine the optimal time for latching and unlatching the absorber. The effect of the controller relies on the observation of the surface elevation, from which the sign of the wave load is estimated. It should be noticed that the wave force is noncausal, which depends on the future surface elevation, so it is necessary to predict the surface elevation at least one vibration period ahead. This is possible in cases of narrow-banded sea states. However, the prediction effect cannot be guaranteed in broad-banded sea states, which can affect the stability of the controller. It has been verified in several publications that latching control can significantly improve the power output for oscillating body WECs (Babarit et al., 2004; Saupe et al., 2014; Wu et al., 2018) and OWC devices (Henriques et al., 2013, 2014, 2016).

Robust closed loop controller has been paid much attention in order to deal with the uncertainties in the open loop controller. Among them, classical PID controller has been put forward by Astrom et al. (2016). The optimal control law was derived by Nielsen et al. (2013) for a heave point absorber, which follows the general PID type but the convolution term replaces the proportional term. Further, the control law is non-causal, which needs to predict the future velocities of the absorber. However, this will cause some uncertainties so the control law is sub-optimal. To handle the indicated non-causality problem, the authors further developed a causal controller, which needs feedback from measurements of the absorber motion.

In practice, the optimal vibration control of WECs is subject to physical

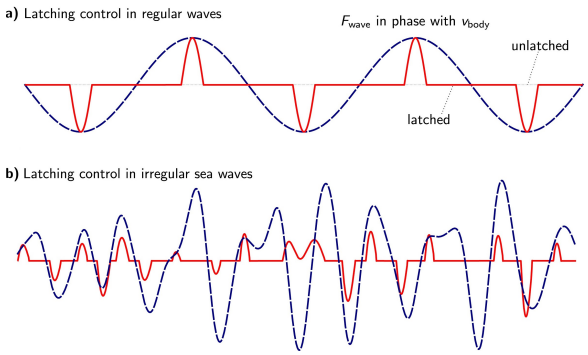

Fig. 1.3: Latching control in a) regular waves and b) irregular waves (Henriques et al., 2016).

constraints on the motion and the actuator force. Constraints are exerted on the magnitude of the control force so as to protect the structure of the absorber safe, or because of the saturation problem. Further, constraints on the absorber motion may be considered, either due to limited strokes of the PTO system or limitation in the mooring. The latter events may cause excessive impulsive loadings on the absorber shell. Evans (1981b), Pizer (1993) and Falnes (2000) presented theoretical analyses for linear wave energy absorber with amplitude constraints in the frequency domain. Sichani et al. (2014) presented a suboptimal control law for a WEC device with the aforementioned two constraints. The displacement constraints are accounted for through adding artificial nonlinear springs to the system equation, which are achieved when the absorber becomes close to the displacement limits. Na et al. (2018) studied an efficient controller for WECs considering nonlinearities and constraints based on adaptive dynamic programming. Adaptive dynamic programming was applied to solve the associated Hamilton-Jacobi-Bellman equation and a neural network is applied for the purpose of approximating the optimal cost value and the control force. The proposed control method was proved to be efficient.

In recent years, model predictive control (MPC) based control strategies have been introduced for optimal control of WECs due to the advantage to deal with the constraints exerted on the motion and control forces. A variety of MPC formulations have been focused by Richter (2011); Richter et al. (2012); Zhan et al. (2019), etc. Cretel et al. (2011) presented an early use of this method, where the absorber motion and actuator force constraints were replaced by inequality constraints related to the increment of actuator force. The constraint on the absorber amplitude was handled with sufficient accuracy but may cause problems for the actuator force constraints. Soltani et al. (2014) suggested a MPC algorithm for a semi-sphere WEC device. The

control problem was transferred to a simple convex optimization problem. The indicated controller requires the future information of the sea state and should be classified as a mixed feedforward and feedback controller. Recently, variations of the MPC method have been applied in WECs. The idea is that the WECs motion and the control force are approximately replaced by a finite linear combination of basis functions while reformulating the objective functional to a convex form. This can effectively reduce the computational burden. According to the choice of test functions, it can be classified to two methods: spectral control and pseudospectral control methods (Faedo, 2017). Bacelli and Ringwood (2014) used a truncated Fourier series based spectral method for WECs to consider the physical constraints. Genest and Ringwood (2016) proposed a half-range Chebyshev Fourier basis functions based pseudospectral control method for WECs device. To hand the signal truncation effect, the receding horizon is used. It has been demonstrated that pseudospectral control can successfully maximize the absorbed energy while reducing the computation burden. Further, Freeman et al. (2014), Fay et al. (2015), Ozkop and Altas (2007) and Wang et al. (2018) provide the relevant summary for the applications of different control strategies for WECs.

1.3 Objective of the thesis

The objective of this study to is carry out fundamental research on control strategies close to optimal power take-off for WECs. Effective control methods for a heave point absorber will be devised with the focus on the pure constrained displacement, the pure constrained control force and the mixed constrained displacement and control force.

Further, a control strategy for OWC device will be explored, based on a novel semi-active control law for the valve for the purpose of maximizing the absorbed power.

1.4 Outline of the thesis

Chapter 1 presents the introduction and motivation of the study, addressing the background, objectives, and structure.

Chapter 2 describes the model and control strategies for oscillating-body heave point absorber. It clearly presents the derivation of the control laws with different constraints.

Chapter 3 presents dynamics and control of floating OWC WECs. A semi-active valve controller is proposed for maximizing the turbine power in ir-

regular sea state.

Chapter 4 provides the general conclusion drawn from this study and possible future extensions.

Appendix presents the discussion of choosing the piston length.

The second part include some published or submitted papers. The detail is shown in the below:

Paper A contains the enclosed journal paper: "Stochastic optimal control of a heave point wave wnergy converter based on a modified LQG approach".

Paper B contains the enclosed journal paper: "Stochastic control of wave energy converters for optimal power absorption with constrained control force".

Paper C contains the enclosed journal paper: "Stochastic control of wave energy converters with constrained displacements for optimal power absorption".

Paper D contains the enclosed journal paper: "Semi-active feedforward control of a floating OWC point absorber for optimal power take-off".

Chapter 2

Control strategies for wave energy point absorbers

This chapter deals with the control of WECs concerning the displacement and control force constraints referring to Papers A, B and C. The optimal control law for the optimization problem with the control force constraints is derived, which turns out to have feedback from the motion of the absorber involving the present displacement, the present acceleration, and future velocities. A prediction algorithm for future velocities has been put forward for the purpose of dealing with the problem. The verification of the mean absorbed power for the proposed controller has been implemented in contrast to the results from both nonlinear programming and a causal closed loop controller. Next, a semi-analytical control law with constrained displacement is derived. The control law is proven to be an open-loop control style, which relies on the wave excitation force during the displacement-activated intervals. In the unconstrained states, the solution follows the theoretical optimal solution for an unconstrained absorber, save an initial constant, which has to be calculated. Methods to estimate the wave excitation force during active displacement constraints, and to predict future velocities during unconstrained states have been proposed. Finally, an alternative control strategy for the absorber with mixed constrained displacement and control force is proposed through a modified LQG approach. The suboptimal solution for the proposed controller has been validated in comparison to the nonlinear programming based optimal solution.

2.1 Description of a point absorber motion and the related constrained optimization problem

Fig. 2.1 shows a somewhat idealized point absorber consisting of cylindrical apart with height H and the diameter D, and semi-sphere with the diameter D , which is constrained to move only in heave and thus may be modeled as a single DOF dynamic system.

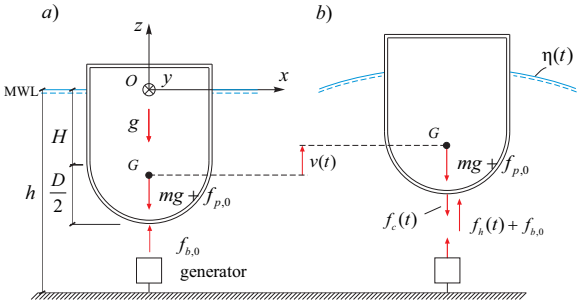

Fig. 2.1: Description of loads on a heave point absorber. a) Static equilibrium state. b) Dynamic state (Sun and Nielsen, 2018).

In the dynamic state in Fig 2.1b), the heave absorber can move up and down, which is driven by a control force $f_c(t)$ and a dynamic hydrodynamic force involving the quasi-static buoyancy $f_b(t)$, the radiation force $f_r(t)$ as well as the wave load $f_e(t)$. Generally, $f_c(t)$ is supplied by the PTO system for capturing wave energy.

$f_b(t) = -r\big(v(t)\big)$ is a nonlinear buoyancy resulting from the displacement $v(t)$ relative to the static equilibrium state. The linearization of $f_b(t)$ in the vicinity of the static equilibrium state can be introduced based on small vertical vibrations (Newman, 1977), which is given as:

$$f_b(t) = -k\,v(t) \quad , \quad k = \frac{1}{4}\pi D^2 \rho g \tag{2.1}$$

The radiation force $f_r(t)$ is produced by the absorber motion in the absence of wave motion. It can be envisioned as a damping force which equivocates the loss of mechanical energy of the absorber when the wave is away from the absorber. Further, $f_r(t)$ can be represented by the acceleration term with the added mass water at infinite frequency, m_h, as a proportional coefficient, and the convolution integral concerning the impulse response function $h_{r\dot{v}}(t)$ and the velocity $\dot{v}(t)$, given as (Cummins, 1962; Faltinsen, 1990):

$$f_r(t) = -m_h \ddot{v}(t) - f_{r,0}(t) \tag{2.2}$$

$$f_{r,0}(t) = \int_{-\infty}^{t} h_{r\dot{v}}(t-\tau)\dot{v}(\tau)\,d\tau \tag{2.3}$$

Finally, the motion equation of the heave point absorber can be given as:

$$\left.\begin{aligned} &\big(m+m_h\big)\ddot{v}(t) + r\big(v(t)\big) + \int_{t_0}^{t} h_{r\dot{v}}(t-\tau)\dot{v}(\tau)\,d\tau = f_e(t) - f_c(t)\ ,\ t > t_0 \\ &v(t_0) = v_0\,, \quad \dot{v}(t_0) = \dot{v}_0 \end{aligned}\right\} \tag{2.4}$$

where m is the dry structural mass of the absorber including possible ballast. v_0 and $\dot{v}_0$ specify the displacement and velocity at the initial time t_0. Eq. (2.4) is known as the Cummins equation.

Table 2.1: Values of physical parameters in the heave absorber

Parameter	Value	Unit	Parameter	Value	Unit
H	7.00	m	m	1.84×10^6	kg
D	14.00	m	m_h	0.44×10^6	kg
h	30.00	m	k	1.51×10^6	N/m

Table 2.1 provides the values of physical parameters in the heave absorber shown in Fig. 2.1. Based on these values, the hydrodynamic parameters including the added mass m_h, the frequency response functions for $f_r(t)$, $H_{r\dot{v}}(\omega)$, and for $f_e(t)$, $H_{e\eta}(\omega)$, can be obtained by the program WAMIT alternatively, and the inverse Fourier transform of $H_{r\dot{v}}(\omega)$ and $H_{e\eta}(\omega)$ is then applied to get the related impulse response functions $h_{r\dot{v}}(t)$ and $h_{e\eta}(t)$, respectively. In Fig. 2.2, $h_{r\dot{v}}(t)$ has been shown with the normalized time relative to the wave peak period T_p. As seen, $h_{r\dot{v}}(t)$ effectively vanishes for $t > T_p$.

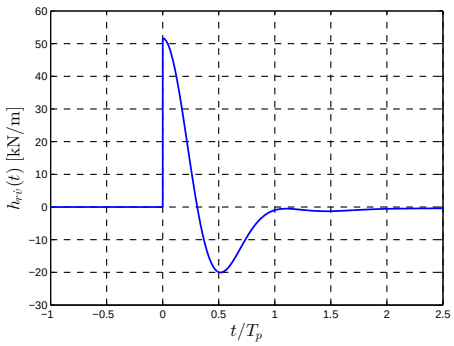

Fig. 2.2: Impulse response function for $h_{r\dot{v}}(t)$ (Sun and Nielsen, 2018).

In order to facilitate the numeral calculation and application in control algorithms, the convolution integration, $f_{r,0}(t)$, can be replaced by a coupled first-order differential equations-based equivalent system, which can be achieved by approximating $H_{r\dot{v}}(\omega)$ with a rational function (Sun and Nielsen, 2018). Fig. 2.3 shows the comparison between the obtained rational approximation and the target frequency response function.

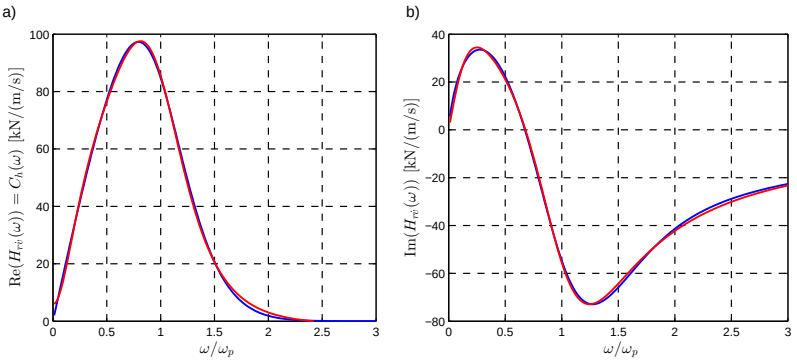

Fig. 2.3: Rational approximation to $H_{r\dot{v}}(\omega)$. a) $\mathrm{Re}(H_{r\dot{v}}(\omega))$. b) $\mathrm{Im}(H_{r\dot{v}}(\omega))$. ——: Target frequency response function. ——: Rational approximation, $(m,n) = (2,3)$ (Sun and Nielsen, 2018).

Then, $f_{r,0}(t)$ can be expressed as (Sun and Nielsen, 2018):

$$\frac{d}{dt}\mathbf{z}_r(t) = \mathbf{A}_r\mathbf{z}_r(t) + \mathbf{b}_r\dot{v}(t) \tag{2.5}$$

$$f_{r,0}(t) = \mathbf{p}_r\mathbf{z}_r(t) \tag{2.6}$$

where $\mathbf{z}_r(t)$, $\mathbf{A}_r$, $\mathbf{b}_r$ and $\mathbf{p}_r$ can be found in Paper B.

In practice, $v(t)$ can only vary in a certain interval $[v_{\min}, v_{\max}]$, either because the actuator stroke is finite or in order to keep the absorber motion in the proper range. Likewise, $f_c(t)$ can only vary in a certain interval $[f_{c,\min}, f_{c,\max}]$, either caused by the actuator saturation or for the purpose of preventing large stresses at specific hot spots of the structure. Under the displacement and control force constraints, the constrained optimization problem during the control interval $[t_0, t_1]$ can be expressed as (Sun and Nielsen, 2018):

$$\max \quad J[f_c(t), \dot{v}(t)] = \int_{t_0}^{t_1} f_c(\tau)\dot{v}(\tau)\, d\tau$$

s.t.

$$\begin{cases} (m + m_h)\ddot{v}(t) + \mathbf{p}_r(t)\mathbf{z}_r(t) + r(v(t)) = f_e(t) - f_c(t) \\ \dot{\mathbf{z}}_r(t) = \mathbf{A}_r\mathbf{z}_r(t) + \mathbf{b}_r\dot{v}(t) \\ v(t_0) = v_0\ , \dot{v}(t_0) = \dot{v}_0 \\ v_{\min} \leq v(t) \leq v_{\max} \\ f_{c,\min} \leq f_c(t) \leq f_{c,\max} \end{cases} \tag{2.7}$$

2.2 Optimal control with constrained control forces

This subsection focuses on the optimal control for WECs considering the control force constraints. No displacement constraints are assumed. Then, Eq. (2.7) is reduced as (Sun and Nielsen, 2019a):

$$\max \quad J[f_c(t), \dot{v}(t)] = \int_{t_0}^{t_1} f_c(\tau)\dot{v}(\tau)\, d\tau$$

s.t.

$$\begin{cases} (m + m_h)\ddot{v}(t) + \mathbf{p}_r(t)\mathbf{z}_r(t) + r(v(t)) = f_e(t) - f_c(t) \\ \dot{\mathbf{z}}_r(t) = \mathbf{A}_r\mathbf{z}_r(t) + \mathbf{b}_r\dot{v}(t) \\ v(t_0) = v_0\ , \dot{v}(t_0) = \dot{v}_0 \\ f_{c,\min} \leq f_c(t) \leq f_{c,\max} \end{cases} \tag{2.8}$$

Pontryagin's maximum principle which states that the optimal control is achieved at stationary value of the Hamiltonian, will be used to handle this control problem (Pontryagin et al., 1962). The resulting control law is given as (Sun and Nielsen, 2019a):

$$f_c(t) = \begin{cases} f_{c,\max} & , \quad f_{c,0}(t) > f_{c,\max} \\ f_{c,0}(t) & \\ f_{c,\min} & , \quad f_{c,0}(t) < f_{c,\min} \end{cases} \tag{2.9}$$

where $f_{c,0}(t)$ is the optimal control force for unconstrained cases, given as (Nielsen et al., 2013)

$$f_{c,0}(t) = -M\ddot{v}(t) + \int_t^{t_1} h_{r\dot{v}}(\tau - t)\, \dot{v}(\tau)\, d\tau - r\big(v(t)\big) \tag{2.10}$$

The control law in Eq. (2.9) has feedback from the motion of the absorber involving $v(t)$ and $\ddot{v}(t)$ as well as future velocities $\dot{v}(\tau)$, $\tau \in]t, t_1]$. Therefore,

it is necessary to apply the prediction algorithm to obtain the future velocities $\dot{v}(\tau)\,,\ \tau \in]t, t_1]$. This will make the proposed controller become suboptimal because of the uncertainty from the prediction algorithm.

It turns out that the response processes of WECs are relatively narrow-banded with the peak angular frequency $\omega_p = \frac{2\pi}{T_p}$ as the center frequency, even though the wave excitation force is broad-banded (Sun et al., 2019). Hence, a van der Pol transformation can be introduced for the purpose of predicting future velocities (Roberts and Spanos, 2003). It should be noted that the time varying amplitude and phase processes in the prediction algorithm are only required to predict one T_p beyond the present time because $h_{r\dot{v}}(t) \simeq 0$ for $t > Tp$ in Fig. 2.2.

Fig. 2.4 shows the predicted $\dot{v}(t)$ from different start times. The black curve indicates a realization of the velocity $\dot{v}(t)$ at optimal control from nonlinear programming. The predicted velocities are in good agreement with the optimal solution at least one T_p ahead. This fulfills the prediction horizon required according to Fig. 2.2.

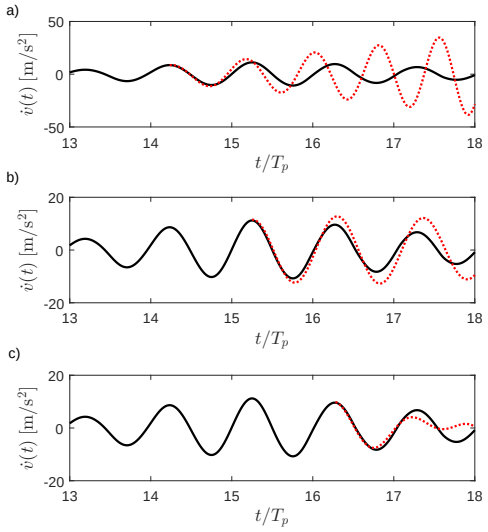

Fig. 2.4: Prediction of $\dot{v}(t)$ from different start times. ——: Nonlinear programming solution. ·····: Prediction velocities (Sun and Nielsen, 2019a).

For the purpose of investigating the impact of the control force constraints on the absorbed power, the boundaries of constrained control force are considered as a variable and the magnitudes of upper and lower boundaries are assumed identical. Assume that the wave load and response processes of the absorber are Gaussian processes, the absorbed mean power at optimal control with constrained control forces can be expressed as (Sun and Nielsen,

2019a):

$$\bar{P}_{\text{opt}} = \alpha\left(f_{c,\min}, f_{c,\max}\right)\bar{P}_{\text{opt},0} \tag{2.11}$$

where $\bar{P}_{\text{opt},0}$ denotes the maximum mean power extracted by the unconstrained optimal control, given as:

$$\bar{P}_{\text{opt},0} = \int_0^\infty \frac{|H_{e\eta}(\omega)|^2}{2\,\text{Re}\big(H_{r\dot{v}}(\omega)\big)} S_{\eta\eta}(\omega)\, d\omega \tag{2.12}$$

$\alpha\left(f_{c,\min}, f_{c,\max}\right)$ indicates a reduction factor caused by the constraints on the control force. The detail is described in Paper A.

Fig. 2.5 shows the variation of $\alpha\big(f_{c,\min}, f_{c,\max}\big)$ as a function of $\frac{f_{c,\max}}{\sigma_{f_{c,0}}}$, $f_{c,\min} = -f_{c,\max}$. As seen, the constraints are only significantly influencing the power takeoff for $\min(f_{c,\max}, -f_{c,\min}) < 3\sigma_{f_{c,0}}$.

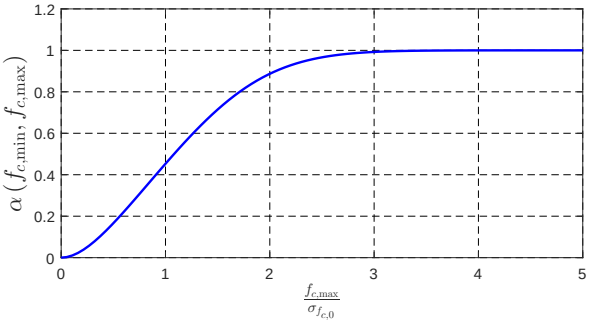

Fig. 2.5: Reduction coefficient $\alpha\left(f_{c,\min}, f_{c,\max}\right)$ as a function of $\frac{f_{c,\max}}{\sigma_{f_{c,0}}}$, $f_{c,\min} = -f_{c,\max}$ (Sun and Nielsen, 2019a).

For evaluating the performance of the proposed controller, the proposed controller has been compared with the following causal controller, where $f_{c,0}(t)$ in Eq. (2.9) is replaced with (Sun and Nielsen, 2019a):

$$f_{c,0}(t) = -\beta_1 M\ddot{v}(t) + c\dot{v}(t) - \beta_2 r\big(v(t)\big) \tag{2.13}$$

where β_1, β_2, c are the optimal tuned gain parameters, which can be found in Paper A.

Three independent realizations of $\eta(t)$ given by a JONSWAP auto-spectral density function with $H_s = 3$m, $T_p = 7.42$s, $\gamma = 5$ have been applied in the control interval $[0, 20T_p]$. There is a comparison of the responses of displacement and velocity, the control force and the instantaneous absorber power at suboptimal control indicated in Eq. (2.10), at feedback control indicated

in Eq. (2.13), and at nonlinear programming based optimal control respectively. Figs. 2.6 shows the results from one of the realizations of $\eta(t)$. There is a small deviation in the displacement and velocity from Eqs. (2.10) and (2.13) based controllers in contrast to the results from nonlinear programming, while the deviations of the control force and the instantaneous power are obvious because of the deviation amplification of the related acceleration signals caused by multiplying M.

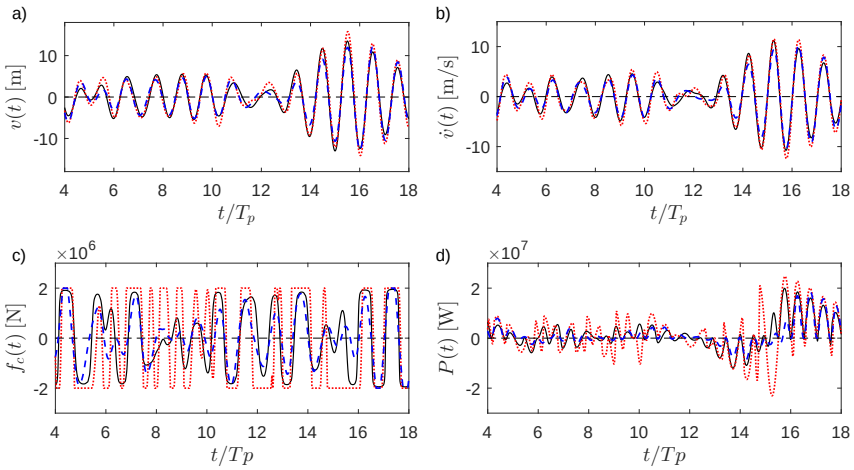

Fig. 2.6: Comparison of solutions with different control strategies for Realization 1. ——: Nonlinear programming solution. ·····: $f_{c,0}(t)$ given by Eq. (2.10). - - - : $f_{c,0}(t)$ given by Eq. (2.13) (Sun and Nielsen, 2019a).

Table 2.2 gives the performance of the proposed controller and the causal controller in comparison to the nonlinear programming based optimal control, using three different realizations of $\eta(t)$. The absorbed mean power $\bar{P}$ has been calculated in the interval $[3.5T_p, 20T_p]$, where the influence from initial values on the vibration of the absorber is assumed to be dissipated. Further, the relative errors compared with the optimal solution have been indicated in brackets.

Table 2.2: Absorbed mean power $\bar{P}$ [MW] (Sun and Nielsen, 2019a).

	Nonlinear programming	$f_{c,0}(t)$ given by Eq. (2.10)	$f_{c,0}(t)$ given by Eq. (2.13)
Realization 1	1.663	1.566 (5.8%)	1.544 (7.2%)
Realization 2	0.521	0.513 (1.2%)	0.467 (10.4%)
Realization 3	0.950	0.945 (0.5%)	0.921 (3.1%)

The absorbed mean power of the proposed controller related to $f_{c,0}(t)$ in

Eq. (2.10) and predicted future velocities is little lower than the optimal solution but it performs better than the causal controller in all three realizations.

2.3 Optimal control with constrained displacements

The focus of the subsection is on the consideration of the displacement-constrained based control for WECs. No control force constraints are assumed. Then Eq. (2.7) is reduced as (Sun et al., 2019):

$$\max \quad J[f_c(t), \dot{v}(t)] = \int_{t_0}^{t_1} f_c(\tau)\dot{v}(\tau)\, d\tau$$

s.t.

$$\begin{cases} (m + m_h)\ddot{v}(t) + \mathbf{p}_r(t)\mathbf{z}_r(t) + r(v(t)) = f_e(t) - f_c(t) \\ \dot{\mathbf{z}}_r(t) = \mathbf{A}_r\mathbf{z}_r(t) + \mathbf{b}_r\dot{v}(t) \\ v(t_0) = v_0\ , \dot{v}(t_0) = \dot{v}_0 \\ v_{\min} \leq v(t) \leq v_{\max} \end{cases} \tag{2.14}$$

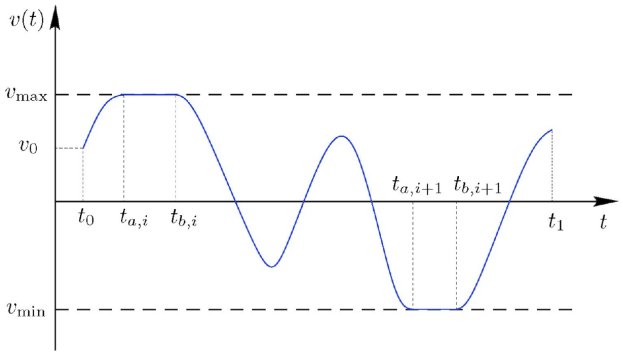

Fig. 2.7: Description of the constrained displacement (Sun et al., 2019).

Let $v_{m,i}$ denote either $v_{\max}$ or $v_{\min}$, and $[t_{a,i}, t_{b,i}]$ the ith constraint-activated interval shown in Fig. 2.7.

Given that $\dot{v}(t) = \ddot{v}(t) \equiv 0$ for $t \in [t_{a,i}, t_{b,i}]$, the control force in the constraint-activated intervals based on Eq. (2.4) can be obtained:

$$f_c(t) = f_e(t) + C_i \tag{2.15}$$

where C_i is a constant depending on previous observed velocities up to the entering of the displacement constraint at the time $t_{a,i}$, given as (Sun et al., 2019):

$$C_i = -\int_{t_0}^{t_{a,i}} h_{r\dot{v}}(t_{a,i}-\tau)\,\dot{v}(\tau)\,d\tau - r(v_{m,i}) \tag{2.16}$$

C_i can be calculated by Eq. (2.16) on the assumption that $\dot{v}(t)$ can be measured continuously in the interval $[t_0, t_{a,i}[$.

The optimal control in Eq. (2.15) is feed-forward so $f_e(t)$ is required to be estimated during constraint-activated intervals.

The optimal control solution during the constraint-unactivated interval $]t_{b,i}, t_{a,i+1}[$ can be given as in Paper B:

$$f_c(t) = f_{c,0}(t) + D_i \tag{2.17}$$

where $f_{c,0}(t)$ indicates the unconstrained optimal control, which has been indicated in Eq. (2.10). D_i is a constant determined based on the information at the interface to the previous constrained interval, expressed as (Sun et al., 2019):

$$D_i = f_e(t_{b,i}) + C_i - \int_{t_{b,i}}^{t_1} h_{r\dot{v}}(\tau - t_{b,i})\,\dot{v}(\tau)\,d\tau + r(v_{m,i}) \tag{2.18}$$

As seen from Eq. (2.18), the calculation of D_i relies on the prediction of future velocities $\dot{v}(\tau), \tau \in [t_{b,i}, t_{b,i} + T_{\dot{v}}]$ where $T_{\dot{v}}$ is the prediction horizon.

In summary, the estimate of wave load and the prediction of future velocity should be performed in order to apply the control law in Eqs. (2.15) - (2.18). Similarly, a van der Pol transformation (Roberts and Spanos, 2003) used in subsection 2.2 has been used for the wave load estimation. Both $f_e(t)$ and $\dot{f}_e(t)$ are narrow banded stochastic processes, which can be represented by harmonic processes with slowly varying amplitude and phase processes, and with wave peak angular frequency (Sun et al., 2019). The details are indicated in Paper B.

Fig. 2.8 shows the prediction results for the wave load $f_e(t)$, one prediction period $T_{f_e} = 0.7T_p$ ahead for $\gamma = 1$ and $\gamma = 5$ with the same $H_s = 3.00$m, $T_p = 7.42$s at different start times. As seen, the predictions for narrow banded processes are more accurate than that for the broad banded processes.

The prediction of velocities is performed based on its approximately skew-symmetric property regarding constraint-activated intervals (Sun et al., 2019) in combination with its narrow banded characteristic (Nielsen and Zhang, 2017). The detailed description can be found in Paper B. Fig. 2.9 shows the predicted velocities for different sea states with different constrains concerning $\gamma = 1, v_{\max} = -v_{\min} = 0.8\,\mathrm{m}$ and $\gamma = 5, v_{\max} = -v_{\min} = 1\,\mathrm{m}$. Further, the figure shows the prediction with different start times. As seen, the prediction effect for responses excited by narrow banded sea states is better than that for responses excited by broad banded sea states.

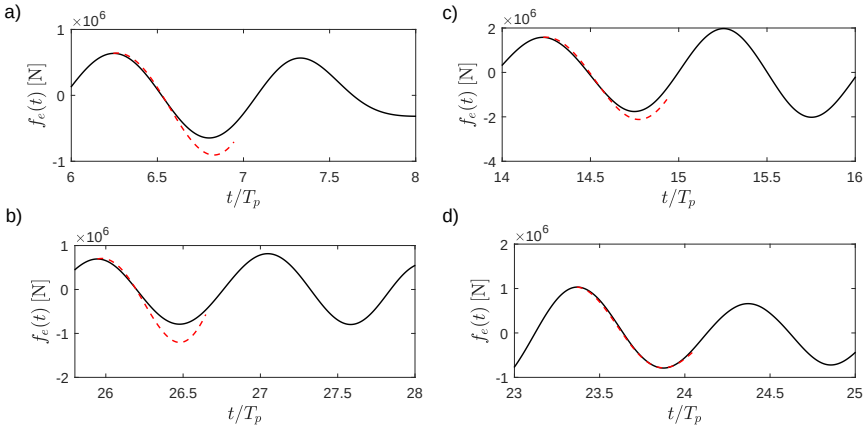

Fig. 2.8: Comparison between the predicted wave loads and the reference wave loads. a), b): $\gamma = 1$. c), d): $\gamma = 5$. ——: Nonlinear programming solution. - - - : Predicted wave load (Sun et al., 2019).

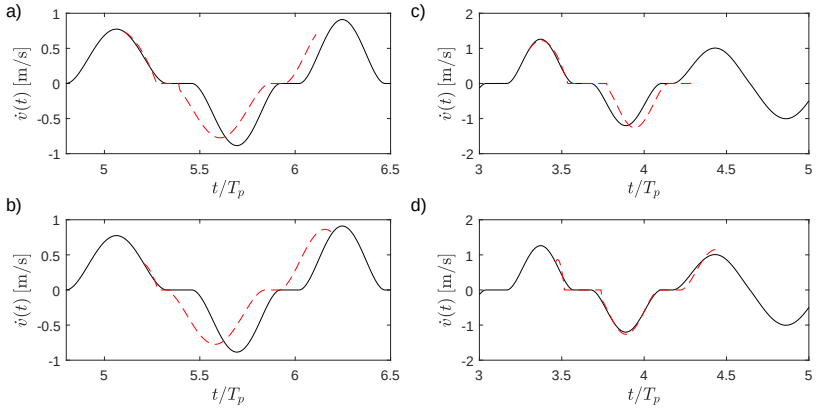

Fig. 2.9: Comparison between the predicted velocities and the reference velocities, H_s=3.00 m, T_p=7.42 s. a), b): γ=1, $v_{\max} = -v_{\min} = 0.8\,\text{m}$. c), d): γ=5, $v_{\max} = -v_{\min} = 1\,\text{m}$. ——: Nonlinear programming solution. - - - : Predicted velocity (Sun et al., 2019).

For the purpose of validating the performance of the devised controller given by Eqs. (2.15)-(2.18), it has been compared with the nonlinear programming based numerical solutions. Fig. 2.10a shows the motion response of the absorber with the displacement constraints $v_{\max} = -v_{\min} = 0.8\,\text{m}$ for $\gamma = 1$ at optimal control. Likewise, Figs. 2.10d shows the response with the constraints $v_{\max} = -v_{\min} = 1\,\text{m}$ for $\gamma = 5$ at optimal control.

Noted that it is necessary to identify the times $t_{a,i}$ and $t_{b,i}$ while devising

the control strategy. Actually, $t_{a,i}$ and $t_{b,i}$ can be obtained based on the measurement of the acceleration $\ddot{v}(t)$ because the discontinuous change of slope for $\ddot{v}(t)$ appears earlier than that for the displacement and velocity at the entrance and exit of constraint-activated intervals, see Figs. 2.10a and 2.10d.

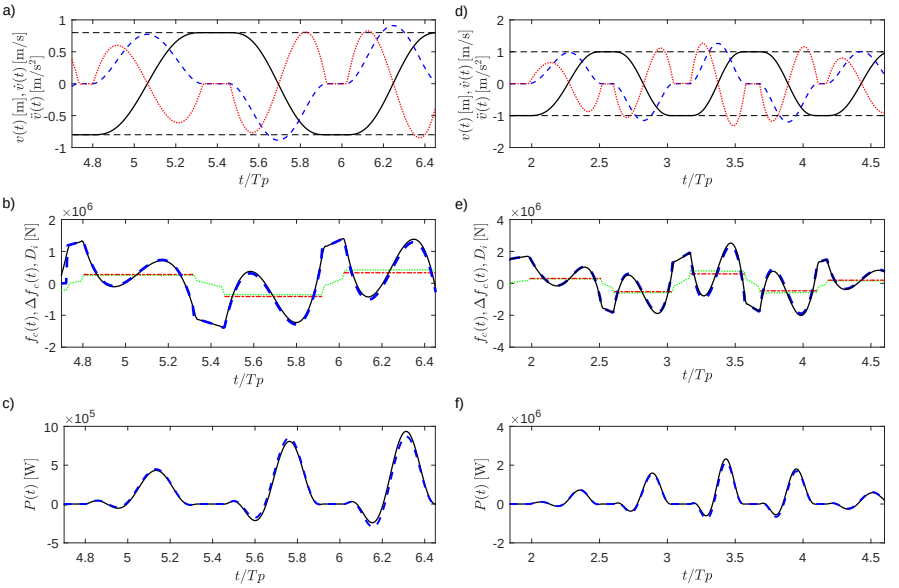

Fig. 2.10: The responses of $v(t)$, $\dot{v}(t)$, $\ddot{v}(t)$ at optimal control, and the control force $f_c(t)$ as well as the instantaneous absorbed power $P(t) = f_c(t)\dot{v}(t)$ from different control strategies, H_s=3.00 m, T_p=7.42 s. a), b), c): γ=1, $v_{\max} = -v_{\min} = 0.8$ m. d), e), f): γ=5, $v_{\max} = -v_{\min} = 1$ m. a),d): ——: $v(t)$. - - -: $\dot{v}(t)$. ·····: $\ddot{v}(t)$. b),e): ——: Nonlinear programming solution. - - -: $f_c(t)$. ·····: $\Delta f_c(t)$. -·-·-: D_i. c),f): ——: $P(t)$ obtained by nonlinear programming. - - -: $P(t)$ obtained by devised algorithm (Sun et al., 2019).

The solid black curves in Figs. 2.10b and 2.10e indicate the optimal control force $f_c(t)$ with different sea states involving γ=1 and γ=5 from nonlinear programming. The dotted blue curves in Figs. 2.10b and 2.10e represent the theoretical solution given in Eqs. (2.15)-(2.18) based on the optimal trajectories shown in Figs. 2.10a and 2.10d. The difference $\Delta f_c(t) = f_c(t) - f_{c,0}(t)$ between constraint-activated intervals, given by the constant D_i, is also shown in the figure. There is a small difference between these because the uncertainties are introduced when calculating the instants t_{a_i} and $t_{b,i}$ with the observation of $\ddot{v}(t)$.

Figs. 2.10c and 2.10f show the comparison of the instantaneous power $P(t)$ between the proposed control and the optimal control for different sea states concerning $\gamma = 1$ and $\gamma = 5$. It can be found that there is a negligible deviation and the time-average power takeoff $\bar{P}$ will deviate even less.

In a word, the devised controller is based on the determination of the sequence of constants C_i and D_i, the wave excitation force estimation and the prediction of future velocities during constraint-unactivated intervals.

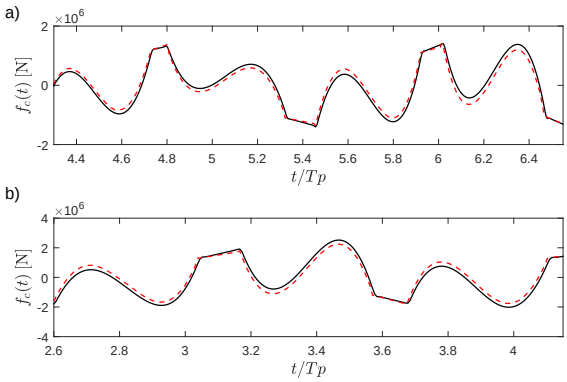

Fig. 2.11: Comparison between the predicted control force and the reference control force, H_s=3.00 m, T_p=7.42 s. a): γ=1 , $v_{\max} = -v_{\min} = 0.8\,\text{m}$. b): γ=5 , $v_{\max} = -v_{\min} = 1\,\text{m}$. ——: Nonlinear programming. - - - : Predicted control force (Sun et al., 2019).

On one hand, the control force during constraint-unactivated intervals is calculated based on the wave load estimation and the determination of the constants D_i. On the other hand, the control force during constraint-activated intervals is obtained based on the continuous measurement of the absorber motion. Fig. 2.11 gives the control forces at proposed control and optimal control for different sea state involving $\gamma = 1$ and $\gamma = 5$. The proposed control is in good agreement with the optimal one. This reveals the effectiveness of the proposed controller.

2.4 Optimal Control with the constrained displacement and control force

This subsection focuses on the optimal control of absorber with the displacement and control force constraints. A modified LQG control is introduced to optimize the absorbed power whilst minimizing these constraints in the objective functional. Hence, the objective functional to be maximized during the control interval $[t_0, t_1]$ in Eq. (2.7) is considered as (Sun and Nielsen, 2018):

$$J_1[f_c(t), \dot{v}(t), v(t)] = \frac{1}{2}\int_{t_0}^{t_1} \big(- qv^2(t) + 2v(t)f_c(t) - rf_c^2(t)\big)dt \tag{2.19}$$

The 2rd integrand indicates the instantaneous power takeoff which should be maximized during the control interval, keeping $|v(t)|$ and $|f_c(t)|$ as small as possible by choosing proper positive gain coefficients q and r. The algorithm does not guarantee that constraints on $v(t)$ and $f_c(t)$ are fulfilled strictly. In traditional LQG control, only the 1st and 3rd term are taken into consideration in the objective functional.

Herein the wave load $f_e(t)$ is modelled as an output of the following differential system excited by Gaussian white noise process $w_1(t)$ with a unit intensity due to its zero-mean stationary Gaussian characteristic, given as:

$$\left.\begin{aligned} \frac{d}{dt}\mathbf{z}_e(t) &= \mathbf{A}_e\mathbf{z}_e(t) + \mathbf{b}_e w_1(t) \\ f_e(t) &= \mathbf{p}_e\mathbf{z}_e(t) \end{aligned}\right\} \tag{2.20}$$

where the detailed definition of $\mathbf{z}_e(t)$, $\mathbf{A}_e$, $\mathbf{b}_e$ and $\mathbf{p}_e$ can be found in Paper C. Fig. 2.12 shows the comparison between the target auto-spectral density function and its rational approximation with the order of $(r, s) = (2, 4)$.

Further, Eq. (2.19) can be transformed into the following expanded matrix format:

$$J_1[f_c(t), \dot{v}(t), v(t)] = \frac{1}{2}\int_{-\infty}^{\infty} \big(- \mathbf{z}(t)^T\mathbf{Q}\mathbf{z}(t) + 2\mathbf{z}(t)^T\mathbf{p}f_c(t) - rf_c^2(t)\big)dt \tag{2.21}$$

where $\mathbf{z}(t)$, $\mathbf{Q}$ and $\mathbf{p}$ are given in detail in Paper C.

The variational approach with Hamiltonian formalism (Naidu, 2002; Pontryagin et al., 1962) has been applied to deal with the aforementioned control problem. The details of the derivation can be found in Paper C. Then, the optimal control law is obtained as (Sun and Nielsen, 2018):

$$f_c(t) = -\frac{1}{r}\big(\mathbf{b}_{f_c}^T\mathbf{S}(t) - \mathbf{p}^T\big)\mathbf{z}(t) \tag{2.22}$$

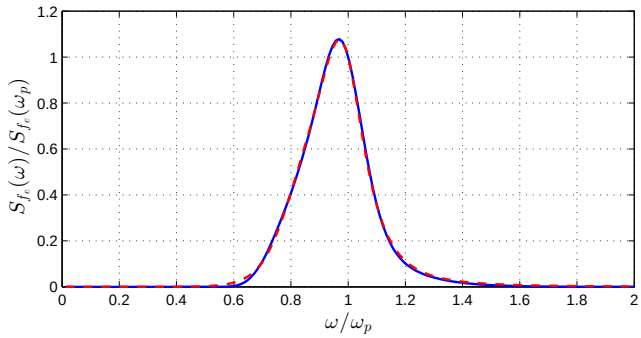

Fig. 2.12: Comparison of the rational approximation to the target function . ——: Numerical determined target auto-spectral density function. - - - : Rational approximation, $(r, s) = (2, 4)$ (Sun and Nielsen, 2018).

where $\mathbf{G}(t)$, $\mathbf{b}_{f_c}$ can be found in Paper C. The control law presumes that the state vector $\mathbf{z}(t)$ is fully measured. However, only the components displacement and velocity can be observed. Hence, Kalman-Bucy filter has been introduced to provide an estimate of the state vector so as to deal with this problem.

For the purpose of verifying the accuracy of the suggested theory, the comparison with the nonlinear programming based solution is performed. Two different sea states described by a JONSWAP auto spectral density function with $H_s = 3$m, $T_p = 7.42$s and $\gamma = 5$ corresponding to narrow banded wave and $H_s = 3$m, $T_p = 7.42$s and $\gamma = 1$ corresponding to broad banded wave are used. The values of the constraints on $v(t)$ and $f_c(t)$ are chosen to $v_{\max} = -v_{\min} = 0.5$m and $f_{c,\max} = -f_{c,\min} = 4 \times 10^5$N. The absorber in Fig. 2.1 has been used and the related paramters have been given in Table 2.1

Noted that the gain parameters q and r in Eq. (2.19) are chosen to make the standard deviations σ_v and σ_{f_c} of the displacement and the control force become identical for solutions from nonlinear programming and full state observation based LQG control. Hence, these parameters have to be optimized for each sea state to be investigated.

Figs. 2.13 and 2.14 show $v(t)$, $\dot{v}(t)$, $f_c(t)$ and the corresponding instantaneous power $P(t)$ under modified LQG control for full and partial state observation, as well as the comparable results from nonlinear programming. As seen, the displacement, the velocity and the control force follow the optimal solution but some deviations are available. Further, the displacement and control force from modified LQG control will violate these constraints at some instants, which is caused by the approximation of the algorithm.

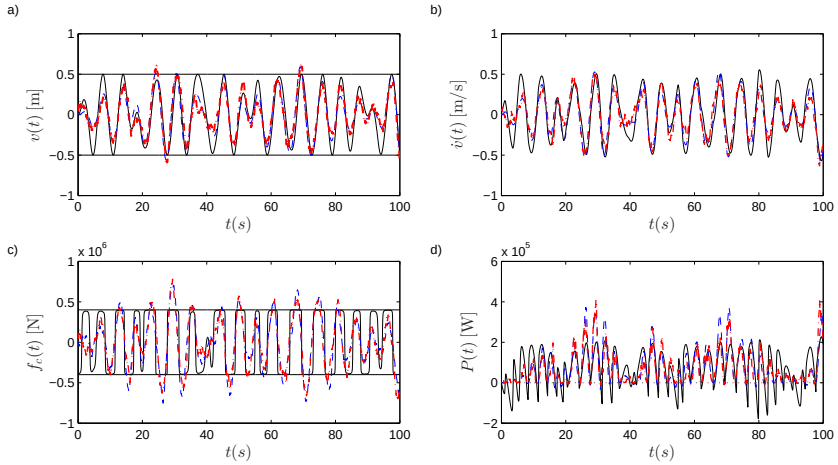

Fig. 2.13: Comparison of $v(t)$, $\dot{v}(t)$, $f_c(t)$ and instantaneous absorbed power $P(t)$ for different control strategies. $\gamma = 5$. $f_{c,\max} = -f_{c,\min} = 4 \times 10^5$N and $v_{\max} = -v_{\min} = 0.5$m. a) $v(t)$. b) $\dot{v}(t)$. c) $f_c(t)$. d) $P(t)$. ——: Nonlinear programming solution. - - - : LQG, full state observation. -·-·-: LQG, partial state observation (Sun and Nielsen, 2018).

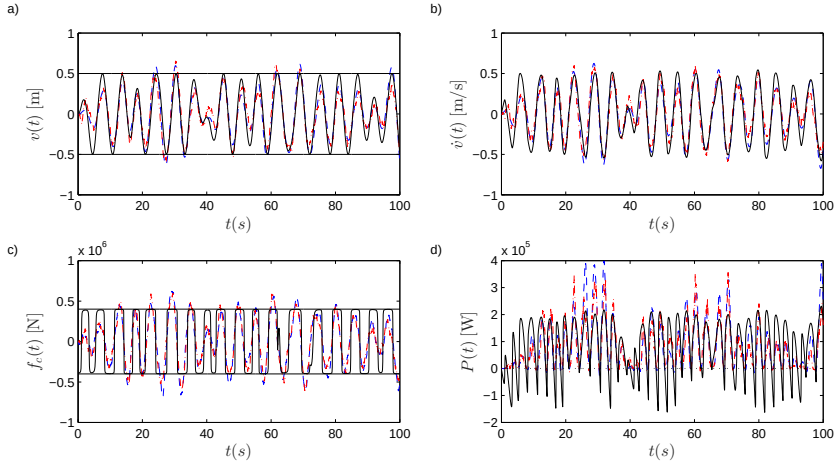

Fig. 2.14: Comparison of $v(t)$, $\dot{v}(t)$, $f_c(t)$ and instantaneous absorbed power $P(t)$ for different control strategies. $\gamma = 1$. $f_{c,\max} = -f_{c,\min} = 4 \times 10^5$N and $v_{\max} = -v_{\min} = 0.5$m. a) $v(t)$. b) $\dot{v}(t)$. c) $f_c(t)$. d) $P(t)$. ——: Nonlinear programming solution. - - - : LQG, full state observation. -·-·-: LQG, partial state observation (Sun and Nielsen, 2018).

Table 2.3 indicates the corresponding mean absorbed power from the modified LQG solution with full and partial observations in comparison to

Table 2.3: Mean absorbed power for different control strategies (Sun and Nielsen, 2018)

	$\gamma = 5$	$\gamma = 1$
Nonlinear programming	78.1005 kW	84.3520 kW
LQG, full state observation	77.0597 kW	83.3994 kW
LQG, partial state observation with (a_2, a_3)=(0.05ms$^{1/2}$, 0,05ms$^{-1/2}$)	73.4893 kW	80.4685 kW
LQG, partial state observation with (a_2, a_3)=(0.5ms$^{1/2}$, 0,5ms$^{-1/2}$)	61.3112 kW	76.2606 kW

the nonlinear programming based optimal solution. As seen, the solution based on full observation is little less than the optimal whilst more than that based on the partial observation. The effect of noise level with two pairs (a_2, a_3) on the absorbed power are also compared in Table 2.3 where a_2 and a_3 specify the noise level related to the measurement of the displacement and velocity. As seen, a_2 and a_3 will generally have a negative influence on the absorbed power. Further, the narrow and board banded waves follow the same analysis results.

Chapter 3

Control for a floating OWC absorber

The chapter considers the control of a floating OWC WEC referring to Paper D. First, the description of dynamic equation for a floating OWC WEC is given. The piston model is applied to model the motion of interval water column, reducing the system to an equivalent 2-DOF system. Further, a linear Wells turbine is applied.

The performance of a floating OWC absorber relies on the pressure variation relative to the atmospheric pressure, which is controlled by a valve. The state of the valve is assumed to be in a binary state of either fully open or fully closed. Further, the closing intervals for a valve are chosen as a constant proportion relative to the peak period associated with waves, and the optimal fraction is then calculated as a part of the control problem. The suggested control strategy can be characterized as a semi-active control, which requires to estimate the wave loads, evently predict the future sea state. Herein a Kalman-Bucy filter is applied to handle this prediction problem. The proposed control has been verified with the optimal control from nonlinear programming.

3.1 Description of dynamic motion for a floating OWC absorber

Fig. 3.1a demonstrates a static equilibrium state for a floating OWC absorber located at sea of the depth h. a and b represent the pressure chamber height and the water column height, separately. D_1 and D_2 specify the outer diameter of the buoyancy tank and the ballast tank respectively. m_1 indicates the combination of the structural mass and ballast.

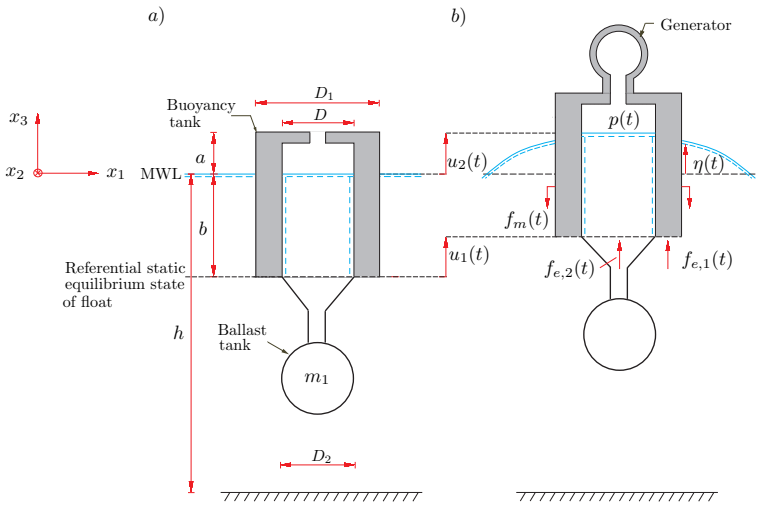

Fig. 3.1: Description of motion for a floating OWC absorber. a) Static equilibrium state. b) Dynamic state (Sun and Nielsen, 2019b).

Fig. 3.1b illustrates the dynamics state of a floating heave OWC device. The air inside the chamber can be compressed and decompressed by the motion of the internal water column excited by waves. In this process the air turbine can be driven by the air flow to produce electricity. $u_1(t)$ and $u_2(t)$ indicate the vertical displacements of the floater and the internal water column relative to the MWL. Herein the piston approximation is chosen to model the internal water column. Further, the discussion for choosing the piston length is indicated in Appendix A.

In the dynamic state, the piston model based vectorial Cummings equation is expressed as (Sun and Nielsen, 2019b):

$$\left.\begin{aligned} &\mathbf{M}\,\ddot{\mathbf{u}}(t) + \mathbf{f}_r(t) + \mathbf{r}\big(\mathbf{u}(t)\big) = \mathbf{f}_e(t) - \mathbf{f}_c(t)\ ,\ t \in]t_0, t_1] \\ &\mathbf{u}(t_0) = \mathbf{u}_0\ ,\ \dot{\mathbf{u}}(t_0) = \dot{\mathbf{u}}_0\ ,\ p(t_0) = 0 \end{aligned}\right\} \tag{3.1}$$

where

$$\left.\begin{aligned}
\mathbf{u}_0 &= \begin{bmatrix} u_{1,0}(t) \\ u_{2,0}(t) \end{bmatrix} \quad , \quad \dot{\mathbf{u}}_0 = \begin{bmatrix} \dot{u}_{1,0}(t) \\ \dot{u}_{2,0}(t) \end{bmatrix} \\
\mathbf{u}(t) &= \begin{bmatrix} u_1(t) \\ u_2(t) \end{bmatrix} \quad , \quad \mathbf{f}_c(t) = \mathbf{a}\, p(t) \quad , \quad \mathbf{a} = \begin{bmatrix} -1 \\ 1 \end{bmatrix} A \\
\mathbf{f}_r(t) &= \begin{bmatrix} f_{r,1}(t) \\ f_{r,2}(t) \end{bmatrix} = \begin{bmatrix} f_{r,11}(t) + f_{r,12}(t) \\ f_{r,21}(t) + f_{r,22}(t) \end{bmatrix} \\
\mathbf{f}_e(t) &= \begin{bmatrix} f_{e,1}(t) \\ f_{e,2}(t) \end{bmatrix} \quad , \quad \mathbf{r}\big(\mathbf{u}(t)\big) = \begin{bmatrix} (k_m + \rho_w\, g\, A_1)\, u_1(t) \\ \rho_w\, g\, A\, u_2(t) \end{bmatrix} \\
\mathbf{M} &= \begin{bmatrix} m_1 + m_{11}(\infty) & m_{12}(\infty) \\ m_{21}(\infty) & m_2 + m_{22}(\infty) \end{bmatrix}
\end{aligned}\right\} \tag{3.2}$$

where the mass matrix $\mathbf{M}$ includes m_1, the piston mass m_2 and the added mass $m_{\alpha\beta}(\infty)(\alpha, \beta = 1, 2)$ at infinite frequency.

$\mathbf{r}\big(\mathbf{u}(t)\big)$ indicates the combined dynamic restoring force which is supplied by the mooring system and buoyancy. Further, it's assumed that the vertical components of the mooring-based restoring force are linear, i.e. $f_m(t) = k_m u_1(t)$, where k_m is the global stiffness coefficient from the mooring system.

$\mathbf{f}_e(t)$ specifies the wave excitation force vector, which can be calculated from the following convolution integral involving the impulse response vector $\mathbf{h}_e(t)$ and the surface elevation $\eta(t)$:

$$\mathbf{f}_e(t) = \int_{-\infty}^{\infty} \mathbf{h}_e(t-\tau)\, \eta(\tau)\, d\tau \tag{3.3}$$

Further, $\mathbf{h}_e(t)$ is non-causal, which implies that the calculation of wave loads requires to predict the surface elevation $\eta(t)$.

$\mathbf{f}_c(t)$ depends on the pressure $p(t)$, which influences the motion of the system. Further, the components of $\mathbf{f}_c(t)$ is linear relevant, which means that there is only one actuator for the 2-DOF system. Therefore, a differential equation of $p(t)$ is required, which is defined later, to make the control of the 2-DOF system becomes reality.

$\mathbf{f}_r(t)$ indicates the radiation force vector including the component $f_{r,\alpha\beta}(t)$ $(\alpha, \beta = 1, 2)$ representing the contribution to $f_{r,\alpha}(t)$ when there is only $\dot{u}_\beta(t)$ in the system. $\mathbf{f}_r(t)$ also can be given as:

$$\mathbf{f}_r(t) = \int_{t_0}^{t} \mathbf{h}_r(t-\tau)\, \dot{\mathbf{u}}(\tau)\, d\tau \tag{3.4}$$

Further, the impulse response matrix $\mathbf{h}_r(t)$ is a causal, which implies that the rational approximation to $\mathbf{f}_r(t)$ is available.

Further, the hydrodynamic parameters including the added mass $m_{\alpha\beta}$, the corresponding frequency response functions $\mathbf{H}_r(\omega)$ and $\mathbf{H}_e(\omega)$ of $\mathbf{h}_r(t)$

and $\mathbf{h}_e(t)$, are computed based on the commercial program WAMIT (Wamit, 2011). $\mathbf{h}_r(t)$ and $\mathbf{h}_e(t)$ can easily be obtained by the Fourier transform of $\mathbf{H}_r(\omega)$ and $\mathbf{H}_e(\omega)$, respectively.

The impulse response function $h_{e,\alpha}(t)$ ($\alpha = 1, 2$) has been indicated in Fig. 3.2. As seen, $h_{e,\alpha}(t)$ approximates to zero when $|t| > T_p$, which reveals that the prediction of the surface elevations with one T_p ahead is reasonable for the estimate of $\mathbf{f}_e(t)$. The parameters $m_{\alpha\beta}(\omega)$, $\mathbf{h}_r(t)$ as well as $\mathbf{H}_r(\omega)$ are indicated in Paper D.

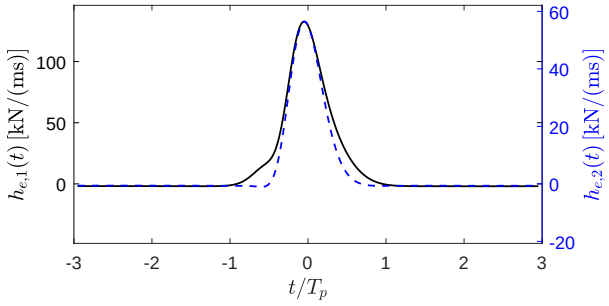

Fig. 3.2: Impulse response functions $h_{e,1}(t)$ and $h_{e,2}(t)$ for wave loads. ——: The float. - - - : The OWC (Sun and Nielsen, 2019b).

Further, the air in the pressure chamber is assumed to be an ideal gas of adiabatic and isentropic characteristics. Based on the constitutive equation (Sarmento and Falcao, 1985), the following differential equations of $p(t)$ can be formulated as:

$$\begin{cases} \dot{p}(t)V(t) + (\gamma p_0 + p(t))\left(\dot{V}(t) + k\,\beta(t)\,p(t)\right) = 0,\ p(t) \geq 0 \\ \dfrac{V(t)}{\gamma p_0}\dot{p}(t) + \left(1 + \dfrac{p(t)}{\gamma p_0}\right)\dot{V}(t) + k\,\beta(t)\,p(t) = 0,\ p(t) < 0 \end{cases} \tag{3.5}$$

where the physical description of the parameters $\rho(t)$, ρ_0, γ, $V(t)$, V_0 and $\dot{V}(t)$ are given in Paper D.

A linear Wells turbine is applied, given as (Brito-Melo et al., 2002):

$$Q(t) = k\,\beta(t)\,p(t) \tag{3.6}$$

This reveals the linear relationship between the mass flow $Q(t)$ and $p(t)$ with the turbine damping k as a proportion coefficient. $\beta(t)$ is the basic control parameter of the semi-active control. In the present case a binary control is assumed, where $\beta(t)$ instantaneously changes between 0 and 1. $\beta(t) = 0$ indicates the valve is fully closed and $\beta = 1$ means the valve is fully open. Hence, the turbine power can be given as (Sarmento et al., 1990):

$$P(t) \;=\; Q(t)\,p(t) \;=\; k\,\beta(t)\,p(t)^2 \tag{3.7}$$

When the valve is closed, the pressure is increasing. At the succeeding opening, this implies an increased volume flow to the generator takes places, and correspondingly an increased power takeoff is achieved. Hence, the aim of the control is to determine the instants of time for optimal opening of the valve, so the absorbed energy energy E during the control horizon $[t_0, t_1]$ is optimized subject to the state constraints given by the equation of motion (3.1), the constitutive equation for the pressure (3.5), and control constraints on the valve and given initial values on the displacement vector, the velocity vector and the pressure, corresponding to the control problem (Sun and Nielsen, 2019b):

$$\left.\begin{aligned}
&\max \quad E \;=\; \int_{t_0}^{t_1} P(\tau)\,d\tau \;=\; \int_{t_0}^{t_1} k\,\beta(\tau)\,p^2(\tau)\,d\tau \\
&\text{s.t.} \\
&\mathbf{M}\,\ddot{\mathbf{u}}(t) \;+\; \mathbf{f}_r(t) \;+\; \mathbf{r}\big(\mathbf{u}(t)\big) \;=\; \mathbf{f}_e(t) \;-\; \mathbf{f}_c(t)\;,\; t \in]t_0, t_1] \\
&\left.\begin{aligned}
\dot{p}(t) + \frac{\gamma p_0 + p(t)}{V(t)}\left(\dot{V}(t) + k\,\beta(t)\,p(t)\right) \;&=\; 0,\; p(t) \geq 0 \\
\dot{p}(t) + \big(\gamma p_0 + p(t)\big)\frac{\dot{V}(t)}{V(t)} + \frac{\gamma\, p_0\, k\,\beta(t)\,p(t)}{V(t)} \;&=\; 0,\; p(t) < 0
\end{aligned}\right\} \\
&\mathbf{u}(t_0) \;=\; \mathbf{u}_0\;,\; \dot{\mathbf{u}}(t_0) \;=\; \dot{\mathbf{u}}_0\;,\; p(t_0) = 0 \\
&\beta(t) = 0, 1
\end{aligned}\right\} \tag{3.8}$$

It should be noted that based on a rational approximation to each component $H_{r,\alpha\beta}(\omega)$ $(\alpha, \beta = 1, 2)$ of $\mathbf{H}_r(\omega)$, an approximate representative for $\mathbf{f}_r(t)$ is introduced to the numerical calculation of (3.8) and the optimal control solution from nonlinear programming. The detailed rational approximation to $\mathbf{f}_r(t)$ has been indicated in Paper D.

3.2 Semi-active control for a floating OWC device

The optimization problem in Eq. (3.8) has been solved by nonlinear programming whose solution is benchmarked in order to validate the subsequent proposed control. $\eta(t)$ is obtained based on the JONSWAP spectrum with significant wave height $H_s = 2.5$m, peak period $T_p = 6.77$s, bandwidth

parameter $\psi = 3.3$ and the related wave load vector $\mathbf{f}_e(t)$ is obtained according to Eq. (3.3). The same $\eta(t)$ and $\mathbf{f}_e(t)$ are used as input of the proposed suboptimal control.

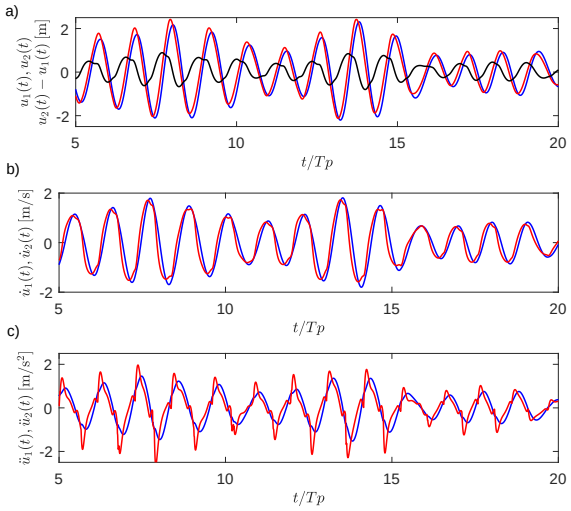

Fig. 3.3: Optimal motion response of the float and OWC. ——: $u_1(t), \dot{u}_1(t), \ddot{u}_1(t)$. ——: $u_2(t), \dot{u}_2(t), \ddot{u}_2(t)$. ——: $u_2(t) - u_1(t)$ (Sun et al., 2019).

Fig. 3.3 gives the optimal motion response of the float and OWC obtained from nonlinear programming. Fig. 3.3a also illustrates the relative displacement $u_2(t) - u_1(t)$.

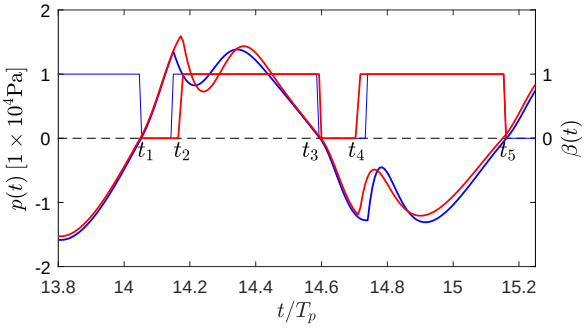

Fig. 3.4: $p(t)$ and $\beta(t)$ from different control strategies, $\alpha = 0.12$. ——: $p(t)$ at optimal control. ——: $p(t)$ at suboptimal control. ——: $\beta(t)$ at optimal control. ——: $\beta(t)$ at suboptimal control (Sun and Nielsen, 2019b).

Fig. 3.4 illustrates the optimal $p(t)$ and $\beta(t)$ obtained by nonlinear programming indicated with a blue signature. $[t_1, t_3]$ and $[t_3, t_5]$ indicate the

time intervals corresponding to $p(t) > 0$ and $p(t) < 0$, respectively. Further, the valve is kept closed in the time intervals $[t_1, t_2]$ and $[t_3, t_4]$, which reveal the pressure can rapidly increase and decrease, respectively. The valve is kept open in the time intervals $[t_2, t_3]$ and $[t_4, t_5]$ where the pressure will temporarily decrease and increase, leading to the local extremes of $p(t)$.

The time intervals for the valve-closed states at optimal control are somewhat different because of the random property of sea states. Herein a suboptimal control is introduced where a fixed time interval of the length $\alpha T_p = t_2 - t_1 = t_4 - t_3$ is applied during valve-closed state for the different valve-closed states. Then, the semi-active valve control is expressed as:

$$\beta(t) = H\big(p(t)\big)H\big(t - t_1 - \alpha T_p\big) + H\big(-p(t)\big)\,H\big(t - t_3 - \alpha T_p\big) \tag{3.9}$$

where $H(t)$ is the unit step function.

The optimal choice for α depends on the considered sea state, and can be determined by comparing the performance for the proposed control with that for the nonlinear programming based optimal control. In Fig. 3.4, $p(t)$ and $\beta(t)$ for the optimal control are compared to that for the suggested suboptimal control with $\alpha = 0.12$, where the same wave load vector $\mathbf{f}_e(t)$ was applied at the two control. As seen, the pressure predicted by the sub-optimal control and nonlinear programming are of equal magnitude. However, there is a phase difference in the signals close to the opening of the valve, because this takes place at slightly different instants of time.

In Eq. (3.8), the inputs to the system are merely $\beta(t)$ and $\mathbf{f}_e(t)$. Based on $\beta(t)$ given by (3.9), a closed system of differential equations can be obtained from which the displacement vector and the pressure variation are calculated, if $\mathbf{f}_e(t)$ can be estimated. According to Eq. (3.3), the estimate of $\mathbf{f}_e(t)$ requires the prediction of $\eta(t)$.

In order to predict $\eta(\tau), \tau > t$, a stochastic model of the surface elevation is at first devised, based on a linear filtration of Gaussian white noise $w_1(t)$ with a unit intensity through a rational filter with the frequency response function $H_{\eta w_1}(s) = \frac{p(s)}{Q_1(s)}$ to the JONSWAP wave spectrum $S_{\eta\eta}(\omega)$ for the surface elevation, see Fig. 3.5.

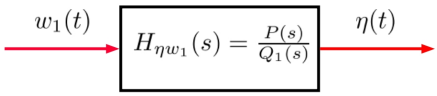

Fig. 3.5: Schematic diagram of the linear rational filter.

The comparison between the rational approximation with order $(r, s) = (3, 6)$ and the target spectrum $S_{\eta\eta}(\omega)$ has been indicated in Fig. 3.6.

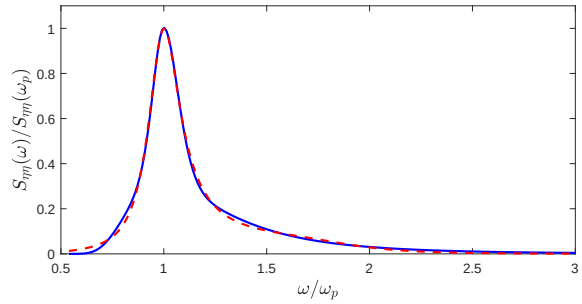

Fig. 3.6: Rational approximation to JONSWAP $S_{\eta\eta}(\omega)$ of order $(r,s) = (3,6)$. ——: Target spectrum $S_{\eta\eta}(\omega)$. - - - : Rational approximation (Sun and Nielsen, 2019b).

The filter equation in the time domain can be formulated as:

$$\begin{cases} \dfrac{d\mathbf{Y}(t)}{dt} = \mathbf{A}_c\mathbf{Y}(t) + \mathbf{b}_c\, w_1(t) \\ \eta(t) = \mathbf{p}_c\, \mathbf{Y}(t) \end{cases} \tag{3.10}$$

where the state vector $\mathbf{Y}(t)$, the system matrix $\mathbf{A}_c$, the load distribution vector $\mathbf{b}_c$ and output gain vector $\mathbf{p}_c$ can be found in Paper D.

It's assumed that $\eta(t)$ can be continuously observed. A certain noise is present in the observation for which reason the output equation in Eq. (3.10) is replaced with the following observation equation.

$$\eta(t) = \mathbf{p}_c\, \mathbf{Y}(t) + c\, w_2(t) \tag{3.11}$$

$c\, w_2(t)$ is the measurement noise where c is used to represent the noise level and $w_2(t)$ is Gaussian white noise with a unit intensity.

Herein a Kalman-Bucy filter is applied to predict $\eta(\tau), \tau > t$. Further, the prediction horizon is approximately one peak period T_p because the impulse response functions have finite support in the interval $[-T_p, T_p]$ as seen from the impulse response functions in Fig. 3.2. Finally, the wave load vector can be estimated by Eq. (3.3).

The physical parameters related to the absorber is given in Table 3.1. Further, the stiffness from the mooring system has been ignored in the present case, i.e. $k_m = 0\mathrm{N/m}$.

Fig. 3.7 shows the comparison between the estimate components and the reference components of $\mathbf{f}_e(t)$. The calculation of the estimate components of $\mathbf{f}_e(t)$ at each time instant requires to predicting the surface elevation one T_p ahead. As seen, there is a deviation between the estimate and the reference value due to the prediction error of η and measurement noise.

The optimal α for a considered sea state was calculated for optimizing the absorbed energy, according to the average of four independent realizations

Table 3.1: The physical parameter for the absorber

Parameter	Value	Unit	Parameter	Value	Unit
a	2.00	m	m_1	8.3695×10^5	kg
b	5.00	m	$m_{11}(\infty)$	3.4515×10^5	kg
h	100.00	m	$m_{12}=m_{21}$	2.5644×10^4	kg
D	5.00	m	$m_{22}(\infty)$	0.3736×10^5	kg
D_1	10.00	m	p_0	101325	Pa
D_2	10.00	m	k_m	0	N/m
ρ_0	1.225	kg/m^3	k	1×10^{-3}	m·s
ρ_w	1025	kg/m^3	c	0.1	m

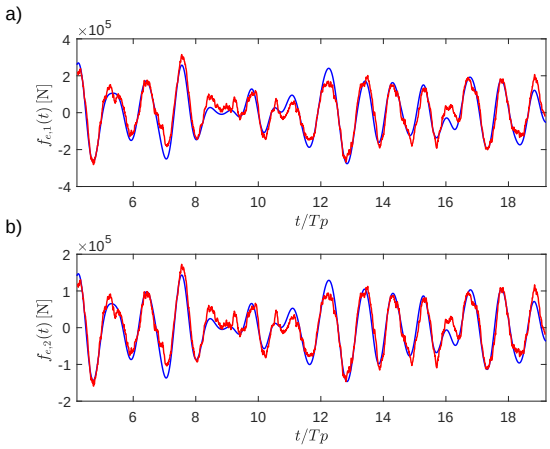

Fig. 3.7: Estimate of $\mathbf{f}_e(\tau)$ with measurement noise level $c = 0.1$m. a) Predicted wave load component $\bar{f}_{e,1}(\tau)$. b) Predicted wave load component $\bar{f}_{e,2}(\tau)$. ——: Reference $\mathbf{f}_e(t)$. ——: Estimated $\bar{\mathbf{f}}_e(\tau)$ (Sun and Nielsen, 2019b).

of $\eta(t)$ of the length $30T_p$. As seen in Fig. 3.9, the red curve indicates the absorbed energy variation with respect to α, using the exact wave loads. It can be found that α with the value around 0.12 reaches a maximum.

Fig. 3.8 gives the time series of $\beta(t)$ and $p(t)$ corresponding to the devised suboptimal controller where $\alpha = 0.12$ and the estimated wave excitation force are used. Compared with the solution at optimal control, the deviation of the pressure variation and the corresponding $\beta(t)$ at suboptimal control is not much.

Fig. 3.9 also shows the average absorbed energy with a black signature corresponding to the suboptimal controller with the combination of the estimated wave excitation forces and $\alpha = 0.12$, based on four considered realizations of $\eta(t)$. The performance of the controller with optimal control parameter α and the exact wave load is less below that of the optimal controller while

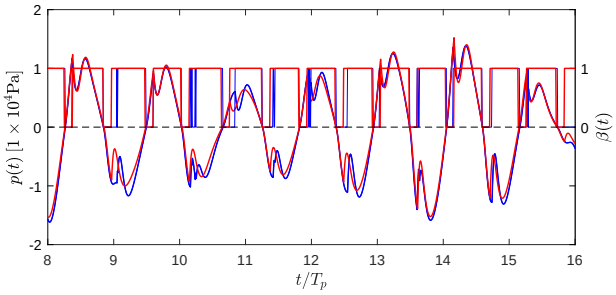

Fig. 3.8: $p(t)$ and $\beta(t)$ at suboptimal control with estimated wave loads, $\alpha = 0.12$ in comparison to that at optimal control. ——: $p(t)$ at optimal control. ——: $p(t)$ at sub-optimal control. ——: $\beta(t)$ at optimal control. ——: $\beta(t)$ at sub-optimal control (Sun and Nielsen, 2019b).

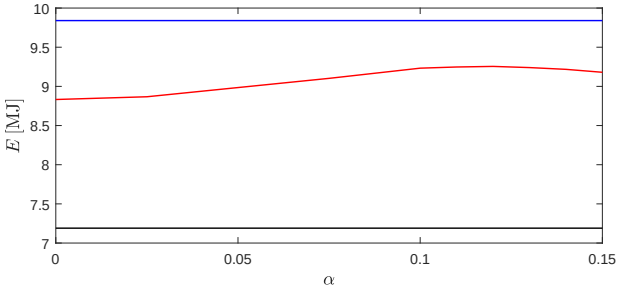

Fig. 3.9: Absorbed energy for different control strategies. ——: Nonlinear programming. ——: Suboptimal controller with respect to α using the exact wave loads. ——: Suboptimal controller with $\alpha = 0.12$ using the estimated wave loads (Sun and Nielsen, 2019b).

it is much better than the suboptimal controller with the estimated wave excitation forces and $\alpha = 0.12$, which reveals that the estimation error of the wave loads has a large negative influence on the absorbed energy.

Chapter 4

Conclusions and future perspectives

The focus of the present study is to indicate new vibration control strategies for point absorbers including two different devices of oscillating body and OWC so as to maximize the absorbed energy. The control laws for oscillating body point absorber under different physical constraints have been derived and analyzed in detail. A semi-active control for floating OWC device has also been devised and analyzed. This final section gives the general conclusions drawn from this study and possible future extensions of this work.

4.1 General conclusions

(1) Based on the variational approach with Hamiltonian formalism, an analytical solution considering the constrained control force for a heave point absorber is presented for the consideration of maximizing the absorbed power. The optimal control force is noncausal, which needs to predict future velocities. To handle this problem, a van der Pol transformation is applied based on the narrow banded character of the response processes. The mean absorbed power for the proposed control is comparable to the nonlinear programming based optimal control. Further, the proposed controller turns out to perform better than a causal controller.

(2) An semi-analytical solution for a heave point absorber concerning the constrained displacements is obtained so as to optimize the absorbed power. The control law depends on the wave excitation force during activated displacement constraints and follows the theoretical optimal control force for an unconstrained case during unconstrained states, where an initial value

needs to be calculated. The solution requires to estimate the wave excitation force during constraint-activated states and to predict future velocities during constraint-unactivated states. In order to solve these problems, the algorithms for the estimation and prediction have been suggested based on the narrow-banded property of the wave excitation force and velocities during unconstrained states, respectively. The solution for the devised control is in good agreement with the nonlinear programming based optimal solution for both relatively narrow-banded and broad-banded sea states.

(3) A LQG approach based control is suggested for the purpose of the optimal absorbed energy of WECs considering the displacement and control force constraints. A Gaussian white noise driven linear stochastic differential equation has been obtained based on the introduction of rational approximations to the wave load and radiation force. In order to deal with the limited observation, i.e. only displacement and velocity, Kalman filter is performed for the purpose of estimating the global state vector. With the proper gain parameters in the modified LQG control, the proposed control can both effectively optimize the absorbed power and keep the displacement and control force within reasonable range during most control horizon in comparison to the solution at optimal control.

(4) Based on a piston model and a Wells turbine, a semi-active control achieving the maximum of the absorbed power for a floating OWC device is proposed. The length of the time interval for the valve-closed states is considered as a constant, which is taken the value of a unchanged proportion with respect to the peak period associated with waves. This optimal constant was calculated through optimizing the absorbed energy to the nonlinear programming based optimal solution. The proposed control requires to estimate the wave loads. This can be achieved by predicting the future surface elevation through Kalman-Bucy filter. Compared with the performance at optimal control, the reduction of the performance for the proposed control primarily is caused by the estimation error of the wave loads.

4.2 Future perspectives

(1) Large motion of WEC devices occurs at extreme waves or at resonance. Therefore, nonlinear potential flow theory will be introduced to the control of WEC devices and the nonlinearities of hydrodynamics on the control effect will be explored. Further, model order reduction techniques will be applied to reduce the computational time when it comes to the calculation of the nonlinear hydrodynamics and the application of the model based control strategies.

(2) Survivability of WEC devices will be investigated, including the extreme response and reliability analysis.

(3) Many of control strategies for WEC devices rely on the availability of the estimation of the wave load and prediction of the surface elevation. An effect and accurate method to those will be explored.

(4) The combined wind turbine and wave energy converter system is designed so as to maximize the exploitation of the wave and wind resources. The dynamic response and the effective control strategies will be focused.

Appendix

Discussion of choosing the piston length for a floating OWC device

The piston model imposes the constraint on the vertical particles displacement which can be specified at any position of the water column because of the incompressibility of the water on the condition that the pressure chamber dimension is relatively small in comparison to the reference incident wavelength (Falnes, 1999; Robinson, 1982).

Fig. B.1 shows the schematic principle of the calculation mesh for 3 different piston lengths. The constraint has been imposed on 3 different pistons along the referential water column length b. The displaced water mass $m_2 = \rho_w A_2 c$ is added to the added mass $m_{22}(\infty)$ obtained by the numerical solution.

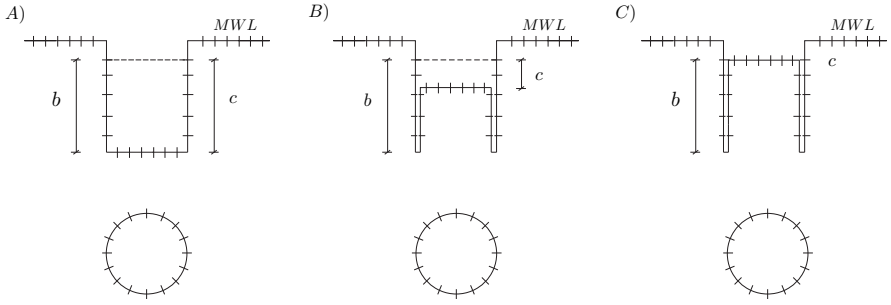

Fig. B.1: Schematic principle of calculation mesh for 3 different piston lengths c. A) $c = 5$m. B) $c = 1.25$m. C) $c = 0.02$m.

The result shows that the hydrodynamics for different piston lengths are identical except the parameters related to the added mass. As seen on Fig. B.2, the combined mass $m_2 + m_{22}(\infty)$ is very close for different piston lengths, even though the added mass m_{22} for different piston lengths is much differ-

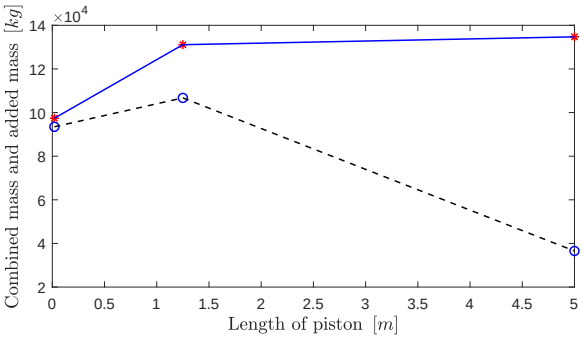

Fig. B.2: The combined mass $m_2 + m_{22}(\infty)$ and added mass $m_{22}(\infty)$ for different piston lengths. ——: $m_2 + m_{22}(\infty)$. - - - : $m_{22}(\infty)$.

ent. The impact of the added mass at infinite frequency on the piston motion can be significant. According to the obtained hydrodynamic parameters, the heave displacement of the piston in the time domain has a good agreement with the result in the frequency domain as long as the piston is long enough Sheng et al. (2014). The length of the piston therefore will be set up to $c = b$ in this paper.

References

Antonio, F.D.O. (2007). Modelling and control of oscillating-body wave energy converters with hydraulic power take-off and gas accumulator. *Ocean engineering*, 34(14-15), 2021-2032.

Astrom, K.J., Hagglund, T., Astrom, K.J. (2006). Advanced PID control (Vol. 461). *Research Triangle Park, NC: ISA-The Instrumentation, Systems, and Automation Society*.

Babarit, A., Duclos, G., Clement, A.H. (2004). Comparison of latching control strategies for a heaving wave energy device in random sea. *Applied Ocean Research*, 26(5), 227-238.

Babarit, A. et al. (2012). Numerical benchmarking study of a selection of wave energy converters. *Renewable Energy*, 41, 44–63.

Bacelli, G., Ringwood, J.V. (2014). Numerical optimal control of wave energy converters. *IEEE Transactions on Sustainable Energy*, 6(2), 294-302.

Basu, B., Staino, A. (2016). Control of a Linear Time-Varying System With a Forward Riccati Formulation in Wavelet Domain. *Journal of Dynamic Systems, Measurement, and Control, ASME*, 138 (10), 104502.

Beatty, S.J. et al. (2015). Experimental and numerical comparisons of self-reacting point absorber wave energy converters in regular waves. *Ocean Engineering*, 104, 370-386.

Beatty, S.J. et al. (2019). Experimental and numerical comparisons of self-reacting point absorber wave energy converters in irregular waves. *Ocean Engineering*, 173, 716-731.

Bhinder, M.A., Rahmati, M.T., Mingham, C.G., Aggidis, G.A. (2015). Numerical hydrodynamic modelling of a pitching wave energy converter. *European Journal of Computational Mechanics*, 24(4), 129-143.

Bingham, H.B., Ducasse, D., Nielsen, K., Read, R. (2015). Hydrodynamic analysis of oscillating water column wave energy devices. *Journal of Ocean Engineering and Marine Energy*, 1(4), 405-419.

Bosma, B., et al. (2012). Wave energy converter modeling in the frequency domain: A design guide. *In 2012 IEEE Energy Conversion Congress and Exposition (ECCE) (pp. 2099-2106)*. IEEE.

Brito-Melo, A., Gato, L.M.C., Sarmento, A.J.N.A. (2002). Analysis of Wells turbine design parameters by numerical simulation of the OWC performance. *Ocean Engineering*, 29(12), 1463-1477.

Cheng, Z., Yang, J., Hu, Z., Xiao, L. (2014). Frequency/time domain modeling of a direct drive point absorber wave energy converter. *Science China Physics, Mechanics and Astronomy*, 57(2), 311-320.

Clement, A.H., Babarit, A. (2012). Discrete control of resonant wave energy devices. *Philosophical Transactions of the Royal Society A: Mathematical, Physical and Engineering Sciences*, 370(1959), 288-314.

Cretel, J.A., Lightbody, G., Thomas, G.P., Lewis, A.W. (2011). Maximisation of energy capture by a wave-energy point absorber using model predictive control. *IFAC Proceedings Volumes*, 44(1), 3714-3721.

Cummins, W.E. (1962). The impulse response function and ship motions. *Schiffstechnik 9*, 101–109.

Elhanafi A., et al. (2017). Numerical hydrodynamic analysis of an offshore stationary floating oscillating water column wave energy converter using CFD. *International Journal of Naval Architecture and Ocean Engineering*, 9, 77–99

Evans, D.V. (1976). A theory for wave-power absorption by oscillating bodies. *Journal of Fluid Mechanics*, 77, 1–25.

Evans, D.V. (1978). The oscillating water column wave-energy device. *IMA Journal of Applied Mathematics*, 22(4), 423-433.

Evans, D.V. (1981). Power from water waves. *Annual review of Fluid mechanics*, 13(1), 157-187.

Evans D.V. (1981). Maximum wave-power absorption under motion constraints. *Applied Ocean Research*, 3(4), 200-203.

Evans, D.V. (1982). Wave-power absorption by systems of oscillating surface pressure distributions. *Journal of Fluid Mechanics*, 114, 481-499.

Eriksson, M., Isberg, J., Leijon, M. (2005). Hydrodynamic modelling of a direct drive wave energy converter. *International Journal of Engineering Science*, 43(17-18), 1377-1387.

Faedo, N., Olaya, S., Ringwood, J.V. (2017). Optimal control, MPC and MPC-like algorithms for wave energy systems: An overview. *IFAC Journal of Systems and Control*, 1, 37-56.

Falcao, A. (2010). Wave energy utilization: a review of the technologies. *Renewable and Sustainable Energy Reviews*, 14(3), 899-918.

Falcao, A.F., Henriques, J.C., Candido, J.J. (2012). Dynamics and optimization of the OWC spar buoy wave energy converter. *Renewable energy*, 48, 369-381.

Falcao, A.F., Henriques, J.C. (2016). Oscillating-water-column wave energy converters and air turbines: A review. *Renewable Energy*, 85, 1391-1424.

Falcao, A.F., Henriques, J.C., Gato, L.M., Gomes, R.P. (2014). Air turbine choice and optimization for floating oscillating-water-column wave energy converter. *Ocean engineering*, 75, 148-156.

Falnes, J. (1978). Wave-Power Conversion by Point Absorber. *Norwegian Maritime Research*, 6(4).

Falnes, J. (1980). Radiation impedance matrix and optimium power absorption for interacting oscillating in surface waves. *Applied Ocean Research*, 2(2), 75–80.

Falnes, J. (1999). Wave-energy conversion through relative motion between two single-mode oscillating bodies. *Journal of Offshore Mechanics and Arctic Engineering*, 121(1), 32-38.

Falnes, J. (2000). Maxiumum wave-energy absorption by oscillating systems consisting of bodies and water columns with restricted or unrestricted amplitudes. *In The Tenth International Offshore and Polar Engineering Conference. International Society of Offshore and Polar Engineers*.

Falnes, J.(2002). Ocean waves and oscillating systems: linear interactions including wave-energy extraction. Cambridge university press.

Falnes, J., Kurniawan, A. (2015). Fundamental formulae for wave-energy conversion vol. 2. *Royal Society Open Science*.

Faltinsen, O. (1990). Sea Loads on Ships and Offshore Structures. *Cambridge University Press*.

Fay, F.X., Henriques, J.C.C., Robles, E., Marcos, M. (2015). Review of control strategies for oscillating water column wave energy converters. *In Proceedings of the European Wave and Tidal Energy Conference*, Nantes, France (pp. 6-11).

Folley, M. (2016). Numerical modelling of wave energy converters: state-of-the-art techniques for single devices and arrays. *Academic Press*.

Freeman, K., Dai, M., Sutton, R. (2014). Control strategies for oscillating water column wave energy converters. *Underwater Technology*, 32(1), 3-13.

French, M.J. (1979). A generalized view of resonant energy transfer. *Journal of Mechanical Engineering Science*, 21(4), 299-300.

Gao, Y., et al. (2016). A fully floating system for a wave energy converter with direct-driven linear generator. *Energy*, 95, 99-109.

Gaspar, J.F., Calvario, M., Kamarlouei, M., Soares, C.G. (2018). Design trade-offs of an oil-hydraulic power take-off for wave energy converters. *Renewable energy*, 129, 245-259.

Genest, R., Ringwood, J.V. (2016). Receding horizon pseudospectral control for energy maximization with application to wave energy devices. *IEEE Transactions on Control Systems Technology*, 25(1), 29-38.

Goh, C.J., Teo, K.L. (1988). Control parametrization: a unified approach to optimal control problems with general constraints. *Automatica*, 24(1), 3-18.

Gomes, R.P.F., Henriques, J.C.C., Gato, L.M.C., Falcao, A.D.O. (2012). Hydrodynamic optimization of an axisymmetric floating oscillating water column for wave energy conversion. *Renewable Energy*, 44, 328-339.

Hansen, R.H., Andersen, T.O., Pedersen, H.C. (2011). Model based design of efficient power take-off systems for wave energy converters. *In 12th Scandinavian International Conference on Fluid Power*, SICFP 2011 (pp. 35-49). Tampere University Press.

Hartl, R.F., Sethi, S.P., Vickson, R.G. (1995). A survey of the maximum principles for optimal control problems with state constraints. *SIAM review*, 37(2), 181-218.

Hashem, I., Hameed, H.A., Mohamed, M.H. (2018). An axial turbine in an innovative oscillating water column (OWC) device for sea-wave energy conversion. *Ocean Engineering*, 164, 536-562.

Henderson, R. (2006). Design, simulation, and testing of a novel hydraulic power take-off system for the Pelamis wave energy converter. *Renewable energy*, 31(2), 271-283.

Henriques, J.C.C., Falcao, A.D.O., Gomes, R.P.F., Gato, L.M.C. (2013). Latching control of an oscillating water column spar-buoy wave energy converter in regular waves. *Journal of Offshore Mechanics and Arctic Engineering*, 135(2), 021902.

Henriques, J.C., Chong, J.C., Falcao, A.F., Gomes, R.P. (2014). Latching control of a floating oscillating water column wave energy converter in irregular waves. *In ASME 2014 33rd International Conference on Ocean, Offshore and Arctic Engineering*. American Society of Mechanical Engineers.

Henriques, J.C.C., et al. (2016). Latching control of a floating oscillating-water-column wave energy converter. *Renewable Energy*, 90, 229-241.

Jefferys, E.R. (1984). Simulation of wave power devices. *Applied Ocean Research*, 6(1), 31-39.

Kim, S.J., Koo, W., Shin, M.J. (2019). Numerical and experimental study on a hemispheric point-absorber-type wave energy converter with a hydraulic power take-off system. *Renewable Energy*, 135, 1260-1269.

Kofoed, J.P., Frigaard, P., Friis-Madsen, E., Sorensen, H.C. (2006). Prototype testing of the wave energy converter wave dragon. *Renewable energy*, 31(2), 181-189.

Kurniawan, A., Hals, J., Moan, T. (2013). Assessment of time-domain models of wave energy conversion systems. *Modelling and geometry optimisation of wave energy converters*.

Li, L., Yuan, Z., Gao, Y. (2018). Maximization of energy absorption for a wave energy converter using the deep machine learning. *Energy*, 165, 340-349.

Margheritini, L., Vicinanza, D., Frigaard, P. (2009). SSG wave energy converter: Design, reliability and hydraulic performance of an innovative overtopping device. *Renewable Energy*, 34(5), 1371-1380.

Na, J., Wang, B., Li, G., Zhan, S., He, W. (2018). Nonlinear Constrained Optimal Control of Wave Energy Converters with Adaptive Dynamic Programming. *IEEE Transactions on Industrial Electronics*.

Naidu, D.S. (2002). Optimal control systems. *CRC press*.

Negahdari, M., Dalayeli, H., Moghadas, M.H. (2018). Design of a two-body wave energy converter by incorporating the effect of hydraulic power take-off parameters. *Journal of Marine Science and Technology*, 26(4), 496-507.

Newman, J. (1977) Marine Hydrodynamics. *The MIT Press*.

Nielsen, S.R.K. et al. (2013). Optimal control of nonlinear wave energy point converters. *Ocean engineering*, 72, 176-187.

Nielsen, S.R.K. et al. (2014). Optimal control of an array of non-linear wave energy point converters. *Ocean Engineering*, 88, 242-254.

Nielsen, S.R.K., Zhang, Z. (2017). Stochastic Dynamics. *Aarhus Unversity Press*.

Ozkop, E., Altas, I.H. (2017). Control, power and electrical components in wave energy conversion systems: A review of the technologies. *Renewable and Sustainable Energy Reviews*, 67, 106-115.

Pastor, J., Liu, Y. (2014). Frequency and time domain modeling and power output for a heaving point absorber wave energy converter. *International Journal of Energy and Environmental Engineering*, 5(2-3), 101.

Penalba, M., Merigaud, A., Gilloteaux, J.C., Ringwood, J.V. (2017). Influence of nonlinear Froude–Krylov forces on the performance of two wave energy points absorbers. *Journal of Ocean Engineering and Marine Energy*, 3(3), 209-220.

Perez, T., Fossen, T.I. (2008). Time-vs. frequency-domain identification of parametric radiation force models for marine structures at zero speed. *Modeling, Identification and Control: A Norwegian Research Bulletin*, 29(1), 1-19.

Pizer, D. (1992). Numerical Prediction Of The Performance of a Solo Duck Technical Report. *Edinburgh University*.

Pizer, D. (1993). Maximum wave-power absorption of point-absorbers under motion constraints. *Applied Ocean Research*, 15(4), 227–234.

Pontryagin, L.S., Boltyanskii, V.G., Gamkrelitze, R.V ., Mishenko, E.F. (1962). The Mathematical Theory of Optimal Processes. *Interscience Publishers, John Wiley and Sons*, New York.

Ransley E., et al. (2017). Survivability of wave energy converters using CFD. *Renewable Energy*, 109, 235–47.

Ricci, P., Saulnier, J.B., Antonio, F.D.O., Pontes, M.T. (2008). Time-domain models and wave energy converters performance assessment. *In ASME 2008 27th International Conference on Offshore Mechanics and Arctic Engineering*. American Society of Mechanical Engineers.

Richter, M. (2011). Different model predictive control approaches for controlling point absorber wave energy converters. *University Stuttgart*, Stuttgart.

Richter, M., Magana, M.E., Sawodny, O., Brekken, T.K. (2012). Nonlinear model predictive control of a point absorber wave energy converter. *IEEE Transactions on Sustainable Energy*, 4(1), 118-126.

Roberts, J.B., Spanos, P.D. (2003). Random vibration and statistical linearization. *Courier Corporation*.

Robinson, R.W. (1982). The effects of geometric-wavefield interactions on the performance of oscillating water column wave energy converters. Queen's University of Belfast.

Ruellan, M., BenAhmed,H., Multon,B., Josset,C., Babarit,A., Clement,A. (2010). Design methodology for a SEAREV wave energy converter. *IEEE Transactions on Energy Conversion*, 25(3), 760-767.

Sarmento, A.J., Falcao, A.D.O. (1985). Wave generation by an oscillating surface-pressure and its application in wave-energy extraction. *Journal of Fluid Mechanics*, 150, 467-485.

Sarmento, A.J.N.A., Gato, L.M.C., Falcao, A.D.O. (1990). Turbine-controlled wave energy absorption by oscillating water column devices. *Ocean engineering*, 17(5), 481-497.

Saupe, F., Gilloteaux, J.C., Bozonnet, P., Creff, Y., Tona, P. (2014). Latching control strategies for a heaving buoy wave energy generator in a random sea. *IFAC Proceedings Volumes*, 47(3), 7710-7716.

Scuotto, M., Falcao, A.D.O. (2005). Wells and impulse turbines in an OWC wave power plant: a comparison. *In Proceedings of 6th European Wave Tidal Energy Conference*, 463-9.

Setoguchi, T., et al. (2001). A review of impulse turbines for wave energy conversion. *Renewable energy*, 23(2), 261-292.

Sheng, W., Alcorn, R., Lewis, A. (2014). Hydrodynamics of oscillating water column wave energy converters. *Renew 2014*.

Sheng, W., Alcorn, R., Lewis, A. (2015). On improving wave energy conversion, part II: Development of latching control technologies. *Renewable energy*, 75, 935-944.

Sheng, W. (2019). Wave energy conversion and hydrodynamics modelling technologies: A review. *Renewable and Sustainable Energy Reviews*, 109, 482-498.

Sheng, W. (2019). Motion and performance of BBDB OWC wave energy converters: I, hydrodynamics. *Renewable Energy*, 138, 106-120.

Sichani, M.T., Chen, J.B., Kramer, M.M., Nielsen, S.R.K. (2014). Constrained optimal stochastic control of non-linear wave energy point absorbers. *Applied Ocean Research*, 47, 255-269.

Soltani, M.N., Sichani, M.T., Mirzaei, M. (2014). Model predictive control of buoy type wave energy converter. *IFAC Proceedings Volumes*, 47(3), 11159-11164.

Sun, T., Nielsen, S.R.K. (2018). Stochastic optimal control of a heave point wave energy converter based on a modified LQG approach. *Ocean Engineering*, 154, 357-366.

Sun, T., Nielsen, S.R.K. (2019a). Stochastic control of wave energy converters for optimal power absorption with constrained control force. *Applied Ocean Research*, 87, 130-141.

Sun, T., Nielsen, S.R.K, Basu, B. (2019). Stochastic control of wave energy converters with constrained displacements for optimal power absorption. *Applied Ocean Research*, 89, 1-11.

Sun, T., Nielsen, S.R.K. (2019b). Semi-active feedforward control of a floating OWC point absorber for optimal power take-off. IEEE Transactions on Sustainable Energy.

Taghipour, R., Perez, T., Moan, T. (2008). Hybrid frequency-time domain models for dynamic response analysis of marine structures. *Ocean Engineering*, 35(7), 685–705.

Temiz, I., Leijon, J., Ekergard, B., Bostrom, C. (2018). Economic aspects of latching control for a wave energy converter with a direct drive linear generator power take-off. *Renewable energy*, 128, 57-67.

Wamit, I. (2011). Wamit user manual.

Wang, L., Isberg, J., Tedeschi, E. (2018). Review of control strategies for wave energy conversion systems and their validation: the wave-to-wire approach. *Renewable and Sustainable Energy Reviews*, 81, 366-379.

Wei, Y. et al. (2019). Frequency-domain hydrodynamic modelling of dense and sparse arrays of wave energy converters. *Renewable Energy*, 135, 775-788.

Wu, J., Yao, Y., Zhou, L., Goteman, M. (2017). Latching and Declutching Control of the Solo Duck Wave-Energy Converter with Different Load Types. *Energies*, 10(12), 2070.

Wu, J., Yao, Y., Zhou, L., Goteman, M. (2018). Real-time latching control strategies for the solo Duck wave energy converter in irregular waves. *Applied energy*, 222, 717-728.

Ye, Y., Chen, W. (2017). Frequency-and time-domain analysis of a multi-degree-of-freedom point absorber wave energy converter. *Advances in Mechanical Engineering*, 9(12), 1687814017722081.

Zhan, S., Li, G., Na, J., He, W. (2019). Feedback noncausal model predictive control of wave energy converters. *Control Engineering Practice*, 85, 110-120.

Zurkinden, A.S. et al(2014). Non-linear numerical modeling and experimental testing of a point absorber wave energy converter. *Ocean Engineering*, 78, 11-21.

Part I

Papers

Paper A

Stochastic Control of Wave Energy Converters for Optimal Power Absorption with Constrained Control Force

Tao Sun, Søren R.K. Nielsen

The paper has been published in the
Applied Ocean Research Vol. 87, pp. 130–X141, 2019.

A.1 Author's Right

Journal author rights

In order for Elsevier to publish and disseminate research articles, we need publishing rights. This is determined by a publishing agreement between the author and Elsevier. This agreement deals with the transfer or license of the copyright to Elsevier and authors retain significant rights to use and share their own published articles. Elsevier supports the need for authors to share, disseminate and maximize the impact of their research and these rights, in Elsevier proprietary journals* are defined below:

For subscription articles	For open access articles
Authors transfer copyright to the publisher as part of a journal publishing agreement, but have the right to: • Share their article for Personal Use, Internal Institutional Use and Scholarly Sharing purposes, with a DOI link to the version of record on ScienceDirect (and with the Creative Commons CC-BY-NC- ND license for author manuscript versions) • Retain patent, trademark and other intellectual property rights (including research data). • Proper attribution and credit for the published work.	Authors sign an exclusive license agreement, where authors have copyright but license exclusive rights in their article to the publisher**. In this case authors have the right to: • Share their article in the same ways permitted to third parties under the relevant user license (together with Personal Use rights) so long as it contains a CrossMark logo, the end user license, and a DOI link to the version of record on ScienceDirect. • Retain patent, trademark and other intellectual property rights (including research data). • Proper attribution and credit for the published work.

https://www.elsevier.com/about/policies/copyright

Applied Ocean Research 87 (2019) 130–141

Contents lists available at ScienceDirect

Applied Ocean Research

journal homepage: www.elsevier.com/locate/apor

Stochastic control of wave energy converters for optimal power absorption with constrained control force

Tao Sun*, Søren R.K. Nielsen

Department of Civil Engineering, Aalborg University, 9000 Aalborg, Denmark

ARTICLE INFO

MSC:
00-01
99-00

Keywords:
Wave energy
Heave point absorber
Optimal power take-off
Actuator force constraints

ABSTRACT

This paper presents an analytical solution derived for optimal control of the power take-off of a single-degree of freedom heave point absorber with constraints on the control force. The optimal control law turns out to be noncausal with a functional dependence on future velocities. To handle this problem, an algorithm for predicting future velocities is derived. Based on the solution the mean (time-averaged) absorbed power in a given sea-state is calculated. The performance of the indicated controller in terms of the mean absorbed power is close to the optimal value obtained by nonlinear programming and better than a controller with feedback from the present displacement, velocity and acceleration, and with optimized gain factors.

1. Introduction

The heave wave energy point absorber is assumed to be constrained by a mooring system or otherwise to enforce a motion only in the vertical direction, and hence the absorber can be modelled as a single-degree-of-freedom oscillator driven by the external wave load.

Significant increase of the power take-off (PTO) of a heave absorber may be achieved by using an active vibration control of the vertical motion [1]. In order to obtain a maximal absorbed power, many studies have proposed control strategies for wave energy converters. Latching control is the most investigated control strategy, independently proposed by Falnes [2] and French [3]. If the velocity and wave load have different signs, so that the wave force supplies a negative power to the device, the absorber is fixed at zero velocity ('latched') by an external mechanism. Hence, the control effort is based on the observation of the wave load and the velocity of the absorber, and hence may be classified as a mixed feedback and feedforward control strategy. For an induction (asynchronous) generator, where the power takeoff force is proportional to the velocity of the absorber, a positive power takeoff is always achieved during the unlatched state. Hoskin and Nichols [4] proved the basic assumption of the latching control strategy to be optimal during the unlatched periods for an induction generator. Subsequently, latching control has been extended to multi-degree-of-freedom wave energy converters [5,6]. Babarit et al. [7] have suggested a somewhat similar semi-active control strategy, known as declutching, where the generator is cut off when the wave force and the absorber velocity are out of phase. Both control strategies require the external wave load to be estimated. Assuming a linear wave theory, this is given as a non-causal convolution of the surface elevation, i.e. there is a need to predict future surface elevations a certain control horizon ahead of the time when the control is applied. This is easy for regular waves or narrow-banded sea states, but the accuracy of the prediction may be affected in broad-banded irregular sea states.

To circumvent the uncertainties related with open-loop control robust closed loop control law in term of classical PID control have been suggested by Astrom and Hagglund [8]. Typically, the control laws will introduce negative control stiffness in order to make the system more flexible [9]. Nielsen et al. [10] derived the optimal control law in the time domain for a heave point absorber with non-linear buoyancy or restoring forces from the mooring system in case of no constraints on the displacements and the control force. The control law is a feedback type depending on the present displacement and acceleration of the absorber and an integral feedback from future velocities. Hence, for practical applications, the indicated control law requires a prediction of future velocities. Because there is no dependence on the wave load, the indicated control law applies to both 2D and 3D irregular sea-states.

Displacement constraints may also be imposed to prevent the absorber from hitting the sea-bottom or jumping out of the water, which may lead to damaging impact loadings. Similarly, constraints may be present on the control force due to saturation in the actuator system or in order to reduce structural fatigue damage accumulation in hot spots in the absorber shell structure. Hansen and Kramer [11] considered constraints on the control force of a WaveStar point converter based on a PD reactive control law and concluded that the constraint

* Corresponding author.
E-mail addresses: tsu@civil.aau.dk (T. Sun), srkn@civil.aau.dk (S.R.K. Nielsen).

https://doi.org/10.1016/j.apor.2019.03.002
Received 6 May 2018; Received in revised form 28 February 2019; Accepted 4 March 2019

significantly influences the mean absorbed power and changes the values of the optimal gain factors of the PD controller. Based on the Pontryagin maximum principle, Hendrikx et al. [12] considered the open-loop optimal control strategy for a WaveStar point absorber with constraints on the control torque. The difference of absorbed power between optimal control and model predictive control strategy was small but the control torque trajectory differed.

A variety of model predictive control (MPC) formulations with the constraints on the state vector and the control force have been reported in the literatures [13,14]. Soltani et al. [15] derived an MPC algorithm to maximize the absorbed power of a Wavestar wave energy converter. The main prerequisite is that the absorber velocity shall be in phase with the wave load. Hence, the controller needs prediction of the future sea state and observation of the absorber velocity.

A recent variation of the general model predictive control (MPC) framework has been suggested by Bacelli and Ringwood [16]. Based on spectral and pseudospectral optimal control methods, the WEC responses and control force are expanded on a functional basis, resulting in a computationally efficient formulation. The spectral method is based on truncated Fourier series, leading to a convex optimization problem and an effective solution for the optimal control. Afterward, Genest and Ringwood [17] developed a receding horizon real-time pseudospectral control algorithm for a wave energy converter with constraints on displacement and control force. The functional basis consists of half-range Chebyshev Fourier functions, which can represent the harmonic signals in the application domain well. Further, the receding horizon is introduced to the control algorithm in order to effectively deal with the signal truncation effects. Compared with alternative MPC formulations, pseudospectral control algorithm shows considerable promise in achieving a good balance between performance and computation.

The present paper presents an analytical solution for the optimal control of a heave point absorber with constraints on the control force. The control law has feedback from present displacement and acceleration and future velocities, which need to be predicted. The obtained control law has been benchmarked against the optimal control obtained from a nonlinear programming algorithm indicated in the appendix to the paper.

The paper is organised as follows. Section 2.1 presents the basic equations of the problem, and the inherent approximations in the nonlinear programming algorithm is justified by comparison to the theoretical unconstrained solution obtained by Nielsen et al. [10]. Section 2.2 derives the optimal control law for a point absorber with constraints on the control force, and the obtained solution is benchmarked against numerical obtained nonlinear programming solution. The obtained control law has feedback from further velocities. For wave energy converters, even if the external wave load is broad-banded, the response is relatively narrow-banded. Therefore, a van der Pol transformation [18] with slowly varying amplitude and phase has been used for the prediction of future velocities in Section 2.3. Section 2.4 derives the analytical mean absorbed power with the constraints on the control force in a given sea-state described by the significant wave height, the peak period and a band-width parameter. Section 3 investigates the performance of the proposed control method, which is compared with the nonlinear programming solution and a causal controller with feedback from the present displacement, velocity and acceleration.

2. Methodology

2.1. Equation of motion of point absorber

Fig. 1 shows the heave absorber to be analyzed. An (x, y, z)-coordinate system is introduced with the origin O placed in the mean water level (MWL) at the centerline of the point absorber. The horizontal x-axis is orientated in the direction of the wave propagation, and the vertical z-axis is orientated in the upward direction. Only two-

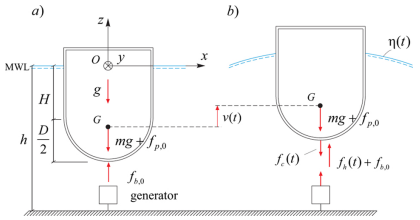

Fig. 1. Loads on heave absorber. (a) Static equilibrium state. (b) Dynamic state.

dimensional (plane) irregular waves are considered. The motion $v(t)$ of the body in the z-direction is measured from the static equilibrium state, where the static buoyancy force $f_{b,0}$ balances the gravity force mg and a possible static pre-stressing force from the mooring system $f_{p,0}$. g is the acceleration of gravity, and m indicates the structural mass including ballast. The center of gravity is denoted G.

In the dynamic state caused by the surface elevation $\eta(t)$, the WEC is excited by an additional dynamic hydrodynamic force $f_h(t)$ and an additional force, $f_c(t)$, from an external hydraulic or electric force generator as the PTO system, which is used to control the motion of the absorber. $f_c(t)$ is considered positive in the opposite direction of $v(t)$, and will be referred to as the control force. In realistic application, the efficiency of the actuator will be smaller than 100% due to energy losses and actuators efficiency influencing the control performance when the large amount of reactive power is involved [19]. In theoretical research, it is assumed that the actuator has ideal efficiency and an ideal PTO system is applied. Further, a PTO system can provide the reactive power. In applications, the cylinder in the PTO system can operate as a pump, producing a bi-directional flow, which drives a hydraulic motor. The motor adapts to the flow and rectifies the flow into a unidirectional turning of the generator. Further, the PTO system absorbs a positive power from the absorber if the control force and the velocity are in counter phase i.e. the actuator is working as a damper. In the other way, the PTO system acts as a motor and supplies energy to the absorber. Assuming linear wave theory, $f_h(t)$ may be written as a superposition of the following contributions:

$$f_h(t) = f_b(t) + f_r(t) + f_e(t) \tag{1}$$

where $f_b(t)$ is the quasi-static restoring force from the static equilibrium state of the buoyancy and the mooring system, $f_r(t)$ is the radiation force generated by the motion of the absorber in still water, and $f_e(t)$ is the wave excitation force caused by the wave action, when the absorber is fixed in the static equilibrium state. The term $f_r(t)$ removes mechanical energy from the absorber by generating an outwards directed radial wave train, whereas $f_e(t)$ supplies energy to the absorber.

$f_b(t)$ may be written as an analytical nonlinear function of the displacement:

$$f_b(t) = -r(v(t)) \tag{2}$$

Assuming small vertical vibrations, Eq. (2) may be linearized around the static equilibrium state as [20]:

$$f_b(t) = -k\,v(t) \quad , k = r'(0) \tag{3}$$

In the numerical results below the linearized relation in Eq. (3) has been assumed with the value of k given in Table 1 below.

The radiation force $f_r(t)$ may be written in terms of the following differential-integro relation [21,22]:

$$f_r(t) = -m_h\ddot{v}(t) - f_{r,0}(t) \tag{4}$$

$$f_{r,0}(t) = \int_{t_0}^{t} h_{rv}(t-\tau)\dot{v}(\tau)\,d\tau \tag{5}$$

Table 1
Heave absorber and wave excitation parameters.

Parameter	Value	Unit	Parameter	Value	Unit
H	7.00	m	H_s	3.00	m
D	14.00	m	T_p	7.42	s
h	30.00	m	γ	5	
m	1.84×10^6	kg	$\sigma_{\dot\psi}$	2.9991	m/s
m_h	0.44×10^6	kg	$\sigma_{f_{e,0}}$	1.8645×10^6	N
k	1.51×10^6	N/m	$P_{\text{opt},0}$	7.2347×10^5	W
β_1	0.82		β_2	0.80	
c	1.0×10^5	kg/s			

where m_h indicates the added water mass at infinite high frequencies, and $h_{r\dot\psi}(t)$ is a causal impulse response function for the radiation force brought forward by the absorber velocity $\dot\psi(\tau)$. t_0 is the initial time of the control.

Due to the causality of the impulse response function, the related frequency response function becomes:

$$H_{r\dot\psi}(\omega) = \int_0^\infty \mathrm{e}^{-\mathrm{i}\omega t} h_{r\dot\psi}(t)\,\mathrm{d}t \tag{6}$$

Combination of Eqs. (2), (4) and (5) provides the following integro-differential equation for $v(t)$ driven by $f_e(t)$ and $f_c(t)$ [21]:

$$\left.\begin{aligned} M\ddot v(t) + r(v(t)) + \int_{t_0}^t h_{r\dot\psi}(t-\tau)\dot v(\tau)\,d\tau = f_e(t) - f_c(t), \quad t\in[t_0,\,t_1] \\ v(t_0) = v_0, \quad \dot v(t_0) = \dot v_0 \end{aligned}\right\} \tag{7}$$

where $M = m + m_h$, and v_0 and $\dot v_0$ are given initial conditions at the time t_0. t_1 is the terminal time of the control.

In Eq. (7), the term $r(v(t))$ represents a combined nonlinear restoring forces from the mooring system and from the buoyancy force due to noncylindrical outer shell of the absorber. In contrast, nonlinearities from the wave loading is ignored. The hydrodynamic nonlinearities originates from the dynamic Froude-Krylov force, the radiation force, the diffraction force and the viscous force. It turns out that the nonlinear radiation-diffraction force for heave point absorber is not significantly different from the one predicted by linear theory, and the viscous effects for heave point absorber seem to be negligible [23]. Hence, the hydrodynamic nonlinearities for heave point absorbers are mainly from the dynamic Froude-Krylov force [24]. It has been demonstrated that the numerical model with linear hydrodynamic coefficients is reasonably accurate for the point absorber oscillating in waves with a steepness factor $\frac{H_s}{\lambda_p} < 0.02$ [25], where H_s is the significant wave height, and λ_p the wavelength. In the numerical example below with $H_s = 3\,\mathrm{m}$ and the peak period $T_p = 7.42\,\mathrm{s}$, this criterion is exceeded. Hence, the theory should be used merely as an approximation for such sea state.

Fig. 2 shows the impulse response function $h_{r\dot\psi}(t)$ based on the data indicated in Table 1 in the numerical example below. The time has been normalized with respect to T_p. As seen, $h_{r\dot\psi}(t)$ effectively vanishes for $t > T_p$.

The wave excitation force $f_e(t)$ may be expressed in terms of the following convolution integral of the sea-surface elevation $\eta(t)$ [26]:

$$f_e(t) = \int_{-\infty}^\infty h_{e\eta}(t-\tau)\eta(\tau)d\tau \tag{8}$$

The sea-surface elevation $\eta(t)$ is assumed to be observed at a sufficient distant position from the absorber, where the measurement is not disturbed by the radiation wave, and $h_{e\eta}(t)$ is a non-causal impulse response function. The related frequency response function and the spectral density function become:

$$H_{e\eta}(\omega) = \int_{-\infty}^\infty \mathrm{e}^{-\mathrm{i}\omega t} h_{e\eta}(t)\mathrm{d}t \tag{9}$$

$$S_{f_e f_e}(\omega) = |H_{e\eta}(\omega)|^2 S_{\eta\eta}(\omega) \tag{10}$$

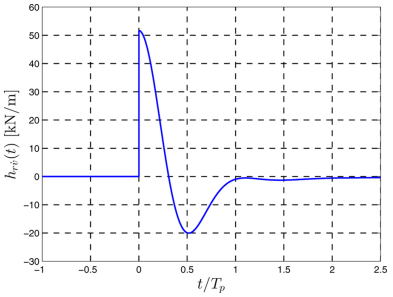

Fig. 2. Impulse response function for the radiation force, $h_{r\dot\psi}(t)$.

The hydrodynamic parameters, i.e. k, m_h, $h_{r\dot\psi}(t)$, $H_{r\dot\psi}(\omega)$, $h_{e\eta}(t)$, $H_{e\eta}(\omega)$ can be calculated numerically. In the present case, the WAMIT program has been used, which is based on the boundary element method [27].

Fig. 3 shows the frequency response function $H_{r\dot\psi}(\omega)$. As follows from Eq. (6), $\mathrm{Re}(H_{r\dot\psi}(\omega)) = \int_0^\infty \cos(\omega t)h_{r\dot\psi}(t)\,\mathrm{d}t$ and $\mathrm{Im}(H_{r\dot\psi}(\omega)) = \int_0^\infty \sin(\omega t)h_{r\dot\psi}(t)\,\mathrm{d}t$. Since $h_{r\dot\psi}(t)$ is real, it follows that $\mathrm{Re}(H_{r\dot\psi}(\omega))$ is an even, and $\mathrm{Im}(H_{r\dot\psi}(\omega))$ an odd function of ω. For this reason, Fig. 3 only shows function values for $\omega > 0$.

In order to verify the theory by comparison to a numerical solution based on nonlinear programming, the convolution integral $f_{r,0}(t) = \int_{t_0}^t h_{r\dot\psi}(t-\tau)\dot\psi(\tau)\,d\tau$ needs to be replaced by a state vector approximation in terms of a system of linear, ordinary filter differential equations driven by the velocity $\dot\psi(t)$. The state vector formulation is based on an initial replacement of the actual frequency response function with an approximating rational function, leading to the following relations in the time domain:

$$\left.\begin{aligned} f_{r,0}(t) &= \mathbf{p}_r\,\mathbf{z}_r(t) \\ \tfrac{d}{\mathrm{d}t}\mathbf{z}_r(t) &= \mathbf{A}_r\,\mathbf{z}_r(t) + \mathbf{b}_r\,\dot\psi(t),\ t\in\,]t_0,\,t_1] \\ \mathbf{z}_r(t_0) &= \mathbf{0} \end{aligned}\right\} \tag{11}$$

The state vector $\mathbf{z}_r(t)$, the column vector $\mathbf{b}_r$, the system matrix $\mathbf{A}_r$ and the row vector $\mathbf{p}_r$ can be found in detail in Nielsen et al. [10]. Further, the initial value $\mathbf{z}_r(t_0) = \mathbf{0}$ follows because $f_{r,0}(t_0) = 0$.

According to the solution to the state vector differential equation in Eq. (11), $f_{r,0}(t)$ can be expressed as:

$$f_{r,0}(t) = \int_{t_0}^t h_{r\dot\psi}(t-\tau)\,\dot\psi(\tau)\,d\tau = \int_{t_0}^t \mathbf{p}_r\,\mathrm{e}^{\mathbf{A}_r(t-\tau)}\mathbf{b}_r\,\dot\psi(\tau)\,d\tau \tag{12}$$

Hence, the impulse response function $h_{r\dot\psi}(t)$ is approximated as:

$$h_{r\dot\psi}(t) = \mathbf{p}_r\,\mathrm{e}^{\mathbf{A}_r t}\mathbf{b}_r \tag{13}$$

Fig. 3 shows the obtained rational approximation of the order $(m, n) = (2, 3)$ to $H_{r\dot\psi}(\omega)$ compared with the target frequency response function.

Based on the double-sided auto-spectral density function $S_{f_e f_e}(\omega)$, a sufficient long time series of the wave load $f_e(t)$ may be generated. The time series in Fig. 4 was generated based on the JONSWAP spectrum defined in Eq. (54) below defined by H_s, T_p and the band-width parameter γ, using a rational linear filtration of a so-called broken line equivalent white noise process [28]. The wave load realization shown in Fig. 4 is used in subsequent numerical investigations.

The nonlinear algorithm indicated in the appendix will be used to validate the derived solution for the optimal constrained control force $f_c(t)$, which maximizes the absorbed power $P(t) = f_c(t)\dot\psi(t)$ in the interval $[t_0, t_1]$. The nonlinear algorithm depends on the accuracy of the state vector representation in Eq. (11) and on a discretization of the

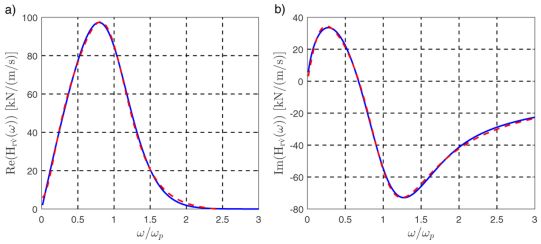

Fig. 3. Frequency response function for the radiation force. (a) $\mathrm{Re}(H_{rv}(\omega))$. (b) $\mathrm{Im}(H_{rv}(\omega))$ ——: Numerical determined target. – – –: Rational approximation with order $(m, n) = (2, 3)$.

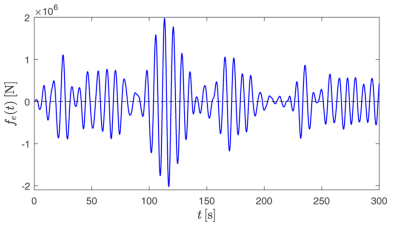

Fig. 4. Realization of the wave load process $f_c(t)$. $H_s = 3$ m, $T_p = 7.42$ s, $\gamma = 5$.

performance functional of the optimization problem. The rational approximation of the order $(m, n) = (2, 3)$ shown in Fig. 3 and a time step $\Delta t = \frac{1}{150}T_p$ will be applied. The validity of the nonlinear programming algorithm with the indicated rational approximation for the radiation force has been tested against the analytical solution for the unconstrained control force given as, [10]:

$$f_{c,0}(t) = -M\ddot{v}(t) - r(v(t)) + \int_t^{t_1} h_{rv}(\tau - t)\dot{v}(\tau)\,d\tau \tag{14}$$

where the trajectories of $v(t)$, $\dot{v}(t)$, $\ddot{v}(t)$ are taken from the nonlinear programming solution.

Fig. 5 indicates the corresponding results. As seen, a perfect agreement is obtained both for the control force $f_{c,0}(t)$ and the instantaneous absorbed power $P_{\mathrm{opt},0}(t) = f_{c,0}(t)\dot{v}(t)$. For this reason, the nonlinear programming algorithm is considered appropriate also in the constrained optimization problem.

2.2. Optimal constrained control force

The displacement response $v(t)$ becomes large at optimal control because the control force $f_{c,0}(t)$ given by Eq. (14) tends to eliminate the nonlinear restoring force $r(v(t))$ and the inertial term $M\ddot{v}(t)$ in Eq. (7), making the system extremely flexible. However, only constraint on the control force caused by saturation of the actuator is considered in the following, given as:

$$f_{c,\min} \le f_c(t) \le f_{c,\max} \tag{15}$$

Maximizing the absorbed power during the control interval$]t_0, t_1]$ with constraints on the control force leads to the following control problem:

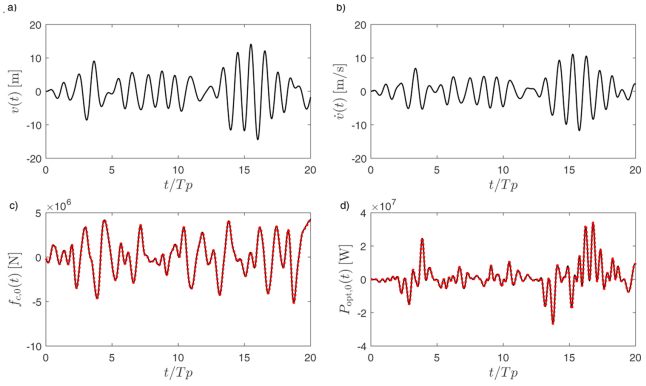

Fig. 5. Unconstrained case, optimal trajectories and power take-off. (a) $v(t)$. (b) $\dot{v}(t)$. (c) $f_{c,0}(t)$. (d) $P_{\mathrm{opt},0}(t)$. —: Nonlinear programming solution. ·····: Unconstrained analytical solution.

$$\left.\begin{aligned}&\max J\left[\dot{v}, f_c\right]=\int_{t_0}^{t_1} f_c(\tau)\dot{v}(\tau)\,d\tau\\&\text{subject to the path and control force constraints:}\\&\begin{cases}\boldsymbol{z}(t)=\boldsymbol{g}(\boldsymbol{z}(t), f_c(t), t), & t\in\,]t_0, t_1]\\ \boldsymbol{z}(t_0)=\boldsymbol{z}_0\end{cases}\\&f_c(t)\in I_{f_c}, \quad t\in\,]t_0, t_1]\end{aligned}\right\} \tag{16}$$

where $I_{f_c}=[f_{c,\min}, f_{c,\max}]$ signifies the interval of admissible control forces. The state vector $\boldsymbol{z}(t)$ and the right-hand side of the state vector equation $\boldsymbol{g}(\boldsymbol{z}(t), f_c(t), t)$ are defined as:

$$\boldsymbol{z}(t)=\begin{bmatrix}v(t)\\ \dot{v}(t)\\ \boldsymbol{z}_r(t)\end{bmatrix} \tag{17}$$

$$\boldsymbol{g}(\boldsymbol{z}(t), f_c(t), t)=\begin{bmatrix}\dot{v}(t)\\ \frac{1}{M}(-\boldsymbol{p}_r\boldsymbol{z}_r(t)-r(v(t))+f_e(t)-f_c(t))\\ \boldsymbol{A}_r\boldsymbol{z}_r(t)+\boldsymbol{b}_r\dot{v}(t)\end{bmatrix} \tag{18}$$

The equivalent unconstrained optimization problem is given as:

$$\begin{aligned}\max J\left[\boldsymbol{z}, \boldsymbol{\lambda}, f_c\right] &= \int_{t_0}^{t_1}\left(f_c(\tau)\dot{v}(\tau)+\lambda^T(\tau)(\boldsymbol{g}(\boldsymbol{z}(\tau), f_c(\tau), \tau)-\dot{\boldsymbol{z}}(\tau))\right)d\tau\\ &= \int_{t_0}^{t_1}\left(H(\boldsymbol{z}(\tau), \boldsymbol{\lambda}(\tau), f_c(\tau), \tau)-\lambda^T(\tau)\dot{\boldsymbol{z}}(\tau)\right)d\tau\end{aligned} \tag{19}$$

where the Hamiltonian $H(\boldsymbol{z}(t), \boldsymbol{\lambda}(t), f_c(t), t)$ of the control problem is given as:

$$\begin{aligned}H(\boldsymbol{z}(t), \boldsymbol{\lambda}(t), f_c(t), t) &= f_c(t)\dot{v}(t)+\lambda^T(t)\boldsymbol{g}(\boldsymbol{z}(t), f_c(t), t)\\ &= -\tfrac{\lambda_{\dot{v}}(t)}{M}r(v(t))+(f_c(t)+\lambda_v(t)\\ &\quad+\boldsymbol{\lambda}_r^T(t)\boldsymbol{b}_r)\dot{v}(t)\\ &\quad+\left(-\tfrac{\lambda_{\dot{v}}(t)}{M}\boldsymbol{p}_r+\boldsymbol{\lambda}_r^T(t)\boldsymbol{A}_r\right)\boldsymbol{z}_r(t)\\ &\quad+\tfrac{\lambda_{\dot{v}}(t)}{M}(f_e(t)-f_c(t))\end{aligned} \tag{20}$$

and $\boldsymbol{\lambda}(t)$ is the co-state vector (Lagrange multiplier) defined as:

$$\boldsymbol{\lambda}(t)=\begin{bmatrix}\lambda_v(t)\\ \lambda_{\dot{v}}(t)\\ \boldsymbol{\lambda}_r(t)\end{bmatrix} \tag{21}$$

Since there are no constraints on $\boldsymbol{z}(t)$ and $\boldsymbol{\lambda}(t)$, the first variation of Eq. (19) provides the following conditions for optimal control, valid for both constrained and unconstrained control forces:

$$\dot{\boldsymbol{z}}(t)=\frac{\partial H}{\partial\boldsymbol{\lambda}}=\boldsymbol{g}(\boldsymbol{z}(t), f_c(t), t) \tag{22}$$

$$\dot{\boldsymbol{\lambda}}(t)=-\frac{\partial H}{\partial\boldsymbol{z}} \tag{23}$$

Eqs. (22) and (23) are known as the Hamiltonian equations (or canonical equations).

Conventionally, the trajectories of the state vector and the co-state vector at optimal control are denoted as $\boldsymbol{z}^*(t)$ and $\boldsymbol{\lambda}^*(t)$. Generally, the asterisks will be omitted in the following for ease of notation.

The terminal boundary condition (or transversality condition) on the co-state vector reads:

$$\boldsymbol{\lambda}(t_1)=\boldsymbol{0}\quad(\lambda_v(t_1)=0, \lambda_{\dot{v}}(t_1)=0, \boldsymbol{\lambda}_r(t_1)=\boldsymbol{0}) \tag{24}$$

From Eqs. (20), (21) and (23) follows:

$$\begin{bmatrix}\dot{\lambda}_v(t)\\ \dot{\lambda}_{\dot{v}}(t)\\ \dot{\boldsymbol{\lambda}}_r(t)\end{bmatrix}=\begin{bmatrix}\frac{\partial r(v(t))}{\partial v}\frac{\lambda_{\dot{v}}(t)}{M}\\ -f_c(t)-\lambda_v(t)-\boldsymbol{b}_r^T\boldsymbol{\lambda}_r(t)\\ \boldsymbol{p}_r^T\frac{\lambda_{\dot{v}}(t)}{M}-\boldsymbol{A}_r^T\boldsymbol{\lambda}_r(t)\end{bmatrix} \tag{25}$$

The 1st and 3rd equations in Eq. (25) in combination with the terminal conditions in Eq. (24) provide the following solutions for $\lambda_v(t)$ and $\boldsymbol{\lambda}_r(t)$:

$$\lambda_v(t)=-\int_t^{t_1}\frac{\partial r(v(\tau))}{\partial v}\frac{\lambda_{\dot{v}}(\tau)}{M}\,d\tau \tag{26}$$

$$\boldsymbol{\lambda}_r(t)=-\int_t^{t_1}\mathrm{e}^{\boldsymbol{A}_r^T(\tau-t)}\boldsymbol{p}_r^T\frac{\lambda_{\dot{v}}(\tau)}{M}\,d\tau \tag{27}$$

Insertion of Eqs. (26) and (27) into the second equation (25) results in the following expression for the optimal control force:

$$\begin{aligned}f_c(t) &= -\dot{\lambda}_{\dot{v}}(t)+\boldsymbol{b}^T\int_t^{t_1}\mathrm{e}^{\boldsymbol{A}_r^T(\tau-t)}\boldsymbol{p}_r^T\frac{\lambda_{\dot{v}}(\tau)}{M}\,d\tau-\int_t^{t_1}\frac{\partial r(v(\tau))}{\partial v}\frac{\lambda_{\dot{v}}(\tau)}{M}\,d\tau\\ &= -\dot{\lambda}_{\dot{v}}(t)+\int_t^{t_1}h_{r\dot{v}}(\tau-t)\frac{\lambda_{\dot{v}}(\tau)}{M}\,d\tau-\int_t^{t_1}\frac{\partial r(v(\tau))}{\partial v}\frac{\lambda_{\dot{v}}(\tau)}{M}\,d\tau\end{aligned} \tag{28}$$

In the last statement it has been used that $\boldsymbol{b}_r^T\mathrm{e}^{\boldsymbol{A}_r^Tt}\boldsymbol{p}_r^T=\boldsymbol{p}_r\mathrm{e}^{\boldsymbol{A}_rt}\boldsymbol{b}_r=h_{r\dot{v}}(t)$, cf. Eq. (13). Eq. (28) holds for both constrained and unconstrained control forces.

The optimal control for constrained control force follows from the Pontryagin maximum principle, [29]:

$$H(\boldsymbol{z}^*(t), \boldsymbol{\lambda}^*(t), f_c^*(t), t)=\max_{f_c(t)\in I_{f_c}}H(\boldsymbol{z}^*(t), \boldsymbol{\lambda}^*(t), f_c(t), t) \tag{29}$$

Based on first order variations, Eqs. (22), (23) and (29) are merely necessary conditions for optimality.

Since the Hamiltonian given by Eq. (20) is linear in the control force $f_c(t)$ with the proportionality factor $\dot{v}(t)-\frac{\lambda_{\dot{v}}(t)}{M}$, Eq. (29) provides the following solution for the optimal control force:

$$f_c(t)=\begin{cases}f_{c,\max}, & \lambda_{\dot{v}}(t)<M\dot{v}(t)\\ f_{c,0}(t), & \lambda_{\dot{v}}(t)=M\dot{v}(t)\\ f_{c,\min}, & \lambda_{\dot{v}}(t)>M\dot{v}(t)\end{cases} \tag{30}$$

The undetermined quantity $f_{c,0}(t)$ is related to the condition:

$$\lambda_{\dot{v}}(t)=M\dot{v}(t) \tag{31}$$

Under the condition in Eq. (31) follows:

$$\frac{\partial r(v(t))}{\partial v}\frac{\lambda_{\dot{v}}(t)}{M}=\frac{\partial r(v(t))}{\partial v}\dot{v}(t)=\frac{\mathrm{d}r(v(t))}{\mathrm{d}t} \tag{32}$$

Then, $f_{c,0}(t)$ is obtained by insertion of Eqs. (31) and (32) in Eq. (28):

$$f_{c,0}(t)=-M\ddot{v}(t)+\int_t^{t_1}h_{r\dot{v}}(\tau-t)\dot{v}(\tau)d\tau-r(v(t))+r(v(t_1)) \tag{33}$$

The term $r(v(t_1))$ indicates a static control force components, which may be used to counteract a static restoring force component corresponding to the static drift $v(t_1)$ of the absorber. Since, the displacement of the absorber is referred to the static equilibrium state, no static offset is present, and so the said term may be set to zero. Hence, Eq. (33) reduces to Eq. (14), which was originally obtained based on the unconstrained first order variation of the performance functional in Eq. (19). This leads to the control law equation $\frac{\partial H}{\partial f_c}=0$, resulting again in Eq. (31).

$f_{c,0}(t)$ may attain arbitrary large positive and negative values. Then, the condition $\lambda_{\dot{v}}(t)<M\dot{v}(t)$ specifies values, where $f_{c,0}(t)>f_{c,\max}$, and the condition $\lambda_{\dot{v}}(t)>M\dot{v}(t)$ correspondingly values fulfilling $f_{c,0}(t)<f_{c,\min}$. Hence, $f_{c,0}(t)$ may be used as a saturation parameter. Then, the final form of the constrained optimal control law may be written as:

$$f_c(t)=\begin{cases}f_{c,\max}, & f_{c,0}(t)>f_{c,\max}\\ f_{c,0}(t)\\ f_{c,\min}, & f_{c,0}(t)<f_{c,\min}\end{cases} \tag{34}$$

Eq. (34) specifies a non-causal control law at the time t with feedback from the present displacement $v(t)$ and acceleration $\ddot{v}(t)$, and feedback

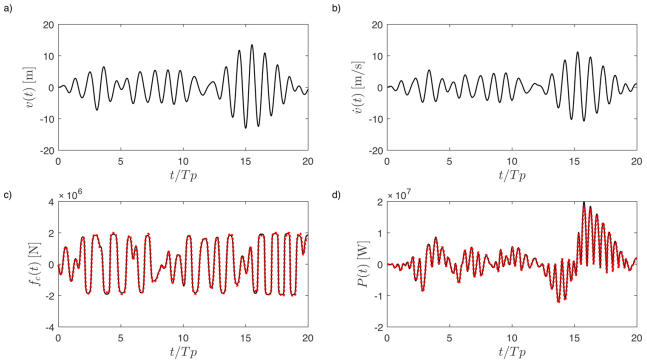

Fig. 6. Constrained control force ($f_{c,\max} = -f_{c,\min} = 2 \times 10^6$ N) and unconstrained displacement. (a) $v(t)$. (b) $\dot{v}(t)$. (c) $f_c(t)$. (d) $P(t)$. —: Nonlinear programming solution. .....: Eq. (34).

from future velocities $\dot{v}(\tau)$, $\tau \in]t, t_1]$. Hence, a prediction algorithm of future velocities $\dot{v}(\tau)$, $\tau \in]t, t_1]$ is needed at practical applications, which will be dealt with in a later section. Due to the inherent uncertainty related to the prediction procedure, the resulting controller will merely be sub-optimal.

In order to verify Eq. (34), the optimal trajectories of $v(t)$, $\dot{v}(t)$ and $\ddot{v}(t)$ obtained from nonlinear programming are inserted in Eq. (34), and the resulting control force and resulting instantaneous absorbed power are compared to the corresponding solutions obtained directly by nonlinear programming. Fig. 6 shows the results for a control force constraint $f_{c,\max} = -f_{c,\min} = 2 \times 10^6$ N and unconstrained displacement. As seen, by comparison of Fig. 6a and b with Fig. 5a and b, the optimal displacement and velocity trajectories are only slightly affected by the control force constraint. Fig. 6c and d show the results for the optimal control force given by Eq. (34) and instantaneous absorbed power, in comparison to the corresponding nonlinear programming solution. As seen, no disagreement is visible.

2.3. Prediction of future velocity

In order to predict the future velocity response $\dot{v}(t)$, $t > t_0$, a van der Pol transformation of the narrow-banded processes $\dot{v}(t)$ and $\ddot{v}(t)$ is introduced, given as [18]:

$$\left.\begin{aligned} \dot{v}(t) &= a(t)\cos(\omega_p t + \varphi(t)) \\ \ddot{v}(t) &= -\omega_p a(t)\sin(\omega_p t + \varphi(t)) \end{aligned}\right\} \tag{35}$$

where $a(t)$ and $\varphi(t)$ signify slowly varying amplitude and phase processes, expressed as:

$$\left.\begin{aligned} a(t) &= \sqrt{\dot{v}^2(t) + \left(\frac{\ddot{v}(t)}{\omega_p}\right)^2} \\ \varphi(t) &= \arctan\left(-\frac{\ddot{v}(t)}{\omega_p \dot{v}(t)}\right) - \omega_p t \end{aligned}\right\} \tag{36}$$

Fig. 7 shows realizations of $a(t)$ and $\varphi(t)$ for the constrained absorber. As seen, the evolution of $a(t)$ and $\varphi(t)$ take place over several periods. Because $h_{rv}(t) \simeq 0$ for $t > T_p$ as shown in Fig. 2, a prediction of $a(t)$, $\varphi(t)$ and hence $\dot{v}(t)$ is only needed one peak wave period T_p ahead of the present time t_0.

Defined the following quantities:

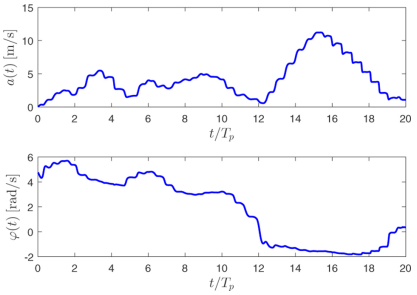

Fig. 7. Realizations of amplitude $a(t)$ and phase $\varphi(t)$ for the unconstrained absorber.

$$\left.\begin{aligned} a_{-j} &= a(t_0 - jT_p) \\ \varphi_{-j} &= \varphi(t_0 - jT_p) \end{aligned}\right\}, \quad j = 0, 1, 2, \ldots \tag{37}$$

Then, the predicted velocities can be formulated as:

$$\dot{v}(t) = a(t)\cos(\omega_p t + \varphi(t)), \quad t > t_0 \tag{38}$$

$a(t)$ and $\varphi(t)$ are estimated by extrapolation from $t = t_0$ of 2nd order Lagrange polynomials calibrated through the function values at t_0, $t_0 - T_p$ and $t - 2T_p$, given as:

$$\left.\begin{aligned} a(t) &= a_0 + \tfrac{1}{2}(3a_0 - 4a_{-1} + a_{-2})\tau + \tfrac{1}{2}(a_0 - 2a_{-1} + a_{-2})\tau^2 \\ \varphi(t) &= \varphi_0 + \tfrac{1}{2}(3\varphi_0 - 4\varphi_{-1} + \varphi_{-2})\tau + \tfrac{1}{2}(\varphi_0 - 2\varphi_{-1} + \varphi_{-2})\tau^2 \end{aligned}\right\}, \quad \tau = \frac{t - t_0}{\mathrm{Tp}} \geq 0 \tag{39}$$

Fig. 8 shows the prediction of $\dot{v}(t)$ from $t = 14.25T_p$, $t = 15.25T_p$ and $t = 16.25T_p$. As seen, the predicted velocities fit well at least one period ahead, which is the required prediction horizon with the impulse response function shown in Fig. 2.

Alternatively, $a(t)$ and $\varphi(t)$ may be estimated by using the Hilbert transformation $\hat{\dot{v}}(t)$ of the velocity response instead of $\frac{\ddot{v}(t)}{\omega_p}$ in Eq. (36)

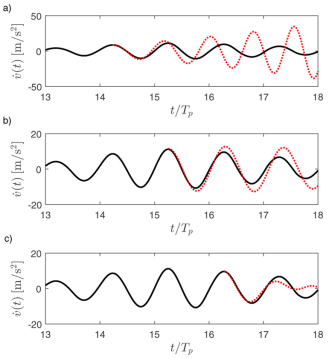

Fig. 8. Prediction of $\dot{v}(t)$. (a) $t = 14.25T_p$. (b) $t = 15.25T_p$. (c) $t = 16.25T_p$. —: Nonlinear programming solution. .....: Prediction velocity response.

[30,31]. The two approaches are identical for harmonic varying functions $\dot{v}(t)$ and $\ddot{v}(t)$.

2.4. Mean absorbed power at optimal control

In the following, the restoring force from buoyancy and mooring is assumed to be linear, i.e. $r(v(t)) = k\,v(t)$.

At optimal unconstrained control, the frequency response function $H_{\dot{v}f_e}(\omega)$ for the velocity response $\dot{v}(t)$ due to the harmonic varying wave load $f_e(t)$ is given as, [26]:

$$H_{\dot{v}f_e}(\omega) = \frac{1}{2\,\mathrm{Re}(H_{rv}(\omega))} \tag{40}$$

Then, the double-sided auto-spectral density function $S_{\dot{v}\dot{v}}(\omega)$ of the related velocity response process becomes, [28]

$$S_{\dot{v}\dot{v}}(\omega) = |H_{\dot{v}f_e}(\omega)|^2\, S_{f_ef_e}(\omega) = \frac{|H_{e\eta}(\omega)|^2}{4\,(\mathrm{Re}(H_{rv}(\omega)))^2}\, S_{\eta\eta}(\omega) \tag{41}$$

where Eq. (10) has been used in the last statement.

Due to the linear relationship between $\dot{v}(t)$ and $f_e(t)$ as reflected by Eq. (40), $\dot{v}(t)$ becomes Gaussian, if the wave load process is Gaussian. Then, the acceleration process $\ddot{v}(t)$ and the displacement process $v(t)$ become Gaussian processes as well.

In turn, $f_{c,0}(t)$ as given by Eq. (14) becomes Gaussian, if the restoring force is linear.

The auto-spectral density function $S_{f_{c,0}f_{c,0}}(\omega)$ of $f_{c,0}(t)$ and the cross-spectral density function $S_{f_{c,0}\dot{v}}(\omega)$ of $f_{c,0}(t)$ and $\dot{v}(t)$ become, [28]:

$$\left.\begin{aligned} S_{f_{c,0}f_{c,0}}(\omega) &= |H_{f_{c,0}\dot{v}}(\omega)|^2 S_{\dot{v}\dot{v}}(\omega) \\ &= \left(\left(\omega M - \tfrac{k}{\omega} - \mathrm{Im}(H_{rv}(\omega))\right)^2 + (\mathrm{Re}(H_{rv}(\omega)))^2\right) S_{\dot{v}\dot{v}}(\omega) \\ S_{f_{c,0}\dot{v}}(\omega) &= H^*_{f_{c,0}\dot{v}}(\omega)\; S_{\dot{v}\dot{v}}(\omega) = \left(i\omega M + H^*_{rv}(\omega) + \tfrac{k}{i\omega}\right) S_{\dot{v}\dot{v}}(\omega) \end{aligned}\right\} \tag{42}$$

where $H^*_{f_{c,0}\dot{v}}(\omega)$ and $H^*_{rv}(\omega)$ signify the complex conjugate of $H_{f_{c,0}\dot{v}}(\omega)$ and $H_{rv}(\omega)$. $H_{f_{c,0}\dot{v}}(\omega)$ is given as:

$$H_{f_{c,0}\dot{v}}(\omega) = -i\omega M + H_{rv}(\omega) - \frac{k}{i\omega} \tag{43}$$

The variances $\sigma^2_{\dot{v}}$ and $\sigma^2_{f_{c,0}}$ and the covariance $\kappa_{f_{c,0}\dot{v}}$ of $f_{c,0}(t)$ and $\dot{v}(t)$ follow from Eqs. (41) and (42), [28]:

$$\left.\begin{aligned} \sigma^2_{\dot{v}} &= \int_{-\infty}^{\infty} S_{\dot{v}\dot{v}}(\omega)\,d\omega = \int_0^{\infty} \tfrac{|H_{e\eta}(\omega)|^2}{2(\mathrm{Re}(H_{rv}(\omega)))^2} S_{\eta\eta}(\omega)\,d\omega \\ \sigma^2_{f_{c,0}} &= \int_{-\infty}^{\infty} |H_{f_{c,0}\dot{v}}(\omega)|^2\, S_{\dot{v}\dot{v}}(\omega)\,d\omega \\ &= 2\int_0^{\infty} \left(\left(\omega M - \tfrac{k}{\omega} - \mathrm{Im}(H_{rv}(\omega))\right)^2 + (\mathrm{Re}(H_{rv}(\omega)))^2\right) S_{\dot{v}\dot{v}}(\omega)\,d\omega \\ \kappa_{f_{c,0}\dot{v}} &= \int_{-\infty}^{\infty} H^*_{f_{c,0}\dot{v}}(\omega)\, S_{\dot{v}\dot{v}}(\omega)\,d\omega = 2\int_0^{\infty} \mathrm{Re}(H_{rv}(\omega))\, S_{\dot{v}\dot{v}}(\omega)\,d\omega \end{aligned}\right\} \tag{44}$$

The final results in Eq. (44) follow, because the real and imaginary parts of the involved frequency response functions are odd and even function of ω, respectively, and $S_{\dot{v}\dot{v}}(\omega)$ is an even function of ω. The quadratures in Eq. (44) need to be evaluated numerically.

The maximum mean power that can be extracted by the unconstrained optimal control from an irregular sea state is expressed as, Nielsen et al. [10]:

$$\bar{P}_{\mathrm{opt},0} = \int_0^{\infty} \frac{|H_{e\eta}(\omega)|^2}{2\,\mathrm{Re}(H_{rv}(\omega))}\, S_{\eta\eta}(\omega)\,d\omega \tag{45}$$

The joint probability density function $p_{f_{c,0}\dot{v}}(f, \dot{v})$ of $f_{c,0}(t)$ and $\dot{v}(t)$ is bivariate normal distributed with the statistical moments given in Eq. (44). $p_{f_{c,0}\dot{v}}(f, \dot{v})$ may be written on the form:

$$p_{f_{c,0}\dot{v}}(f, \dot{v}) = \frac{1}{\sigma_{f_{c,0}}}\varphi\left(\frac{f}{\sigma_{f_{c,0}}}\right)\frac{1}{\sigma}\varphi\left(\frac{\dot{v} - \mu(f)}{\sigma}\right) \tag{46}$$

$\varphi(\cdot)$ indicates the standardized normal probability density function, $\mu(f)$ and σ signifies the mean value and standard deviation of $\dot{v}(t)$ on condition of the sample $f_{c,0}(t) = f$, given as:

$$\left.\begin{aligned} \mu(f) &= \rho\tfrac{\sigma_{\dot{v}}}{\sigma_{f_{c,0}}} f \\ \sigma &= \sqrt{1-\rho^2}\,\sigma_{\dot{v}} \end{aligned}\right\} \tag{47}$$

ρ is the correlation coefficient of $\dot{v}(t)$ and $f_{c,0}(t)$ given as:

$$\rho = \frac{\kappa_{f_{c,0}\dot{v}}}{\sigma_{f_{c,0}}\sigma_{\dot{v}}} \tag{48}$$

Next, the maximal mean power absorbed by the constrained control force $f_c(t)$ given by Eq. (34) may be calculated from the following linear combination of conditional expectations:

$$\begin{aligned} \bar{P}_{\mathrm{opt}} = {} & E[f_c(t)\dot{v}(t)] \\ = {} & E[f_c(t)\dot{v}(t)\,|\,f_c(t) = f_{c,\max}]\,P(f_{c,0}(t) > f_{c,\max}) \\ & + E[f_c(t)\dot{v}(t)\,|\,f_{c,\min} \le f_c(t) \le f_{c,\max}]\,P(f_{c,\min} \le f_{c,0}(t) \le f_{c,\max}) \\ & + E[f_c(t)\dot{v}(t)\,|\,f_c(t) = f_{c,\min}]\,P(f_{c,0}(t) < f_{c,\min}) \end{aligned} \tag{49}$$

where:

$$\left.\begin{aligned} P(f_{c,0}(t) > f_{c,\max}) &= 1 - \Phi\left(\tfrac{f_{c,\max}}{\sigma_{f_{c,0}}}\right) \\ P(f_{c,\min} \le f_{c,0}(t) \le f_{c,\max}) &= \Phi\left(\tfrac{f_{c,\max}}{\sigma_{f_{c,0}}}\right) - \Phi\left(\tfrac{f_{c,\min}}{\sigma_{f_{c,0}}}\right) \\ P(f_{c,0}(t) < f_{c,\min}) &= \Phi\left(\tfrac{f_{c,\min}}{\sigma_{f_{c,0}}}\right) \end{aligned}\right\} \tag{50}$$

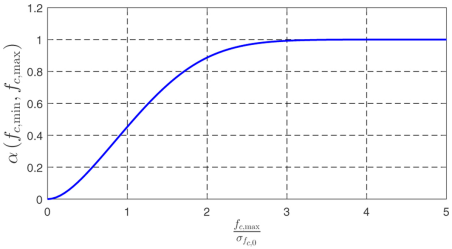

Fig. 9. Reduction coefficient $\alpha(f_{c,\min}, f_{c,\max})$ as a function of $\frac{f_{c,\max}}{\sigma_{f_{c,0}}}$, $f_{c,\min} = -f_{c,\max}$.

$$\left.\begin{aligned}
E[f_c(t)\dot{v}(t)\,|\,f_c(t) &= f_{c,\max}] = f_{c,\max}\,E[\dot{v}(t)\,|\,f_{c,0}(t) = f_{c,\max}] \\
&= f_{c,\max}\,\mu(f_{c,\max}) = \left(\frac{f_{c,\max}}{\sigma_{f_{c,0}}}\right)^2 \bar{P}_{\text{opt},0} \\
E[f_c(t)\dot{v}(t)\,|\,f_{c,\min} \le f_c(t) \le f_{c,\max}] &= \int_{f_{c,\min}}^{f_{c,\max}} f \int_{-\infty}^{\infty} \dot{v}\, p_{f_{c,0}\dot{v}}(f,\dot{v})\,\mathrm{d}\dot{v}\,\mathrm{d}f \\
&= \int_{f_{c,\min}}^{f_{c,\max}} f\,\mu(f)\frac{1}{\sigma_{f_{c,0}}}\varphi\left(\frac{f}{\sigma_{f_{c,0}}}\right)\mathrm{d}f \\
&= \left(\Phi\left(\frac{f_{c,\max}}{\sigma_{f_{c,0}}}\right) - \Phi\left(\frac{f_{c,\min}}{\sigma_{f_{c,0}}}\right) - \frac{f_{c,\max}}{\sigma_{f_{c,0}}}\varphi\left(\frac{f_{c,\max}}{\sigma_{f_{c,0}}}\right)\right. \\
&\quad \left. + \frac{f_{c,\min}}{\sigma_{f_{c,0}}}\varphi\left(\frac{f_{c,\min}}{\sigma_{f_{c,0}}}\right)\right)\bar{P}_{\text{opt},0} \\
E[f_c(t)\dot{v}(t)|f_c(t) = f_{c,\min}] &= f_{c,\min}\,E[\dot{v}(t)|f_{c,0}(t) = f_{c,\min}] \\
&= f_{c,\min}\,\mu(f_{c,\min}) = \left(\frac{f_{c,\min}}{\sigma_{f_{c,0}}}\right)^2 \bar{P}_{\text{opt},0}
\end{aligned}\right\} \tag{51}$$

where $\Phi(\cdot)$ indicates the standardized normal probability distribution function.

Insertion of the results in Eqs. (50) and (51) in Eq. (49) provides the following solution for the maximal mean power that can be absorbed by the constrained control force:

$$\bar{P}_{\text{opt}} = \alpha(f_{c,\min}, f_{c,\max})\bar{P}_{\text{opt},0} \tag{52}$$

where $\alpha(f_{c,\min}, f_{c,\max})$ is a reduction factor caused by the constraints on the control force:

$$\begin{aligned}
\alpha(f_{c,\min}, f_{c,\max}) = &\left(\Phi\left(\frac{f_{c,\max}}{\sigma_{f_{c,0}}}\right) - \Phi\left(\frac{f_{c,\min}}{\sigma_{f_{c,0}}}\right)\right)^2 \\
&- \left(\frac{f_{c,\max}}{\sigma_{f_{c,0}}}\varphi\left(\frac{f_{c,\max}}{\sigma_{f_{c,0}}}\right) - \frac{f_{c,\min}}{\sigma_{f_{c,0}}}\varphi\left(\frac{f_{c,\min}}{\sigma_{f_{c,0}}}\right)\right)\left(\Phi\left(\frac{f_{c,\max}}{\sigma_{f_{c,0}}}\right)\right. \\
&\left. - \Phi\left(\frac{f_{c,\min}}{\sigma_{f_{c,0}}}\right)\right) \\
&+ \left(\frac{f_{c,\max}}{\sigma_{f_{c,0}}}\right)^2\left(1 - \Phi\left(\frac{f_{c,\max}}{\sigma_{f_{c,0}}}\right)\right) + \left(\frac{f_{c,\min}}{\sigma_{f_{c,0}}}\right)^2 \Phi\left(\frac{f_{c,\min}}{\sigma_{f_{c,0}}}\right)
\end{aligned} \tag{53}$$

Fig. 9 shows the variation of $\alpha(f_{c,\min}, f_{c,\max})$ as a function of $\frac{f_{c,\max}}{\sigma_{f_{c,0}}}$, $f_{c,\min} = -f_{c,\max}$. As seen, the constraints are only active for $\min(f_{c,\max}, -f_{c,\min}) < 3\sigma_{f_{c,0}}$.

3. Numerical example

A point heave wave energy converter indicated in Fig. 1 is considered in the numerical simulation. Table 1 indicates the relevant data of the absorber and the wave excitation parameters and the optimized gain parameters in Eq. (57).

$S_{\eta\eta}(\omega)$ is taken as the double-sided JONSWAP auto spectral density function given as [32]:

$$S_{\eta\eta}(\omega) = \delta\frac{H_s^2}{\omega_p}\gamma^{\beta}\left(\frac{|\omega|}{\omega_p}\right)^{-5}\exp\left(-\frac{5}{4}\left(\frac{\omega}{\omega_p}\right)^{-4}\right) \tag{54}$$

where

$$\left.\begin{aligned}
\delta &= \frac{0.0312}{0.230 + 0.0336\gamma - \frac{0.185}{1.9+\gamma}} \\
\beta &= \exp\left(-\frac{1}{2}\left(\frac{|\omega| - \omega_p}{\sigma\omega_p}\right)^2\right) \\
\sigma &= \begin{cases} 0.07, & |\omega| \le \omega_p \\ 0.09, & |\omega| > \omega_p \end{cases}
\end{aligned}\right\} \tag{55}$$

T_p is the peak period, $\omega_p = \frac{2\pi}{T_p}$ is the related angular peak frequency and H_s is the significant wave height. γ is the so-called peak enhancement parameter which controls the bandwidth of the spectrum.

It is well known that the optimal control of point absorber in monochromatic waves is achieved when the control force enforces the absorber into resonance with the harmonic varying wave force. In this respect, the value of $k = 1.51 \times 10^5$ N/m has been chosen in the numerical analysis below, corresponding to the undamped angular eigenfrequency $\omega_0 = 0.81$ rad/s, which is close to the peak angular eigenfrequency $\omega_p = 0.85$ rad/s, in order to reduce the control effort even in irregular sea states.

In applications, $\ddot{v}(t)$ may be measured by an accelerometer, from which $v(t)$ and $\dot{v}(t)$ are obtained by numerical integration. However, $\ddot{v}(t)$ may be corrupted by measurement noise. In order to analyze the influence of the noise on the quality of the control, $\ddot{v}(t)$ is written in the form:

$$\ddot{v}(t) = \ddot{v}_0(t) + a_1 w(t) \tag{56}$$

where $\ddot{v}_0(t)$ is the acceleration predicted by nonlinear programming. The parameter a_1 indicates the level of noise, and $w(t)$ signifies a zero mean, stationary, broadbanded Gaussian stochastic process with an auto spectral density function, which is flat at the value $\frac{1}{2\pi}$ in the angular frequency interval $[0, 2\omega_p]$, mimicking a unit intensity Gaussian white noise [28]. Fig. 10 shows the obtained control forces with different noise levels $a_1 = 0.5\ \text{m/s}^{1/2}$, $a_1 = 0.05\ \text{m/s}^{1/2}$ and $a_1 = 0.001\ \text{m/s}^{1/2}$.

As seen, the obtained control force is sensible to observation noise when $a_1 \ge 0.05\ \text{m/s}^{1/2}$. The reason is that the inertial term is dominating in the solution Eq. (34), and the noise in the acceleration signal is amplified by multiplication with M.

The quality of the estimated control force will influence the future response. The extent of this will next be investigated. The detail of the procedure can be expressed as:

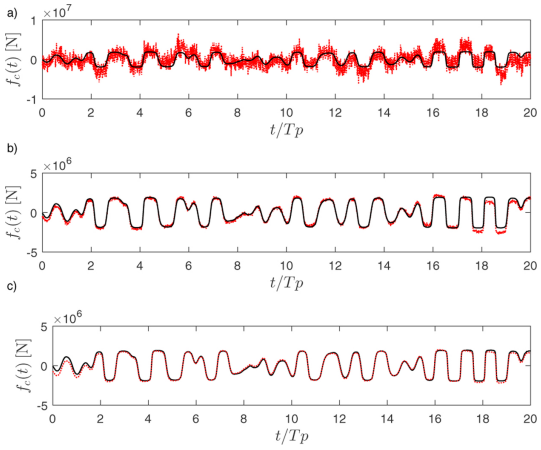

Fig. 10. Comparison of control force $f_c(t)$ with different noise level on the observation of the acceleration singal. (a) $a_1 = 0.5\,\mathrm{m/s^{1/2}}$. (b) $a_1 = 0.05\,\mathrm{m/s^{1/2}}$. (c) $a_1 = 0.001\,\mathrm{m/s^{1/2}}$. —: Nonlinear programming solution. - - -: Noise affected solution.

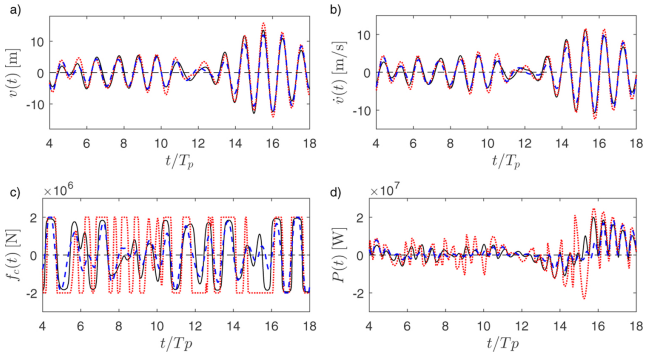

Fig. 11. Realization 1: Comparison of trajectories for different control strategies. —: Nonlinear programming solution. .....: $f_{c,0}(t)$ given by Eq. (33). - - -: $f_{c,0}(t)$ given by Eq. (57).

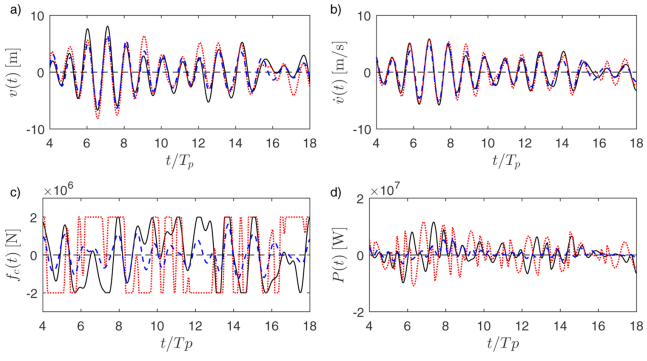

Fig. 12. Realization 2: Comparison of trajectories for different control strategies. —: Nonlinear programming solution. .....: $f_{c,0}(t)$ given by Eq. (33). - - -: $f_{c,0}(t)$ given by Eq. (57).

(1) At the time t, predict $\dot{v}(\tau)$ for τ in the interval $[t, t + T_p]$.
(2) Calculate $f_{c,0}(t)$ and $f_c(t)$ from Eqs. (33) and (34).
(3) Integrate Eq. (7) one time step Δt ahead to obtain $v(t + \Delta t)$, $\dot{v}(t + \Delta t)$ and $\ddot{v}(t + \Delta t)$, keeping $f_c(t)$ constant in the interval $[t, t + \Delta t]$.
(4) Update $f_c(t)$.

The procedure mimics the practical application of the control, where the control force needs to be applied as a piecewise constant function.

Additionally, comparison will be made with the following causal unconstrained control force in Eq. (34):

$$f_{c,0}(t) = -\beta_1 M\ddot{v}(t) + c\dot{v}(t) - \beta_2 r(v(t)) \tag{57}$$

Eq. (57) can be characterized as a controller with feedback from the displacement, velocity and the present acceleration. The first and the third terms introduce negative inertia and stiffness into the system. Guided by the theoretical solution in Eq. (33), these parameters should be close to one. The viscous damping term replaces the radiation damping term in Eq. (33). Obviously, the gain parameters β_1, β_2, c depend on the considered sea-state.

Figs. 11–13 indicate the performance of the suggested control law compared to those obtained by nonlinear programming and the feedback control in Eq. (57) for three independent realizations of the surface elevation of a sea-state defined by $H_s = 3$ m, $T_p = 7.42$ s, $\gamma = 5$. The control interval is chosen as $[t_0, t_1] = [0, 20T_p]$, and the same optimized parameters β_1, β_2, c as indicated in Table 1 are used for three realizations. The related absorbed mean power have been indicated in Table 2.

As seen from Figs. 11, 12 and 13, the displacement and velocity estimates based on the two approximate control related to Eqs. (34) and (57) are not deviating much from the nonlinear programming solution. However, the control force and the instantaneous power takeoff deviate substantially. Again, this is because the deviations in the related acceleration signals are amplified significantly when multiplied by M.

Table 2 compares the mean absorbed power $\bar{P}$ in the indicated interval $[3.5T_p, 20T_p]$ for the considered control strategy with the solutions from nonlinear programming and the optimized causal control with $f_{c,0}(t)$ given by Eq. (57).

Table 2
Absorbed mean power $\bar{P}$ [MW].

	Nonlinear programming	$f_{c,0}(t)$ given by Eq. (33)	$f_{c,0}(t)$ given by Eq. (57)
Realization 1	1.663	1.566 (5.8%)	1.544 (7.2%)
Realization 2	0.521	0.513 (1.2%)	0.467 (10.4%)
Realization 3	0.950	0.945 (0.5%)	0.921 (3.1%)

Values in brackets indicate the error relative to the nonlinear programming solution.

As seen, the absorbed mean power by the control laws is less deviating than the instantaneous power takeoff. As shown in Table 2, the absorbed mean power for the control law with $f_{c,0}(t)$ given by Eq. (33) and with predicted future velocities are between 0.5% and 5.8% lower than the nonlinear programming solution for the optimal control. Further, the mean power takeoff for the control law with $f_{c,0}(t)$ given by Eq. (57) is further reduced compared to the suggested control law.

4. Conclusions

This paper presents an analytical solution for the optimal power takeoff of a heave point wave energy converter with the constrained control force. Based on the solution for the optimal control force, the mean absorbed power take-off in a given sea-state has been derived. The optimal control force has a noncausal dependence on future velocities, which need to be predicted. The response processes turn out to be narrow-banded with the peak angular frequency as center frequency. This

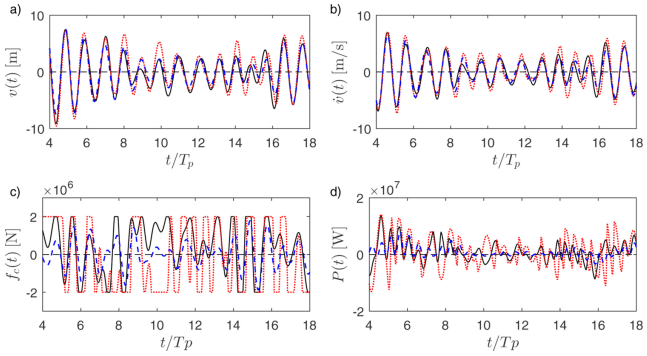

Fig. 13. Realization 3: Comparison of trajectories for different control strategies. —: Nonlinear programming solution. ·····: $f_{c,0}(t)$ given by Eq. (33). - - -: $f_{c,0}(t)$ given by Eq. (57).

observation is used in the prediction algorithm, which is based on a van der Pol transformation of velocity and acceleration of the absorber. The mean power takeoff of the suggested control law, applied in a way mimicking the application in reality, was compared to that of optimal control obtained by nonlinear programming for three independent realizations of a given sea-state. The reduction in efficiency varied between 0.5% and 5.8%. Finally, the controller was compared to a causal controller with feedback from the present displacement, velocity and acceleration, which turn out to perform worse in all three cases.

Acknowledgements

The authors gratefully acknowledge the financial support from project 675659-ICONN-H2020-MSCA-ITN-2015.

Appendix A. Nonlinear programming algorithm

The optimal control problem in Eq. (16) is reformulated as a nonlinear programming problem by discretizing the objective functional and the state vector in time:

$$\begin{aligned}&\max\ J(\mathbf{X}(\tau_M)) = x_{n+3}(\tau_M)\\ &\text{subject to the path and inequality constraints:}\\ &\left.\begin{aligned}&\mathbf{c}(\mathbf{X}(\tau_j)) = \mathbf{0}\\ &\mathbf{h}(\mathbf{X}(\tau_j)) = \begin{bmatrix} v(\tau_j) - v_{\max} \\ -v(\tau_j) + v_{\min} \\ f_c(\tau_j) - f_{c,\max} \\ -f_c(\tau_j) + f_{c,\min} \end{bmatrix} - \mathbf{s}(\tau_j) = \mathbf{0}\\ &\mathbf{s}(\tau_j) \geq \mathbf{0}\end{aligned}\right\}\end{aligned} \tag{58}$$

where $\tau_j = t_0 + j\Delta\tau\ j = 0, 1, \ldots, M$.

$\mathbf{s}(t)$ indicates a vector function of slack variables. The time step in the discretization of the interval$]t_0, t_1]$ is given as $\Delta\tau = \frac{t_1 - t_0}{M}$. The vector $\mathbf{X}(t)$ of dimension $2n + 6$ and the path constrain vector $\mathbf{c}(\mathbf{X}(t))$ of dimension $n + 3$ are defined as:

$$\mathbf{X}(t) = \left[v(t),\ \dot{v}(t),\ \mathbf{z}_r^T(t),\ x_{n+3}(t),\ \frac{d}{\mathrm{d}t}v(t),\ \frac{d}{\mathrm{d}t}\dot{v}(t),\ \frac{d}{\mathrm{d}t}\mathbf{z}_r^T(t),\ \frac{d}{\mathrm{d}t}x_{n+3}(t)\right]^T \tag{59}$$

$$\mathbf{c}(\mathbf{X}(t)) = \begin{bmatrix} \frac{d}{\mathrm{d}t}v(t) - \dot{v}(t) \\ M\frac{d}{\mathrm{d}t}\dot{v}(t) + \mathbf{p}_r\mathbf{z}_r(t) + r(v(t)) - f_e(t) + f_c(t) \\ \frac{d}{\mathrm{d}t}\mathbf{z}_r(t) - \mathbf{A}_r\,\mathbf{z}_r(t) - \mathbf{b}_r\,\dot{v}(t) \\ \frac{d}{\mathrm{d}t}x_{n+3}(t) - f_c(t)\dot{v}(t) \end{bmatrix} \tag{60}$$

The inherent approximation in the indicated nonlinear programming formulation concerns the discretization of the time continuous problem into $M + 1$ discrete instants of time for optimization, and the use of the rational approximation in Eq. (13) for the force $f_{r,0}(t)$.

The formulation applies to both displacement constraints and control force constraints. In case, merely control force constraints are prescribed the algorithm is applied by using large values of $v_{\max}$ and small values of $v_{\min}$.

The applied algorithm for solving the indicated nonlinear programming problem is described in [33].

References

[1] J.V. Ringwood, G. Bacelli, F. Fusco, Energy-maximizing control of wave-energy converters: the development of control system technology to optimize their operation, IEEE Control Syst. 34 (5) (2014) 30–55.
[2] J. Falnes, Wave-power conversion by point absorber, Nor. Marit. Res. 6 (4) (1978).
[3] M.J. French, A generalized view of resonant energy transfer, J. Mech. Eng. Sci. 21 (4) (1979) 299–300.
[4] R.E. Hoskin, N.K. Nichols, Latching Control for the Point-absorber Wave-power Device, University of Reading. Department of Mathematics, 1986.
[5] U.A. Korde, Latching control of deep water wave energy devices using an active reference, Ocean Eng. 29 (11) (2002) 1343–1355.
[6] A. Babarit, A.H. Clement, Optimal latching control of a wave energy device in regular and irregular waves, Appl. Ocean Res. 28 (2) (2006) 77–91.
[7] A. Babarit, M. Guglielmi, A.H. Clement, Declutching control of a wave energy converter, Ocean Eng. 36 (12-13) (2009) 1015–1024.
[8] K.J. Åström, T. Hägglund, Advanced PID Control, ISA – The Instrumentation, Systems and Automation Society, 2006.
[9] S. Peretta, P. Ruol, L. Martinelli, A. Tetu, J.P. Kofoed, Effect of a negative stiffness mechanism on the performance of the WEPTOS rotors, International Conference on Computational Methods in Marine Engineering, CNR, 2015, pp. 58–72.
[10] S.R.K. Nielsen, Q. Zhou, M.M. Kramer, B. Basu, Z. Zhang, Optimal control of nonlinear wave energy point converters, Ocean Eng. 72 (2013) 176–187.
[11] R. Hansen, M.M. Kramer, Modelling and control of the wavestar prototype, Proceedings of the 9th European Wave and Tidal Conference (2011).
[12] R.W.M. Hendrikx, J. Leth, P. Andersen, W.P.M.H. Heemels, Optimal control of a wave energy converter, Proceedings of the 2017 IEEE Conference on Control Technology and Applications (CCTA), Kohala Coast, HI, USA, 27–30 August, 2017, pp. 779–786.
[13] J. Hals, J. Falnes, T. Moan, Constrained optimal control of a heaving buoy wave-energy converter, J. Offsh. Mech. Arct. Eng. 133 (1) (2010) 011401.
[14] M. Richter, M.E. Magana, O. Sawodny, T.K.A. Brekken, Nonlinear model predictive control of a point absorber wave energy converter, IEEE Trans. Sustain. Energy 4 (1) (2013) 118–126.
[15] M.N. Soltani, M.T. Sichani, M. Mirzaei, Model predictive control of buoy type wave energy converter, IFAC Proc. Vol. 47 (3) (2014) 11159–11164.
[16] G. Bacelli, J.V. Ringwood, Numerical optimal control of wave energy converters, IEEE Trans. Sustain. Energy 6 (2) (2015) 294–302.
[17] R. Genest, J.V. Ringwood, Receding horizon pseudospectral control for energy maximization with application to wave energy devices, IEEE Trans. Control Syst. Technol. 25 (1) (2017) 29–38.
[18] J.B. Roberts, P.D. Spanos, Random Vibration and Statistical Linearization, Courier Corporation, 2003.
[19] R. Genest, F. Bonnefoy, A.H. Clement, A. Babarit, Effect of non-ideal power take-off on the energy absorption of a reactively controlled one degree of freedom wave energy converter, Appl. Ocean Res. 48 (2014) 236–243.
[20] J. Newman, Marine Hydrodynamics, The MIT Press, 1977.
[21] W. Cummins, The impulse response functions and ship motions, Schiff-stechnik 9 (1962) 101–109.
[22] O. Faltinsen, Sea Loads on Ships and Offshore Structures, Cambridge University Press, 1990.
[23] M. Penalba Retes, G. Giorgi, J. Ringwood, A review of non-linear approaches for wave energy converter modelling. Proceedings of the 11th European Wave and Tidal Energy Conference. European Wave and Tidal Energy Conference (2015).
[24] G. Giorgi, J.V. Ringwood, Comparing nonlinear hydrodynamic forces in heaving point absorbers and oscillating wave surge converters, J. Ocean Eng. Mar. Energy 4 (1) (2018) 25–35.
[25] A.S. Zurkinden, F. Ferri, S. Beatty, J.P. Kofoed, M.M. Kramer, Non-linear numerical modeling and experimental testing of a point absorber wave energy converter,

Ocean Eng. 78 (2014) 11–21.
[26] J. Falnes, Ocean Waves and Oscillating Systems: Linear Interactions Including Wave-Energy Extraction, Cambridge University Press, 2002.
[27] WAMIT, WAMIT User Manual, version 7.0. Technical Report, (2011).
[28] S.R.K. Nielsen, Z. Zhang, Stochastic Dynamics, Aarhus Unversity Press, 2017.
[29] D.S. Naidu, Optimal Control Systems, CRC Press, 2002.
[30] N.E. Huang, Z. Shen, S.R. Long, M.C. Wu, H.H. Shih, Q. Zheng, N.C. Yen, C.C. Tung, H.H. Liu, The empirical mode decomposition and the Hilbert spectrum for nonlinear and non-stationary time series analysis, Proceedings of the Royal Society of London A: Mathematical, Physical and Engineering Sciences (1998) The Royal Society.
[31] H. Cramér, M.R. Leadbetter, Stationary and Related Stochastic Processes: Sample Function Properties and Their Applications, Courier Corporation, 2013.
[32] K. Hasselmann, T.P. Barnett, E. Bouws, et al., Measurements of Wind Wave Growth and Swell Decay During the Joint North Sea Project (JONSWAP), Deutches Hydrographisches Institut, 1973.
[33] A.S. El-Bakry, R.A. Tapia, T. Tsuchiya, Y. Zhang, On the formulation and theory of the Newton interior-point method for nonlinear programming, J. Optim. Theory Appl. 89 (3) (1996) 507–541.

Paper B

Stochastic Cntrol of Wave Energy Converters with Constrained Displacements for Optimal Power Absorption

Tao Sun, Søren R.K. Nielsen, Biswajit Basu

The paper has been published in the
Applied Ocean Research Vol. 89, pp.1-11, 2019.

B.1 Author's Right

Journal author rights

In order for Elsevier to publish and disseminate research articles, we need publishing rights. This is determined by a publishing agreement between the author and Elsevier. This agreement deals with the transfer or license of the copyright to Elsevier and authors retain significant rights to use and share their own published articles. Elsevier supports the need for authors to share, disseminate and maximize the impact of their research and these rights, in Elsevier proprietary journals* are defined below:

For subscription articles	For open access articles
Authors transfer copyright to the publisher as part of a journal publishing agreement, but have the right to: • Share their article for Personal Use, Internal Institutional Use and Scholarly Sharing purposes, with a DOI link to the version of record on ScienceDirect (and with the Creative Commons CC-BY-NC- ND license for author manuscript versions) • Retain patent, trademark and other intellectual property rights (including research data). • Proper attribution and credit for the published work.	Authors sign an exclusive license agreement, where authors have copyright but license exclusive rights in their article to the publisher**. In this case authors have the right to: • Share their article in the same ways permitted to third parties under the relevant user license (together with Personal Use rights) so long as it contains a CrossMark logo, the end user license, and a DOI link to the version of record on ScienceDirect. • Retain patent, trademark and other intellectual property rights (including research data). • Proper attribution and credit for the published work.

https://www.elsevier.com/about/policies/copyright

Applied Ocean Research 89 (2019) 1–11

Contents lists available at ScienceDirect

Applied Ocean Research

journal homepage: www.elsevier.com/locate/apor

Stochastic control of wave energy converters with constrained displacements for optimal power absorption

Tao Sun[a,*], Søren R.K. Nielsen[a], Biswajit Basu[b]

[a] Department of Civil Engineering, Aalborg University, 9000 Aalborg, Denmark
[b] Department of Civil, Structural and Environmental Engineering, Trinity College Dublin, Dublin 2, Ireland

ARTICLE INFO

Keywords:
Wave energy
Heave point absorber
Optimal power take-off
Displacement constraints

ABSTRACT

An semi-analytical solution is derived for the optimal control of the power take-off of a single-degree of freedom heave point absorber with constraints on the displacement. At first the control force is derived during states, where the displacement constraint is active. This results in an open-loop control law dependent on the external wave load on the absorber. Next, the analytical solution for the optimal control in the unconstrained state is indicated, which turns out to be of the closed loop type with feedback from the present displacement and acceleration and from future velocities. The derived control law contains an undetermined constant, which is calibrated at the interface to the previous constrained state. The approach requires the estimation of the wave load during the constrained states, and the prediction of the future velocity response during unconstrained states. An algorithm has been devised in the paper for handling these problems. The theory has been validated against numerical solutions obtained by nonlinear programming.

1. Introduction

A wave energy point absorber has horizontal dimensions significantly smaller than the dominating wave length. Especially, a heave point absorber is constrained by a mooring system or otherwise to enforce a motion merely in the vertical direction, and hence can be modeled as a single-degree-of-freedom oscillator.

In reality constraints are present on the displacement of the absorber, because the actuator has a limited stroke. Displacement constraints may also be imposed to prevent the absorber from hitting the sea-bottom or jumping out of the water, which may lead to damaging impact loadings on the outer shell of the absorber. Similarly, constraints are present on the control force due to saturation in the actuator system.

In this paper only displacement constraints of the absorber is considered. Displacement constraints are difficult to deal with since the constraint does not depend explicitly on the control force and the state variables can only be controlled indirectly through the equation of the motion of the system. Hartl et al. [1] presented a survey of maximum principles for optimal control problems with state constraints. In the so-called the direct adjoining approach, also known as the penalty function method [2], the state constraints are introduced into the Hamiltonian via adding Lagrange multipliers. The indirect adjoining approach, also known as the slack variable method, is based on the differentiation of the state constraints which explicitly depends on the control force and is adjoined to the Hamiltonian. Jacobson and Lee [3] transformed an optimal control problem with a state inequality constraint into an unconstrained problem of higher dimension by slack variable method where the slack variable becomes the new control variable. The necessary conditions of optimality is presented based on Pontryagin's maximum principle and is solved by conjugate gradient method [4]. However, numerical difficulties may occur due to the increase dimension of the state vector. Eidsmoen [5] utilized an end-stop device modeled by a friction force to restrict the oscillating amplitude for a floating wave energy converter and determined an optimal control strategy based on variations of a Lagrange functional, subsequently solved by numerical method. Further, the unconstrained case and constrained case in regular an irregular sea-states are compared. Perez and Garcia [6] presented a state constrained optimal control strategy applied for monitoring supervisory control in hybrid electric vehicles. The solution with constraints on both the control force and state vector is derived based on Pontryagin's maximum principle. However, it is difficult to use the method straightforwardly, since the future instants of time at which these switching occur are unknown. Further, the co-state vector is also unknown. Instead, a nonlinear programming approached based on projected augmented Lagrangian algorithm was used to solve this constrained optimization problem. This is only applicable if the external loading is known throughout the control

* Corresponding author.
E-mail addresses: tsu@civil.aau.dk (T. Sun), srkn@civil.aau.dk (S.R.K. Nielsen), BASUB@tcd.ie (B. Basu).

https://doi.org/10.1016/j.apor.2019.04.022
Received 1 September 2018; Received in revised form 23 April 2019; Accepted 24 April 2019

horizon. Hals et al. [7] studied optimal constrained motion of wave-energy converters based on a heaving, semi-submerged sphere. They formulated the dynamic programming problem with the maximum absorbed power considering the constraints on the heave excursion and the machinery force. Again, the future wave loading is required. It shows how amplitude constraint affects the amount of absorbed power. Sichani et al. [8] studied the optimal control law of a non-linear wave energy point absorber under the displacement and the control force constraints. Further, the displacement constraints were considered in terms of increasing control stiffness as the absorber approaches the boundary. Wang et al. [9] investigated the optimal control of a WEC with the constrained PTO force and the constrained motions of the converter in term of truncated Fourier series in time domain, where the problem is converted to a optimization problem with a convex quadratic objective functional and nonlinear constraints.

The present paper presents a semi-analytical solution for the optimal control of a heave point absorber with constraints on the displacement. The suggested solution is optimal between the intervals, where the displacement constraints are not active. During the intervals with active displacement constraints, an approximate feedforward control is applied. Because the time intervals with active constraints diminish as the level of the constraints is increased, the suggested solution will approach the optimal solution asymptotically at high displacement constraints. The optimal solution to the control problem may be achieved by nonlinear programming. However, this requires the full length of the time series of the surface elevation to be known. For irregular sea states this can only be predicted at most one peak period ahead of the time where any control strategy is applied. As a consequence, any realizable control strategy is necessary. The nonlinear programming solution is applied as a benchmark for the validation of the suggested control. The paper is organized as follows. In Section 2.1 the basic motion equation of point absorber is presented. In Section 2.2 the optimal control law for a point absorber with constraints on the displacement is derived and the obtained solution is benchmarked against a numerical solution from nonlinear programming. The obtained control law has feedback from further velocities and depends on the further wave load. The quantities need to be predicted at the time the control is applied, which is dealt with in Section 2.3. Finally, in Section 3 a numerical example is provided to investigate the quality of the theory.

2. Methodology

2.1. Equation of motion of point absorber

The heave absorber to be analyzed is shown in Fig. 1. An (x, y, z)-coordinate system is introduced with the origin O placed in the mean water level (MWL) at the centerline of the point absorber. The horizontal x-axis is orientated in the direction of the wave propagation, and the vertical z-axis is orientated in the upward direction. Only two-dimensional (plane) irregular waves are considered. The motion $v(t)$ of the body in the z-direction is measured from the static equilibrium state with no wave motion, where the static buoyancy force $f_{b,0}$ balances the gravity force mg and a possible static pre-stressing force from the mooring system $f_{p,0}$. g is the acceleration of gravity, and m indicates the structural mass including ballast.

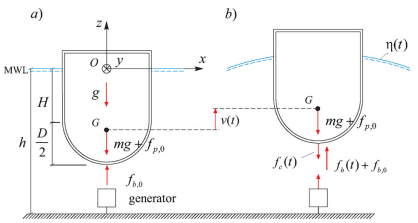

Fig. 1. Loads on heave absorber. (a) Static equilibrium state. (b) Dynamic state.

In the dynamic state caused by the surface elevation $\eta(t)$ the indicated static forces disappear from the dynamic equation of motion. Assuming linear wave theory, $v(t)$ is given by the following linear integro-differential equation [10]:

$$\left.\begin{aligned} M\ddot{v}(t) + r(v(t)) + \int_{t_0}^{t} h_{rv}(t-\tau)\dot{v}(\tau)\,d\tau &= f_e(t) - f_c(t), \quad t \in [t_0, t_1] \\ v(t_0) = v_0, \quad \dot{v}(t_0) &= \dot{v}_0 \end{aligned}\right\} \tag{1}$$

$f_e(t)$ is the wave excitation force on the absorber, and $f_c(t)$ is the reaction force from the power take-off system, which is used to control the motion of the absorber. The signs of $f_e(t)$ and $f_c(t)$ are defined in Fig. 1.

$r(v(t))$ is the quasi-static restoring force due to the buoyancy and the mooring system, caused by displacements from the static equilibrium state. Assuming small vertical vibrations, $r(v(t))$ may be linearized around the static equilibrium state as:

$$f_b(t) = -k\,v(t), \quad k = r'(0) \tag{2}$$

In the numerical results below the linearized relation in Eq. (7) has been assumed with the value of k given in Table 1.

$M = m + m_h$, where m_h indicates the added water mass at infinite high frequencies. v_0 and $\dot{v}_0$ are given initial conditions at the time t_0. t_1 is the terminal time of the control.

The impulse response function $h_{rv}(t)$ in the convolution integral is causal, i.e. $h_{rv}(t) = 0,\ t < 0$. The related frequency response function becomes [11]:

$$H_{rv}(\omega) = \int_0^\infty \mathrm{e}^{-i\omega t} h_{rv}(t)\,\mathrm{d}t \tag{3}$$

Fig. 2 shows the impulse response function $h_{rv}(t)$ and the frequency response function $H_{rv}(\omega)$ for the radiation force, based on the data of the absorber indicated in Table 1 in the numerical example below. In Fig. 2a the time has been normalized with respect to the peak period T_p. As seen, $h_{rv}(t)$ effectively vanishes for $t > T_\dot{v},\ T_\dot{v} \simeq T_p$. Below, it is shown that $T_\dot{v}$ indicates the prediction horizon of future velocities affecting the optimal control force in the unconstrained case. The angular frequency ω in Fig. 2b and c has been normalized with respect to the peak angular frequency $\omega_p = \frac{2\pi}{T_p}$. Since the real part is an even function of ω, and the imaginary part an odd function of ω, only results for positive values of the angular frequencies have been indicated. Further, the frequency response function $H_{rv}(\omega)$ is approximated by a rational function of the order (m, n), where m and n indicate the order of the numerator and the denominator polynomials, respectively. The details of the approach can be found in Appendix B. The rational approximation to $H_{rv}(\omega)$ of order (m, n) = (2, 3) has been illustrated in Fig. 2b and c.

The wave excitation force $f_e(t)$ may be expressed in terms of the following convolution integral of the sea-surface elevation $\eta(t)$ [12]:

$$f_e(t) = \int_{-\infty}^{\infty} h_{e\eta}(t-\tau)\,\eta(\tau)\,d\tau \tag{4}$$

The sea-surface elevation $\eta(t)$ is assumed to be observed at a sufficient distant position from the absorber, where the measurement is not

Table 1
Heave absorber and wave excitation parameters.

Parameter	Value	Unit	Parameter	Value	Unit
H	7.00	m	m_h	0.44×10^6	kg
D	14.00	m	k	1.51×10^6	N/m
h	30.00	m	H_s	3.00	m
m	1.84×10^6	kg	T_p	7.42	s

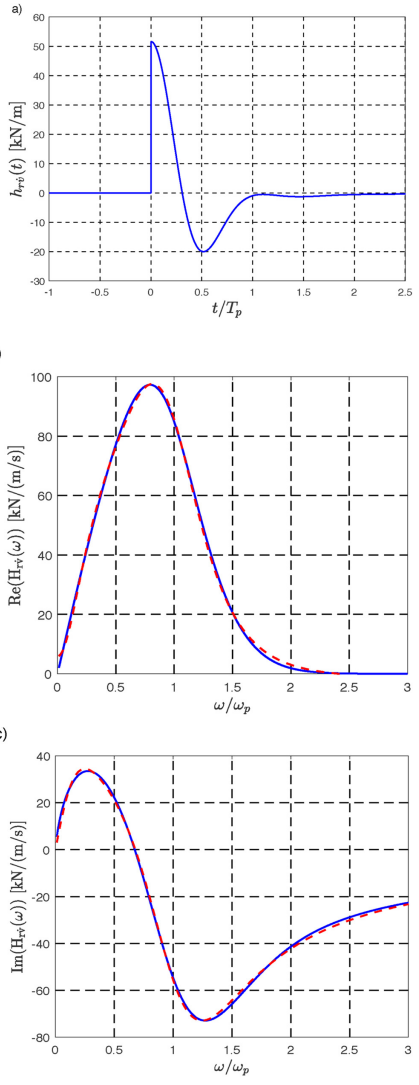

Fig. 2. Radiation force. (a) Impulse response function, $h_{rr}(t)$. (b) Real part $\mathrm{Re}(H_{rr}(\omega))$ of frequency response function. (c) Imaginary part $\mathrm{Im}(H_{rr}(\omega))$ of frequency response function. ——: Numerical determined target. - - -: Rational approximation of order $(m, n) = (2, 3)$.

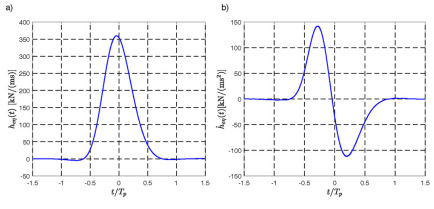

Fig. 3. Impulse response functions for wave excitation force. (a) $h_{e\eta}(t)$. (b) $\dot{h}_{e\eta}(t)$.

disturbed by the radiation wave.

The time derivative of the wave excitation force, $\dot{f}_e(t)$, is given as:

$$\dot{f}_e(t) = \int_{-\infty}^{\infty} \dot{h}_{e\eta}(t-\tau)\eta(\tau)\,d\tau \tag{5}$$

Alternatively, $\dot{f}_e(t)$ may be obtained by numerical differentiation of the realizations of $f_e(t)$. $\dot{f}_e(t)$ is later used in the devised prediction algorithm for the wave excitation force.

The impulse response function $\dot{h}_{e\eta}(t)$ in Eq. (5) may be calculated from the following Fourier transform [11]:

$$\dot{h}_{e\eta}(t) = \frac{1}{2\pi}\int_{-\infty}^{\infty} e^{i\omega t}\, i\omega\, H_{e\eta}(\omega)\,d\omega \tag{6}$$

where $H_{e\eta}(\omega)$ indicates the frequency response function for the wave force, which can be calculated numerically by a boundary element method. In the present paper, the WAMIT program [13] has been applied.

Fig. 3 shows the impulse response function $h_{e\eta}(t)$ and $\dot{h}_{e\eta}(t)$ for the considered point absorber. As seen, both impulse response functions effectively vanishes for $|t| > T_{f_e}$, $T_{f_e} \simeq 0.7\,T_p$. T_{f_e} indicates the prediction horizon for the wave excitation force.

Fig. 4a and b show simulated realizations of the Gaussian surface elevation process $\eta(t)$ defined by the double-sided JONSWAP auto-spectral density function given by Eq. (29) with the the indicated values of the significant wave height H_s and the peak period T_p, and with the bandwidth parameters $\gamma = 1$ and $\gamma = 5$, respectively. $\gamma = 1$ specifies the sea-state in open sea with unlimited fetch, whereas $\gamma = 5$ applies to a relatively small fetch.

Fig. 5a and c show realizations of the wave excitation force process $f_e(t)$ for $\gamma = 1$ and $\gamma = 5$, respectively, as calculated by Eq. (4) based on the corresponding realizations of the surface elevation process $\eta(t)$ shown in Fig. 4. Fig. 5b and d show the corresponding realization of the

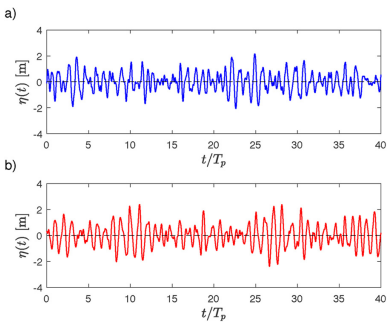

Fig. 4. Realizations of the surface elevation process $\eta(t)$, $H_s = 3.00$ m, $T_p = 7.42$ s. (a) $\gamma = 1$. (b) $\gamma = 5$.

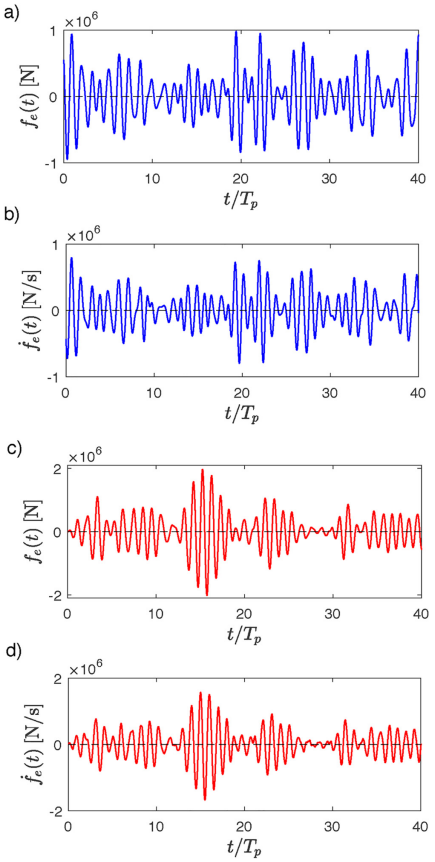

Fig. 5. Realizations of the wave excitation force process $f_e(t)$ and its derivative $\dot{f}_e(t)$, $H_s = 3.00$ m, $T_p = 7.42$ s. (a, b) $\gamma = 1$. (c, d) $\gamma = 5$.

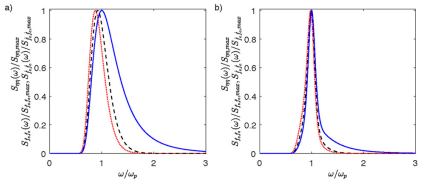

Fig. 6. Normalized double-sided auto-spectral density functions of $\eta(t)$, $f_e(t)$, $\dot{f}_e(t)$. (a) $\gamma = 1$. (b) $\gamma = 5$. ——: $\eta(t)$. ·····: $f_e(t)$. – – –: $\dot{f}_e(t)$.

time derivative $\dot{f}_e(t)$. As seen, the realizations of $f_e(t)$ and $\dot{f}_e(t)$ are significantly more narrow-banded than the underlying surface elevations realizations. The double-sided auto-spectral density functions of the surface elevation $\eta(t)$, the wave load $f_e(t)$ and its time derivative $\dot{f}_e(t)$ have been shown in Fig. 6a and b for the wave spectrum bandwidth parameters $\gamma = 1$ and $\gamma = 5$ indicating broadbanded and narrowbanded sea-states, respectively. As seen, the wave spectrum $S_{\eta\eta}(\omega)$ is significantly more broadbanded than $S_{f_e f_e}(\omega)$ and $S_{\dot{f}_e \dot{f}_e}(\omega)$ for both cases of γ. This observation will be used in the estimation algorithm of the wave excitation force $f_e(t)$ presented in Section 2.3.1.

2.2. Optimal control problem

The control problem for maximizing the absorbed power during the interval $]t_0,\ t_1]$ with constraints on the absorber displacement may be defined as:

$$\left.\begin{array}{l} \max J\,[\dot{v}, f_c] = \int_{t_0}^{t_1} f_c(\tau)\dot{v}(\tau)\,d\tau \\ \text{subject to the path constraint given by Eq. (1),} \\ \text{and to the displacement constraint:} \\ v_{\min} \le v(t) \le v_{\max} \end{array}\right\} \tag{7}$$

Let $v_{m,i}$ denote either $v_{\max}$ or $v_{\min}$, and let $[t_{a,i},\ t_{b,i}]$ indicate the ith interval where the constrain $v_{m,i}$ is activated, see Fig. 7.

Since $\dot{v}(t) = \ddot{v}(t) = 0$ in the constraint intervals, the integro-differential equation (1) provides the following relation for the control force for $t \in [t_{a,i},\ t_{b,i}]$:

$$f_c(t) = f_e(t) + C_i \tag{8}$$

where C_i is a constant given as:

$$C_i = -\int_{t_0}^{t_{a,i}} h_{r\dot{v}}(t_{a,i} - \tau)\,\dot{v}(\tau)\,d\tau - r(v_{m,i}) \tag{9}$$

Assume that $\dot{v}(t)$ is observed continuously in the interval $[t_0,\ t_{a,i}[$. Then, C_i can be calculated by Eq. (9).

Eq. (8) indicates that the optimal control law is of the open loop type, whenever the displacement constraint is active. Hence, the wave excitation force $f_e(t)$ needs to be estimated in these intervals.

The corresponding optimal control problem in the interval $]t_{b,i},\ t_{a,i+1}[$, where no constraint is active, has previously been solved by the authors [14]. The solution may be given as:

$$f_c(t) = f_{c,0}(t) + D_i \tag{10}$$

where:

$$f_{c,0}(t) = -M\ddot{v}(t) + \int_t^{t_1} h_{r\dot{v}}(\tau - t)\,\dot{v}(\tau)\,d\tau - r(v(t)) \tag{11}$$

D_i is a constant, which can be calibrated at the interface to the previous constrained interval. From Eqs. (8) and (10) follows:

$$f_c(t_{b,i}) = f_e(t_{b,i}) + C_i = f_{c,0}(t_{b,i}) + D_i \tag{12}$$

Similarly, we have for the previous unconstrained interval at the boundary at $t = t_{a,i}$:

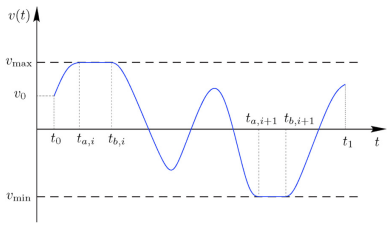

Fig. 7. Constrained displacement response. Definition of parameters.

$$f_c(t_{a,i}) = f_e(t_{a,i}) + C_i = f_{c,0}(t_{a,i}) + D_{i-1} \tag{13}$$

Since, $f_{c,0}(t_{a,i}) = f_{c,0}(t_{b,i})$ it follows from Eqs. (12) and (13):

$$D_i = D_{i-1} + f_e(t_{a,i}) - f_e(t_{b,i}), \quad i = 1, 2, \ldots \tag{14}$$

$f_c(t) = f_{c,0}(t)$ during the first unconstrained interval $[t_0, t_{a,1}]$, so $D_0 = 0$. Hence, Eq. (14) provides a recursive relation for the determination of the constants D_i, if the wave excitation force at the boundaries of the constrained intervals can be determined.

Due to accumulated estimation errors of the wave excitation forces, Eq. (14) becomes increasingly inaccurate. To remedy this, D_i should occasionally be calculated directly from Eq. (12) leading to:

$$D_i = f_e(t_{b,i}) + C_i - \int_{t_{b,i}}^{t_i} h_{rv}(\tau - t_{b,i})\,\dot{v}(\tau)\,d\tau + r(v_{m,i}) \tag{15}$$

where it has been used that $\ddot{v}(t_{b,i}) = 0$ in the expression for $f_{c,0}(t_{b,i})$ given by Eq. (11). Eq. (15) requires a prediction of $\dot{v}(\tau)$, $\tau \in [t_{b,i}, t_{b,i} + T_v]$.

2.3. Estimation and prediction problems

The solution for the optimal control law $f_c(t)$ as given by Eqs. (8)–(12) requires that the wave excitation force $f_e(t)$ can be estimated during the constrained time intervals, cf. Eq. (8). In the unconstrained intervals the evaluation of the function $f_{c,0}(t)$ given by Eq. (11) requires that the velocity $\dot{v}(\tau)$ ahead of the present time t to be predicted. Because the support of the impulse response function $h_{rv}(t)$ is effectively confined to the interval $[0, T_p]$, the prediction horizon is limited to $T_v \simeq T_p$, cf. Fig. 2a.

The estimation and prediction procedures described below presume that the surface elevation $\eta(t)$ and the vertical acceleration $\ddot{v}(t)$ of the absorber are continuously measured. The displacement $v(t)$ and velocity $\dot{v}(t)$ are obtained by online integration of the acceleration signal.

2.3.1. Estimation of wave excitation force

The wave excitation force and its derivative at the time $t - T_{f_e}$ may be written as, cf. Eqs. (4) and (6):

$$\left.\begin{aligned} f_e(t - T_{f_e}) &\simeq \int_{-\infty}^{t} h_{e\eta}(t - T_{f_e} - \tau)\,\eta(\tau)\,d\tau \\ \dot{f}_e(t - T_{f_e}) &\simeq \int_{-\infty}^{t} \dot{h}_{e\eta}(t - T_{f_e} - \tau)\,\eta(\tau)\,d\tau \end{aligned}\right\} \tag{16}$$

Eq. (16) is based on the fact that $h_{e\eta}(-T_{f_e}) \simeq \dot{h}_{e\eta}(-T_{f_e}) \simeq 0$, cf. Fig. 3a and b, so surface elevations beyond the time t will not affect the left-hand sides of Eq. (16). Further, the surface elevation $\eta(\tau)$ is available up to and including the time t.

$f_e(t)$ and $\dot{f}_e(t)$ may be represented by a van der Pol transformation defined as, [15]:

$$\left.\begin{aligned} f_e(t) &= a_e(t)\cos(\omega_p t + \varphi_e(t)) \\ \dot{f}_e(t) &= -\omega_p\, a_e(t)\sin(\omega_p t + \varphi_e(t)) \end{aligned}\right\} \tag{17}$$

where the amplitude process $a_e(t)$ and the phase process $\varphi_e(t)$ are given as:

$$\left.\begin{aligned} a_e(t) &= \sqrt{f_e^2(t) + \left(\frac{\dot{f}_e(t)}{\omega_p}\right)^2} \\ \varphi_e(t) &= \arctan\left(-\frac{\dot{f}_e(t)}{\omega_p f_e(t)}\right) - \omega_p t \end{aligned}\right\} \tag{18}$$

Because $f_e(t)$ and $\dot{f}_e(t)$ are narrow-banded stochastic processes, $a_e(t)$ and the $\varphi_e(t)$ become slowly varying functions with time. Alternatively, the Hilbert-Huang transform may be used, where $\frac{\dot{f}_e(t)}{\omega_p}$ is replaced by the Hilbert transform $\hat{f}_e(t)$ [16,17]. Actually, these alternatives are equivalent for harmonic varying signals.

Fig. 8 shows the realizations of $a_e(t)$ and $\varphi_e(t)$ for $\gamma = 1$ and $\gamma = 5$,

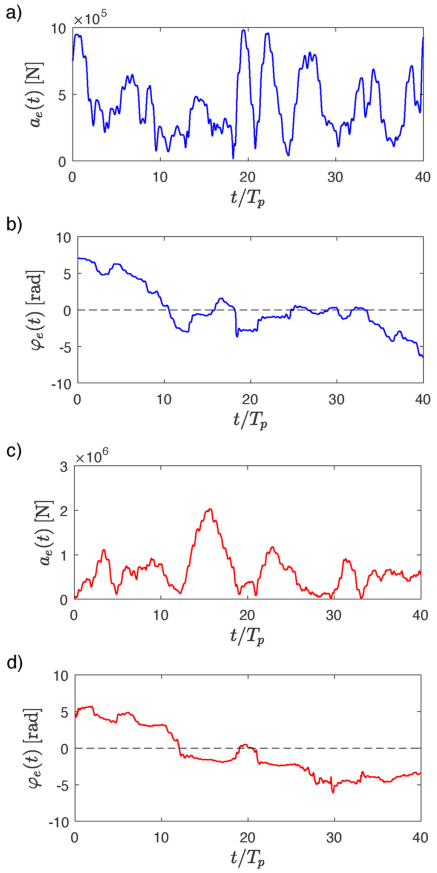

Fig. 8. Time-series of amplitude process $a_e(t)$ and phase process $\varphi_e(t)$, $H_s = 3.00$ m, $T_p = 7.42$ s. (a, b) $\gamma = 1$. (c, d) $\gamma = 5$.

respectively, based on the realizations of $f_e(t)$ and $\dot{f}_e(t)$ shown in Fig. 5.

Define the following quantities:

$$\left.\begin{aligned} a_{-j} &= a_e(t - T_{f_e} - j\,T_p) \\ \varphi_{-j} &= \varphi_e(t - T_{f_e} - j\,T_p) \end{aligned}\right\}, \quad j = 0, 1, 2, \ldots \tag{19}$$

Next, the values of $a_e(\tau)$ and $\varphi_e(\tau)$ for $\tau \in]t - T_{f_e}, t]$ are estimated by extrapolation from $\tau = t - T$ by means of 2nd order Lagrange polynomials calibrated by the function values at $t - T_{f_e}$, $t - T_{f_e} - T_p$ and $t - T_{f_e} - 2T_p$, given as:

$$\left.\begin{aligned} a_e(\tau) &= a_0 + \frac{1}{2}(3a_0 - 4a_{-1} + a_{-2})\,u + \frac{1}{2}(a_0 - 2a_{-1} + a_{-2})\,u^2 \\ \varphi_e(\tau) &= \varphi_0 + \frac{1}{2}(3\varphi_0 - 4\varphi_{-1} + \varphi_{-2})\,u + \frac{1}{2}(\varphi_0 - 2\varphi_{-1} + \varphi_{-2})\,u^2 \end{aligned}\right\} \tag{20}$$

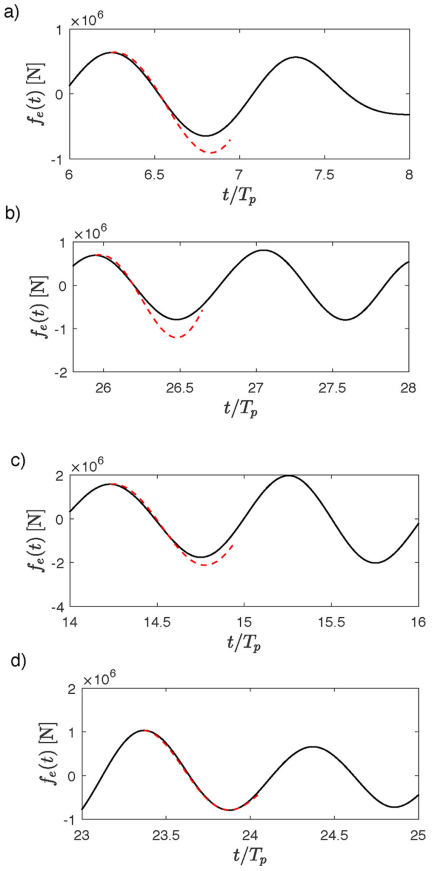

Fig. 9. Prediction of wave excitation force $f_e(t)$. (a, b) $\gamma = 1$. (c, d) $\gamma = 5$. ——: Nonlinear programming solution. – – –: Predicted wave load.

where

$$u = \frac{\tau - t + T_{f_e}}{T_p} \tag{21}$$

Then, $f_e(\tau)$ in the interval $]t - T_{f_e}, t]$ is predicted from:

$$f_e(\tau) = a_e(\tau)\cos(\omega_p \tau + \varphi_e(\tau)) \tag{22}$$

Fig. 9 illustrates prediction results for the wave excitation force $f_e(t)$ one prediction period $T_{f_e} = 0.7T_p$ ahead. Fig. 9a and b show predictions for $\gamma = 1$ at the instants of time $t = 6.2T_p$ and $t = 25.9T_p$ on the time-series shown in Fig. 5a. Fig. 9c and d show similar results for $\gamma = 5$ predicted at the instants of time $t = 14.2T_p$ and $t = 23.4T_p$ on the time-series shown in Fig. 5c. The predictions are more accurate for $\gamma = 5$, due to the enhanced narrow-bandedness of the time-series in this case.

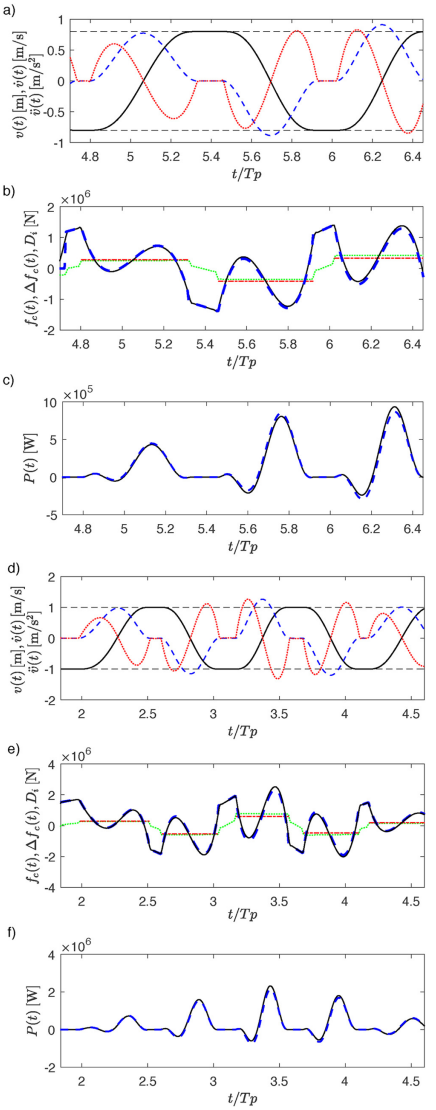

Fig. 12. Time-series of $v(t)$, $\dot{v}(t)$, $\ddot{v}(t)$, control force $f_e(t)$ and instantaneous absorbed power $P(t)$ at optimal control, $H_s = 3.00$ m, $T_p = 7.42$ s. (a–c) $\gamma = 1$, $v_{max} = -v_{min} = 0.8$ m. (d–f) $\gamma = 5$, $v_{max} = -v_{min} = 1$ m. (a, d) ——: $v(t)$. – – –: $\dot{v}(t)$. ·····: $\ddot{v}(t)$. (b, e) ——: Nonlinear programming solution. – – –: $f_e(t)$. – – –: $\Delta f_e(t)$. – · – ·: D_t. (c, f) ——: Nonlinear programming solution. – – –: $P(t)$.

2.3.2. Prediction of future velocities

The velocity response in the vicinity to the constrained interval is significantly influenced by the initial values $\dot{v}(t_{b,i}) = 0$. This initial values needs to be taken into consideration at the prediction of $\dot{v}(t)$, $t > t_{b,i}$.

As seen from Fig. 12a and b, $\dot{v}(t)$ is approximately skew-symmetric before and after the constrained interval $[t_{a,i}, t_{b,i}]$ corresponding to the relation:

$$\dot{v}(t) \simeq -\dot{v}(t_{a,i} + t_{b,i} - t), \quad t \in [t_{b,i}, t_{b,i} + T_{\dot{v}}] \tag{23}$$

The right hand side of Eq. (23) is available from previous measurements of the velocity response. Hence, Eq. (23) may be used to evaluate $f_{c,0}(t)$ for $t \in]t_{b,i}, t_{b,i} + T_{\dot{v}}]$. Further, the constant D_i given by Eq. (15) may be approximated as:

$$\begin{aligned} D_i &\simeq f_e(t_{b_i}) + C_i - \int_{t_{b_i}}^{t_{b,i}+T_{\dot{v}}} h_{rv}(\tau - t_{b_i})\,\dot{v}(\tau)\,d\tau + r(v_{m,i}) \\ &\simeq f_e(t_{b_i}) + C_i + \int_{t_{a_i}-T_{\dot{v}}}^{t_{a,i}} h_{rv}(t_{a,i} - \tau)\,\dot{v}(\tau)\,d\tau + r(v_{m,i}) \end{aligned} \tag{24}$$

Around one prediction interval $T_{\dot{v}}$ away from the constraints, corresponding to the time interval $[t_{b,i} + T_{\dot{v}}, t_{a,i+1} - T_{\dot{v}}]$, the response processes $v(t)$ and $\dot{v}(t)$ become stationary and narrow-banded for both $\gamma = 1$ and $\gamma = 5$, see Fig. 10. $v(t)$ is at an absolute extremum, when the displacement constraints are active, and may have one or more local maxima or minima between these states. At any of these extremes the velocity $\dot{v}(t) = 0$. As seen from Fig. 10, $\dot{v}(t)$ have exactly one local maximum or local minimum between the zeros, which is characterizing a narrowbanded response [11].

Then, velocities $\dot{v}(\tau)$, $\tau \in]t, t + T_{\dot{v}}]$ ahead of the present time t may be predicted by based on a van der Pol transformation similar to the one used for predictions of future wave excitation forces defined by Eqs. (17) and (18):

$$\left.\begin{aligned} v(t) &= a_v(t)\cos(\omega_p t + \varphi_v(t)) \\ \dot{v}(t) &= -\omega_p\, a_v(t)\sin(\omega_p t + \varphi_v(t)) \end{aligned}\right\} \tag{25}$$

where the slowly varying amplitude process $a_v(t)$ and the phase process $\varphi_v(t)$ given as:

$$\left.\begin{aligned} a_v(t) &= \sqrt{v^2(t) + \left(\frac{\dot{v}(t)}{\omega_p}\right)^2} \\ \varphi_v(t) &= \arctan\left(-\frac{\dot{v}(t)}{\omega_p\, v(t)}\right) - \omega_p t \end{aligned}\right\} \tag{26}$$

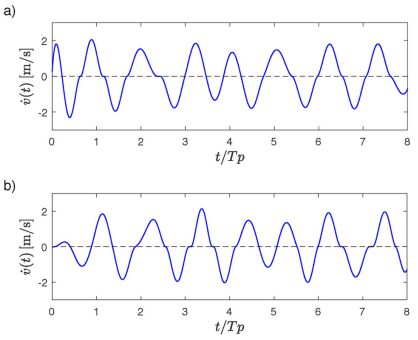

Fig. 10. Time-series of $\dot{v}(t)$, $H_s = 3.00$ m, $T_p = 7.42$ s, $v_{\max} = -v_{\min} = 2$ m. (a) $\gamma = 1$. (b) $\gamma = 5$.

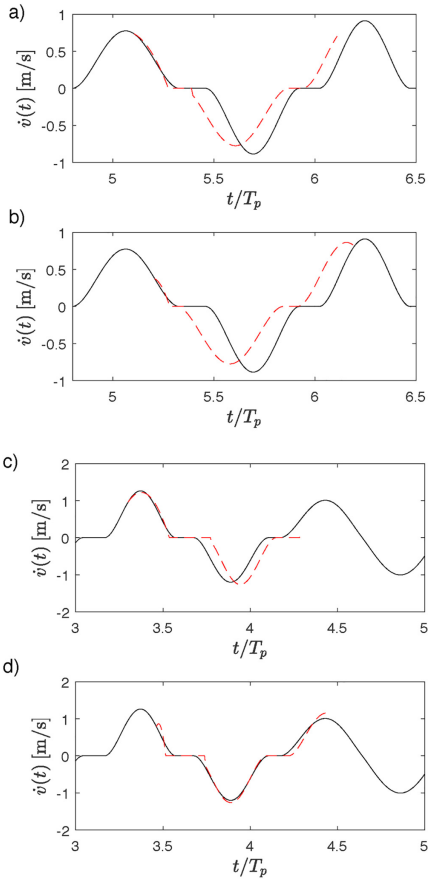

Fig. 11. Prediction of $\dot{v}(t)$, $H_s = 3.00$ m, $T_p = 7.42$ s. (a, b) $\gamma = 1$, $v_{\max} = -v_{\min} = 0.8$ m. (c, d) $\gamma = 5$, $v_{\max} = -v_{\min} = 1$ m. ——: Nonlinear programming solution. - - -: Predicted velocity.

At a certain instant of time t is checked whether the predicted displacement exceeds the boundaries during the prediction interval $[t, t + T_p]$. If so, the time $t_{a,i+1}$ is estimated from the prediction, and a cubic interpolation is applied for $v(t)$ in the interval $[t, t_{a,i+1}]$, given as:

$$v(\tau) = v(t) + \dot{v}(t)(\tau - t_{a,i+1}) + a(\tau - t_{a,i+1})^2 + b(\tau - t_{a,i+1})^3 \tag{27}$$

where

$$\left.\begin{aligned} a &= \frac{1}{(t_{a,i+1} - t_0)^2}(3(v_{m,i+1} - v(t)) + 2\dot{v}(t)(t_{a,i+1} - t)) \\ b &= \frac{1}{(t_{a,i+1} - t_0)^3}(-2(v_{m,i+1} - v(t)) + \dot{v}(t)(t_{a,i+1} - t)) \end{aligned}\right\} \tag{28}$$

a and b are determined so $v(t_{a,i+1}) = v_{m,i+1}$ and $\dot{v}(t_{a,i+1}) = 0$.

Finally, the predicted velocity in the interval $[t_{a,i+1} - T_0, t_{a,i+1}]$ can be obtained by the derivative of the displacement indicated in Eq. (27). Combination with the skew-symmetric property of the velocity indicated in Eq. (23), the predicted velocity at least one period ahead can be obtained. Fig. 11 shows the predicted velocities for $\gamma = 1$ and $\gamma = 5$, separately.

3. Numerical example

A point heave wave energy converter indicated in Fig. 1 is considered in the numerical simulation. The relevant data of the absorber and the wave excitation parameters have been indicated in Table 1.

$S_{\eta\eta}(\omega)$ is taken as the double-sided JONSWAP auto spectral density function given as [18]:

$$S_{\eta\eta}(\omega) = \delta \frac{H_s^2}{\omega_p} \gamma^{\beta} \left(\frac{|\omega|}{\omega_p}\right)^{-5} \exp\left(-\frac{5}{4}\left(\frac{\omega}{\omega_p}\right)^{-4}\right) \tag{29}$$

where

$$\left.\begin{aligned} \delta &= \frac{0.0312}{0.230 + 0.0336\gamma - \frac{0.185}{1.9+\gamma}} \\ \beta &= \exp\left(-\frac{1}{2}\left(\frac{|\omega| - \omega_p}{\sigma\,\omega_p}\right)^2\right) \\ \sigma &= \begin{cases} 0.07, & |\omega| \le \omega_p \\ 0.09, & |\omega| > \omega_p \end{cases} \end{aligned}\right\} \tag{30}$$

T_p is the peak period, $\omega_p = \frac{2\pi}{T_p}$ is the related angular peak frequency and H_s is the significant wave height. γ is the so-called peak enhancement parameter which controls the bandwidth of the spectrum.

The validity of the theoretical optimal control solution given by Eqs. (8)–(12) has been verified by comparison to a numerical solution obtained by the nonlinear programming algorithm described in Appendix A.

Fig. 12a and d show the trajectories of $v(t)$, $\dot{v}(t)$, $\ddot{v}(t)$ with the displacement constraints $v_{\max} = -v_{\min} = 0.8\,\mathrm{m}$ and $v_{\max} = -v_{\min} = 1.0\,\mathrm{m}$ at optimal control determined by the nonlinear programming algorithm for $\gamma = 1$ and $\gamma = 5$, respectively. The nonlinear programming solutions are merely available at discrete points separated at the distance $\Delta t = \frac{T_p}{150}$.

Because, the first and second derivative of the displacement response and the first derivative of the velocity response vanish in the constrain intervals $[t_{a,i}, t_{b,i}]$, these responses are flat at the boundaries of these intervals. Hence, neither of these responses are suitable for identifying the times $t_{a,i}$ and $t_{b,i}$, which are essential to the devised control algorithm. Instead, $t_{a,i}$ and $t_{b,i}$ should be determined from the observed time series of the acceleration response which has an early detected discontinuous change of slope at the entrance and exit of the constrained interval as shown in Fig. 7a and d. Further, the velocity response between the constrained intervals turns out to be significantly narrow-banded. This observation will be used in the estimation algorithm of the unconstrained control force $f_{c,0}(t)$ given by Eq. (11).

Fig. 12b and e show the variation with time of the optimal control force $f_c(t)$ and the theoretical solution given by Eqs. (8)–(12) for $\gamma = 1$ and $\gamma = 5$, respectively, using the optimal response trajectories shown in Fig. 7a and d in the theoretical solution. Also shown in the figure is the difference $\Delta f_c(t) = f_c(t) - f_{c,0}(t)$ between the constrained intervals. According to Eq. (11) this difference is given by the constant D_i. The small deviation between these is assumed to be caused by uncertainty in the determination of the boundaries t_{a_i} and $t_{b,i}$ of the constrained interval from the available discrete time specification of $\ddot{v}(t)$. As seen,

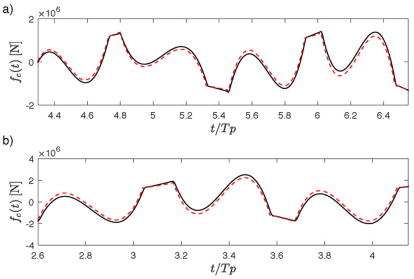

Fig. 13. Prediction of $f_c(t)$, $H_s = 3.00$ m, $T_p = 7.42$ s. (a) $\gamma = 1$, $v_{\max} = -v_{\min} = 0.8\,\mathrm{m}$. (b) $\gamma = 5$, $v_{\max} = -v_{\min} = 1\,\mathrm{m}$. ——: Nonlinear programming. - - -: Predicted control force.

the estimate of D_i is valid up to and including the time $t_{a,i+1}$, although this constant has been calibrated at the time $t_{b,i}$ at the end of the previous constrained interval.

Fig. 12c and f show the variation with time of the instantaneous absorbed power $P(t) = f_c(t)\dot{v}(t)$ at optimal control for $\gamma = 1$ and $\gamma = 5$, respectively. The deviation is quite insignificant.

Summing up, the devised control algorithm for optimal power take-off requires the sequence of constants C_i and D_i to be determined, along with estimation of the wave load $f_e(t)$ and the unconstrained control force $f_{c,0}(t)$. C_i is obtained from Eq. (9) and D_i from Eq. (14) or Eq. (15). The instants of time for entrance and exit of the constrained intervals is most reliable obtained from observation of the acceleration signal.

Based on Eqs. (10) and (24) the control force for unconstrained parts can be obtained. The constrained parts can be determined from the continuous measurement of the responses of the absorber. Fig. 13 shows the predicted control forces for $\gamma = 1$ and $\gamma = 5$. As seen, a good agreement is shown in Fig. 13.

Here the influence of the deviation of the predicted control force on the trajectory will not be considered. It assumed that the acceleration of the absorber can be measured continuously. Correspondingly, the times $t_{a,i}$ and $t_{b,i}$ can be determined in real time.

4. Conclusions

The paper presents a semi-analytical solution for the optimal power take-off of a heave point wave energy converter with the constrained displacements. The solution requires that the wave excitation force can be estimated during active displacement constraints, and that the velocity response between constrained states can be predicted at least one wave period ahead. To handle these problems physical based estimation and prediction algorithms have been devised, which make use of the narrow-banded character of the wave excitation force and the unconstrained velocity response. The obtained control law has been verified against numerical solutions based on nonlinear programming for relatively broad-banded and narrow-banded sea states. In both cases a good agreement is obtained.

Acknowledgements

The authors gratefully acknowledge the financial support from project 675659-ICONN-H2020-MSCA-ITN-2015.

Appendix A. Nonlinear programming algorithm

The optimal control problem in Eq. (7) is reformulated as a nonlinear programming problem by discretizing the objective functional and the state

vector in time:

$$\left.\begin{array}{l}\max \quad J(\mathbf{X}(\tau_M)) = x_{n+3}(\tau_M)\\ \text{subjecttothepathandinequalityconstraints:}\\ \mathbf{c}(\mathbf{X}(\tau_j)) = \mathbf{0}\\ \mathbf{h}(\mathbf{X}(\tau_j)) = \begin{bmatrix} v(\tau_j) & -v_{\max} \\ -v(\tau_j) & +v_{\min}\end{bmatrix} - \mathbf{s}(\tau_j) = \mathbf{0}\\ \mathbf{s}(\tau_j) \geq \mathbf{0}\end{array}\right\} \tag{31}$$

where $\tau_j = t_0 + j\,\Delta\tau\; j = 0, 1, \ldots, M$.

$\mathbf{s}(t)$ indicates a vector function of slack variables. The time step in the discretization of the interval$]t_0, t_1]$ is given as $\Delta\tau = \frac{t_1 - t_0}{M}$. The vector $\mathbf{X}(t)$ of dimension $2n + 6$ and the path constrain vector $\mathbf{c}(\mathbf{X}(t))$ of dimension $n + 3$ are defined as:

$$\mathbf{X}(t) = \left[v(t),\ \dot{v}(t),\ \mathbf{z}_r^T(t),\ x_{n+3}(t),\ \frac{d}{\mathrm{d}t}v(t),\ \frac{d}{\mathrm{d}t}\dot{v}(t),\ \frac{d}{\mathrm{d}t}\mathbf{z}_r^T(t),\ \frac{d}{\mathrm{d}t}x_{n+3}(t)\right]^T \tag{32}$$

$$\mathbf{c}(\mathbf{X}(t)) = \begin{bmatrix} \dfrac{d}{\mathrm{d}t}v(t) - \dot{v}(t) \\ M\dfrac{d}{\mathrm{d}t}\dot{v}(t) + \mathbf{p}_r\,\mathbf{z}_r(t) + r(v(t)) - f_c(t) + f_c(t) \\ \dfrac{d}{\mathrm{d}t}\mathbf{z}_r(t) - \mathbf{A}_r\,\mathbf{z}_r(t) - \mathbf{b}_r\,\dot{v}(t) \\ \dfrac{d}{\mathrm{d}t}x_{n+3}(t) - f_c(t)\dot{v}(t)\end{bmatrix} \tag{33}$$

$\mathbf{z}_r(t)$ is a state vector, $\mathbf{A}_r$ is a quadratic matrix, and $\mathbf{b}_r$ and $\mathbf{p}_r$ are column and row vectors related to the convolution integral in Eq. (1), all defined in Appendix B.

The inherent approximation in the indicated nonlinear programming formulation concerns the discretization of the time continuous problem into $M + 1$ discrete instants of time for optimization, and the use of the rational approximation in Eq. (38) for the force $f_{r,0}(t)$.

The formulation applies to both displacement constraints and control force constraints. In case, merely control force constraints are prescribed the algorithm is applied by using large values of $v_{\max}$ and small values of $v_{\min}$.

The applied algorithm for solving the indicated nonlinear programming problem is described in El-Bakry et al. [19].

It should be noted that the optimal solution obtained by the nonlinear programming depends qualitatively and quantitatively on the applied time step $\Delta\tau$. Fig. 14a and c show the obtained time series of displacement $v(t)$ and the acceleration $\ddot{v}(t)$ for $v_{\max} = -v_{\min} = 4$m with the constraints checked the intervals $\Delta\tau = 0.05$s and $\Delta\tau = 0.01$s, respectively. In Fig. 14a, the acceleration is not zero when the displacement reaches the boundary, which means that the displacement constraint is not active in a finite time interval, and $v(t)$ is merely tangential to the constraint. In contrast, in Fig. 14c the constraint is everywhere active in a finite time interval, as assumed in the theory.

Fig. 14b and d indicate the instantaneous absorbed power $P(t)$ as predicted by the nonlinear programming algorithm during a control interval $[0, 8T_p]$ for the two time steps. The absorbed energy $E = \int P(\tau)d\tau$ during the interval becomes $E = 29.87$MJ for $\Delta\tau = 0.05$s and $E = 30.61$MJ for $\Delta\tau = 0.01$s. Actually, E turns out to be monotonously decreasing function of $\Delta\tau$, as shown in Fig. 15. The theoretical solution given by Eqs. (8) and (10) checks the constraints throughout the control interval $[t_0, t_1]$. Hence, it is expected that the nonlinear programming solutions approach the theoretical solution in the limit $\Delta\tau \to 0$.

Appendix B. State vector formulation of equation of motion

The nonlinear programming algorithm presumes a state vector description of the integro-differential equation of motion (1). To achieve this the frequency response function $H_{rv}(\omega)$ given by Eq. (3) is approximated by a rational function:

$$\tilde{H}_{rv}(\omega) = \frac{P(s)}{Q(s)}, \quad s = i\omega \tag{34}$$

$$\left.\begin{array}{ll} P(s) & = p_0\,s^m + \cdots + p_{m-1}\,s + p_m \\ Q(s) & = s^n + q_1\,s^{n-1} + \cdots + q_{n-1}\,s + q_n \\ & = (s - s_1)\cdots(s - s_{n-1})(s - s_n)\end{array}\right\} \tag{35}$$

where $m < n$. $p_0, \ldots, p_m$ and $q_1, \ldots, q_n$ are real constants determined, so $\tilde{H}_{rv}(\omega)$ approximates the target frequency function $H_{rv}(\omega)$ at best in some normed sense, and so the poles (roots of the denominator polynomial) s_j, $j = 1, \ldots, n$ all have negative real part, $\mathrm{Re}(s_j) < 0$. The latter condition is the necessary and sufficient condition for causality and asymptotic stability of the filter defined by Eq. (34). A rational approximation of the order $(m, n) = (2, 3)$ has been shown with a dashed signature in Fig. 2b and c, and was used in the nonlinear programming analysis.

Consider the convolution integral:

$$f_{c,0}(t) = \int_{t_0}^{t} h_{rv}(t - \tau)\,\dot{v}(\tau)\,d\tau \tag{36}$$

Then, $f_{r,0}(t)$ may be obtained as output to the following system of linear, ordinary filter differential equations driven by the velocity $\dot{v}(t)$:

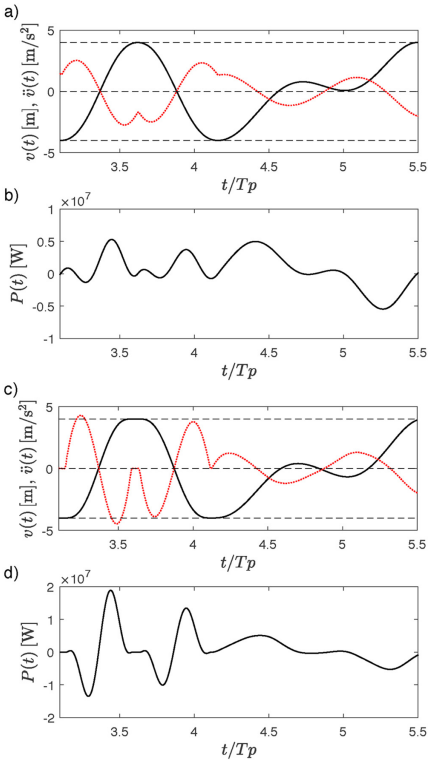

Fig. 14. Time-series of $v(t)$, $\ddot{v}(t)$ and instantaneous absorbed power $P(t)$ at optimal control, $\gamma = 5$, $H_s = 3.00$ m, $T_p = 7.42$ s, $v_{\max} = -v_{\min} = 4$ m. (a, b) $\Delta\tau = 0.05$s. (c, d) $\Delta\tau = 0.01$s.

$$\left.\begin{aligned} f_{r,0}(t) &= p_0 \frac{d^m x(t)}{\mathrm{d}t^m} + p_1 \frac{d^{m-1} x(t)}{\mathrm{d}t^{m-1}} + \cdots + p_{m-1} \frac{\mathrm{d}x(t)}{\mathrm{d}t} + p_m x(t) \\ \frac{d^n x(t)}{\mathrm{d}t^n} &+ q_1 \frac{d^{n-1} x(t)}{\mathrm{d}t^{n-1}} + \cdots + q_{n-1} \frac{\mathrm{d}x(t)}{\mathrm{d}t} + q_n x(t) = \dot{v}(t) \end{aligned}\right\} \tag{37}$$

where $x(t)$ is an auxiliary response process without any physical interpretation.

Eq. (37) may be represented on the state vector form:

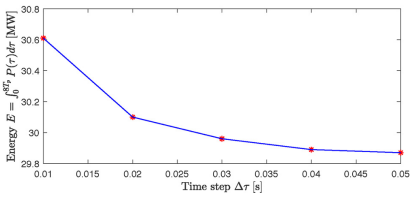

Fig. 15. Variation of the absorbed energy with different time step $\Delta\tau$.

$$\left.\begin{aligned} f_{r,0}(t) &= \mathbf{p}_r\,\mathbf{z}_r(t) \\ \frac{d}{\mathrm{d}t}\mathbf{z}_r(t) &= \mathbf{A}_r\,\mathbf{z}_r(t) + \mathbf{b}_r\,\dot{v}(t), \quad t \in]t_0, t_1] \\ \mathbf{z}_r(t_0) &= \mathbf{0} \end{aligned}\right\} \tag{38}$$

The initial value $\mathbf{z}_r(t_0) = \mathbf{0}$ follows because $f_{r,0}(t_0) = 0$.

The state vector $\mathbf{z}_r(t)$, the column vector $\mathbf{b}_r$, the system matrix $\mathbf{A}_r$ and the row vector $\mathbf{p}_r$ are given as:

$$\left.\begin{aligned} \mathbf{z}_r(t) &= \begin{bmatrix} x(t) \\ \frac{d}{\mathrm{d}t}x(t) \\ \vdots \\ \frac{d^{n-2}}{\mathrm{d}t^{n-2}}x(t) \\ \frac{d^{n-1}}{\mathrm{d}t^{n-1}}x(t) \end{bmatrix}, \quad \mathbf{b}_r = \begin{bmatrix} 0 \\ 0 \\ \vdots \\ 0 \\ 1 \end{bmatrix} \\ \mathbf{A}_r &= \begin{bmatrix} 0 & 1 & \cdots & 0 & 0 \\ 0 & 0 & \cdots & 0 & 0 \\ \vdots & \vdots & \ddots & \vdots & \vdots \\ 0 & 0 & \cdots & 0 & 1 \\ -q_n & -q_{n-1} & \cdots & -q_2 & -q_1 \end{bmatrix} \\ \mathbf{p}_r &= [p_m \quad p_{m-1} \cdots p_1 \quad p_0 \quad 0 \cdots 0] \end{aligned}\right\} \tag{39}$$

Then, Eq. (1) may be represented by the state vector differential equation:

$$\left.\begin{aligned} \frac{d}{\mathrm{d}t}\mathbf{z}(t) &= \mathbf{g}(\mathbf{z}(t), f_c(t), t), \quad t \in [t_0, t_1] \\ \mathbf{z}(t_0) &= \mathbf{z}_0 \end{aligned}\right\} \tag{40}$$

The state vector $\mathbf{z}(t)$, the initial value vector $\mathbf{z}_0$ and the right hand side of the state vector equation $\mathbf{g}(\mathbf{z}(t), f_c(t), t)$ are given as:

$$\mathbf{z}(t) = \begin{bmatrix} v(t) \\ \dot{v}(t) \\ \mathbf{z}_r(t) \end{bmatrix}, \quad \mathbf{z}_0 = \begin{bmatrix} v(t_0) \\ \dot{v}(t_0) \\ \mathbf{0} \end{bmatrix} \tag{41}$$

$$\mathbf{g}(\mathbf{z}(t), f_c(t), t) = \begin{bmatrix} \dot{v}(t) \\ \frac{1}{M}\Big(-\mathbf{p}_r\mathbf{z}_r(t) - r(v(t)) + f_e(t) - f_c(t)\Big) \\ \mathbf{A}_r\mathbf{z}_r(t) + \mathbf{b}_r\dot{v}(t) \end{bmatrix} \tag{42}$$

References

[1] R.F. Hartl, S.P. Sethi, R.G. Vickson, A survey of the maximum principles for optimal control problems with state constraints, SIAM Rev. 37 (2) (1995) 181–218.

[2] D.S. Naidu, Optimal Control Systems, CRC Press, 2002.

[3] D. Jacobson, M. Lee, A transformation technique for optimal control problems with a state variable inequality constraint, IEEE Trans. Autom. Control 14 (5) (1969) 457–464.

[4] L. Lasdon, S. Mitter, A. Waren, The conjugate gradient method for optimal control problems, IEEE Trans. Autom. Control 12 (2) (1967) 132–138.

[5] H. Eidsmoen, Optimum control of a floating wave-energy converter with restricted amplitude, J. Offshore Mech. Arct. Eng. 118 (2) (1996) 96–102.

[6] L.V. Perez, G.O. Garcia, State constrained optimal control applied to supervisory control in HEVs, Oil Gas Sci. Technol. – Revue de l'Institut Francais du Petrole 65 (1) (2010) 191–201.

[7] J. Hals, J. Falnes, T. Moan, Constrained optimal control of a heaving buoy wave-energy converter, J. Offshore Mech. Arct. Eng. 133 (1) (2011) 011401.

[8] M.T. Sichani, J.B. Chen, M.M. Kramer, S.R.K. Nielsen, Constrained optimal stochastic control of non-linear wave energy point absorbers, Appl. Ocean Res. 47 (2014) 255–269.

[9] L. Wang, J. Engstrom, M. Goteman, J. Isberg, Constrained optimal control of a point absorber wave energy converter with linear generator, J. Renew. Sustain. Energy 7 (4) (2015) 043127.

[10] W. Cummins, The impulse response functions and ship motions, Schiffstechnik 9 (1962) 101–109.

[11] S.R.K. Nielsen, Z. Zhang, Stochastic Dynamics, Aarhus University Press, 2017.

[12] J. Falnes, Ocean Waves and Oscillating Systems: Linear Interactions Including Wave-Energy Extraction, Cambridge University Press, 2002.

[13] WAMIT, User Manual, Version 7.0, Technical Report, (2011).

[14] S.R.K. Nielsen, Q. Zhou, M.M. Kramer, B. Basu, Z. Zhang, Optimal control of non-linear wave energy point converters, Ocean Eng. 72 (2013) 176–187.

[15] J.B. Roberts, P.D. Spanos, Random Vibration and Statistical Linearization, Courier Corporation, 2003.

[16] N.E. Huang, et al., The empirical mode decomposition and the Hilbert spectrum for nonlinear and non-stationary time series analysis, Proc. R. Soc. Lond. A: Math. Phys. Eng. Sci. 454 (1998) 903–995.

[17] H. Cramer, M.R. Leadbetter, Stationary and Related Stochastic Processes, Wiley, New York, 1967.

[18] K. Hasselmann, T.P. Barnett, E. Bouws, et al., Measurements of Wind Wave Growth and Swell Decay During the Joint North Sea Project (JONSWAP), Deutches Hydrographisches Institut, 1973.

[19] A.S. El-Bakry, R.A. Tapia, T. Tsuchiya, Y. Zhang, On the formulation and theory of the Newton interior-point method for nonlinear programming, J. Optim. Theory Appl. 89 (3) (1996) 507–541.

Paper C

Stochastic Optimal Control of a Heave Point Wave Energy Converter based on a Modified LQG Approach

Tao Sun, Søren R.K. Nielsen

The paper has been published in the
Ocean Engineering Vol. 154, pp. 357–366, 2018.

C.1 Author's Right

Journal author rights

In order for Elsevier to publish and disseminate research articles, we need publishing rights. This is determined by a publishing agreement between the author and Elsevier. This agreement deals with the transfer or license of the copyright to Elsevier and authors retain significant rights to use and share their own published articles. Elsevier supports the need for authors to share, disseminate and maximize the impact of their research and these rights, in Elsevier proprietary journals* are defined below:

For subscription articles	For open access articles
Authors transfer copyright to the publisher as part of a journal publishing agreement, but have the right to: • Share their article for Personal Use, Internal Institutional Use and Scholarly Sharing purposes, with a DOI link to the version of record on ScienceDirect (and with the Creative Commons CC-BY-NC- ND license for author manuscript versions) • Retain patent, trademark and other intellectual property rights (including research data). • Proper attribution and credit for the published work.	Authors sign an exclusive license agreement, where authors have copyright but license exclusive rights in their article to the publisher**. In this case authors have the right to: • Share their article in the same ways permitted to third parties under the relevant user license (together with Personal Use rights) so long as it contains a CrossMark logo, the end user license, and a DOI link to the version of record on ScienceDirect. • Retain patent, trademark and other intellectual property rights (including research data). • Proper attribution and credit for the published work.

https://www.elsevier.com/about/policies/copyright

Ocean Engineering 154 (2018) 357–366

Contents lists available at ScienceDirect

Ocean Engineering

journal homepage: www.elsevier.com/locate/oceaneng

Stochastic optimal control of a heave point wave energy converter based on a modified LQG approach

Tao Sun *, Søren R.K. Nielsen

Department of Civil Engineering, Aalborg University, 9000 Aalborg, Denmark

ARTICLE INFO

Keywords:
Wave energy
Heave absorber
Modified LQG control
Displacement and control force restriction
Kalman filtration

ABSTRACT

The optimal control constrain problem of a wave energy point absorber is constrained due to limited stroke and saturation of the control force actuator. The basic idea of this paper is to control the motion of the absorber by a modified LQG control where the constraints on the displacement and actuator force are approximately considered by counteracting the absorbed power in the objective quadratic functional. Based on rational approximations to the radiation force and the wave load, the integrated dynamic system can be reformulated as a linear stochastic differential equation which is driven by a unit intensity Gaussian white noise. The optimal LQG control force becomes a linear function of the state vector of the integrated system, which can only be partially observed. In order to remedy this problem, the control is combined with a Kalman filter observer. The obtained sub-optimal solution has been compared to the numerical optimal solution obtained by nonlinear programming. With suitable calculated gain parameters, the LQG controller can provide approximately the amount of the averaged absorbed power as that of the numerical optimum.

1. Introduction

A wave energy converter (WEC) extracts the mechanical energy in the wave motion and converts it into electric energy. Different kinds of WEC devices have been developed such as the oscillating water column plant (Ozkop and Altas, 2017), overtopping types like the Wave Dragon (Wavedragon, 2005), the Pelamis (Pelamis Wave, 2012), Archimedes Wave Swing (Archimedes Wave Swing, 2004), and the Wave Star Energy plant (Wave Star Energy, 2003).

A wave energy point absorber is a wave energy converter (WEC) with horizontal dimensions significantly smaller than the dominating wave length, which is capable of absorbing energy from waves propagating in arbitrary directions. Especially, a heave absorber is constrained by a mooring system or otherwise to move merely in the vertical direction.

Significant increase of the power take-off (PTO) of a heave absorber may be achieved by using an active vibration control of the vertical motion (Ringwood et al., 2014). In this connection many control strategies typical of the proportional derivative (PD) type have been suggested in the literatures. Nielsen et al. (2013) derived the optimal control law in irregular sea-states for a heave point absorber with non-linear buoyancy in case of no constraints on the displacements and the control force. The optimal control force turns out to make the absorber maximal flexible by eliminating the inertial load and the buoyancy stiffness totally. Further, the control law has feed-back from the present displacement and acceleration of the absorber and a non-causal feedback from the future velocities. Hence, for practical applications the indicated control law requires a prediction of future velocities. The predictor introduces uncertainty in the problem and makes the control sub-optimal.

Generally, there are constraints on the motion of the absorber due to the limited stroke of the actuator of the control system. Similarly, the available control force will be constrained between certain limits due to saturation. Based on the optimal control for the unconstrained case, Sichani et al. (2014) proposed an extension to the unconstrained case, where the displacement were achieved by adding the nonlinear artificial springs to the buoyancy, which were achieved close to the boundaries. Using predictive PD control, Wang et al. (2015) analyzed the motions of a point absorber. Based on truncated Fourier series of the control force and the velocity, the problem is converted to an optimization problem with a convex quadratic objective functional and nonlinear constraints. Cretel et al. (2011) proposed a control scheme to maximize the absorbed energy by a wave energy point absorber based on model predictive control. As a result of the introduction of triangle-hold discretization approach where the control force and the wave load need to be continuous piecewise linear, the objective functional is reformulated as a convex quadratic

* Corresponding author.
E-mail addresses: tsu@civil.aau.dk (T. Sun), srkn@civil.aau.dk (S.R.K. Nielsen).

https://doi.org/10.1016/j.oceaneng.2018.02.021
Received 1 May 2017; Received in revised form 3 January 2018; Accepted 5 February 2018

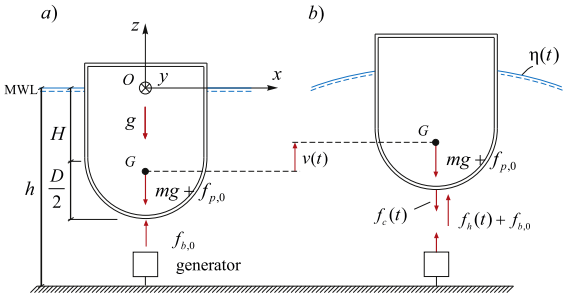

Fig. 1. Loads on heave absorber. a) Static equilibrium state. b) Dynamic state.

function of the increment of the control force. Constraints on the displacement of the absorber and the control force can be enforced to the system by affine inequality constraints on the input increment control force. However, the control law may give rise to feasibility issues for the hard constraints on the control force and may cause large amounts of energy flowing in and out of the system. Especially, it turns out that the instantaneous absorbed power may undergo large negative excursions which is not the care for the optimal control. Li et al. (2012) analyzed the nearly optimal control of wave energy converter with the state and control input constraints based on Pontryagins Minimum Principle. Further, the interior penalty term included in the cost functional replaces the state constraints, preventing the optimal state trajectory from approaching the boundary of the permitted region. The nearly optimal control approximated using discretization and dynamic programming turns out to be bang-bang control on the condition that the portions of the singular arc assuming that the times in which this happens are negligible are ignored, without rigorous proof for that. Zou et al. (2017) demonstrated that the singular arc part of the optimal control cannot be neglected and significant portions of time may become on singular arcs depending on the initial conditions and on the maximum control level. Hartl et al. (1995) presented the Pontryagins maximum principle for optimal control problems with both pure state and mixed variables inequality constraints. Further, the mixed constraints are the constraints on control variables that may depend on the state variables and the time.

As the optimal control turns out to be noncausal, i.e. the control law depends on the future motion of the absorber or wave load, prediction of the motion of the absorber or wave load should be considered. To remedy this question, a causal closed-loop controller with the feedback information is proposed. In case of infinite control horizon this problem can be circumvented by LQG control. Lattanzio and Scruggs (2011) derived the optimal causal controller for wave energy converter and the determination of the optimal causal controller distills to a nonstandard LQG optimal control problem, which can be solved easily. Scruggs et al. (2013) formulated the LQG control problem for wave energy converter and compared the results with the optimal noncausal control through choosing proper weights. Kassem et al. (2015) maximized the take-off power from a two-body point absorber with a mooring wave energy converter based on LQG approach and demonstrated the feasibility and effectiveness of the LQG control. In the present paper the basic idea is to deal with stochastic optimal control of a heave point wave absorber with constraints on the displacement and the control force, and with noisy observation on the displacement and the velocity. The radiation force and the wave load are reformulated as output of rational approximate filters. The integrated dynamic system may be given by a linear stochastic state vector differential equation driven by a Gaussian white noise. The idea of the paper is to take the constraints on the displacement and the control force into consideration by introducing negative penalty terms of the two parameters in the Lagrangian of a LQG approach, where the weights are calibrated against a nonlinear programming solution to provide the same mean power take-off. This does not guarantee a local observation of the indicated constraints, but merely that these are fulfilled in average. Further, the controller is combined with a Kalman filter, for which the reason is merely that the displacement and the velocity can be observed. The obtained sub-optimal results from assumed full state observation and partial state observation will be discussed and compared to numerical optimal controller from nonlinear programming. The stochasticity of the control problem origins partially from the nonobservable wave load and the noise related to the measured displacements and velocities. Hence, the indicated quantities need to be modelled by stochastic process.

2. Equation of motion of point absorber

Although, only the heave absorber shown in Fig. 1 will be analyzed, all results, including the equation of motion and control laws, may easily be carried over to other single-degree-of-freedom systems by slight modifications. The (x,y,z)-coordinate system is introduced as shown in Fig. 1. The original O is placed in the mean water level (MWL) at the centerline of the point absorber. The x-axis is the horizonal orientation in the direction of the wave propagation, and the z-axis is vertical orientation in the upward direction. Only two-dimensional (plane) regular or irregular waves are considered. The motion $v(t)$ of the body in the vertical z direction is defined relative to the static equilibrium state, where the static buoyancy force balances the gravity force and a possible static pre-stressing force from the generator.

In the dynamic state caused by the surface elevation $\eta(t)$ the WEC is excited by dynamic hydrodynamic force, $f_h(t)$, in addition to the static buoyancy force, and by an additional control force, $f_c(t)$ from an external hydraulic or electric force generator as the PTO system, which is used to control the motion of the absorber and to achieve maximal wave energy absorption. In theoretical research, it's assumed that the PTO system can provide the reactive power. In applications, the cylinder can operate as a pump, producing a bi-directional flow, which drives a hydraulic motor. The motor adapts to the flow and rectifies the flow into a unidirectional turning of the generator. Further, The PTO system will absorb a positive power from the absorber if the control force $f_c(t)$ and the velocity $\dot{v}(t)$ are in counter phase. In opposite case, the PTO system acts as a motor and supplies energy to the absorber. Next, the mechanical energy stored in the absorber is converted into electrical energy via an generator. Henceforth, $f_c(t)$ considered positive in the opposite direction of $v(t)$ will be referred to as the control force. Then, the equation of motion becomes:

$$m\ddot{v}(t) = f_h(t) - f_c(t) \tag{1}$$

Assuming linear wave theory $f_h(t)$ may be written as a superposition of the following contributions:

$$f_h(t) = f_b(t) + f_r(t) + f_e(t) \tag{2}$$

where $f_b(t)$ is the quasi-static increment of the buoyancy force, $f_r(t)$ is the radiation force generated by the motion of the absorber in still water, and $f_e(t)$ is the wave excitation force caused by the wave action, when the absorber is fixed in the static equilibrium state. The term $f_r(t)$ removes mechanical energy by generating a wave train propagating away from the absorber, whereas $f_e(t)$ supplies energy to the absorber. $f_b(t)$ is given as:

$$f_b(t) = \rho(D(v(t)) - D(0))\, g = -r(v(t)) \tag{3}$$

where ρ is the mass density of water, and $D(v(t))$ denotes the displaced water volume at the displacement $v(t)$. The nonlinear buoyancy function $r(v(t))$ is limited between the value r_1 corresponding to a fully submerged absorber, and the value $r_0 = -f_{b,0}$, when the absorber is jumping out of the water. Assuming small vertical vibrations, Eq. (3) may be linearized around the static equilibrium state as (Newman, 1977):

$$f_b(t) = -k\, v(t) \quad , \quad k = r'(0) = \rho\, D'(0)\, g = \frac{1}{4}\pi D^2 \rho g \tag{4}$$

The radiation force $f_r(t)$ may be written in terms of the following differential-integro relation (Cummins, 1962; Faltinsen, 1990):

$$f_r(t) = -m_h \ddot{v}(t) - f_{r,0}(t) \tag{5}$$

$$f_{r,0}(t) = \int_{-\infty}^{t} h_{rv}(t-\tau)\dot{v}(\tau)d\tau \tag{6}$$

The term m_h is the added water mass at infinite high frequencies, and $h_{rv}(t)$ is a causal impulse response function for the radiation force brought forward by the absorber velocity $\dot{v}(\tau)$.

Insertion of Eqs. (3), (5) and (6) in Eq. (1) provides the following integro-differential equation for $v(t)$ driven by $f_e(t)$ and $f_c(t)$:

$$\left.\begin{aligned} &(m+m_h)\ddot{v}(t) + r(v(t)) + \int_{t_0}^{t} h_{rv}(t-\tau)\dot{v}(\tau)d\tau = f_e(t) - f_c(t), t > t_0 \\ &v(t_0) = v_0, \dot{v}(t_0) = \dot{v}_0 \end{aligned}\right\} \tag{7}$$

where v_0 and $\dot{v}_0$ are given initial conditions at the time t_0.

Due to the causality of the impulse response function, the related frequency response function becomes:

$$H_{rv}(\omega) = \int_0^\infty \mathrm{e}^{-i\omega t} h_{rv}(t)dt \tag{8}$$

$M_h(\omega)$ and $C_h(\omega)$ denote the hydrodynamic added mass and the hydrodynamic radiation damping coefficient during monochromatic wave excitation. These are related to the imaginary and real parts of $H_{rv}(\omega)$ by the following sine and cosine transforms (Nielsen et al., 2013):

$$\left.\begin{aligned} &M_h(\omega) = m_h + \frac{1}{\omega}\mathrm{Im}(H_{rv}(\omega)) = m_h - \frac{1}{\omega}\int_0^\infty \sin(\omega t) h_{rv}(t)dt \\ &C_h(\omega) = \mathrm{Re}(H_{rv}(\omega)) = \int_0^\infty \cos(\omega t) h_{rv}(t)dt \end{aligned}\right\} \tag{9}$$

The wave excitation force $f_e(t)$ may be expressed in terms of the following convolution integral of the sea-surface elevation $\eta(t)$ (Falnes, 2002):

$$f_e(t) = \int_{-\infty}^{\infty} h_{e\eta}(t-\tau)\eta(\tau)d\tau \tag{10}$$

the sea-surface elevation $\eta(t)$ is assumed to be observed at a sufficient distant position where the measurement is not disturbed by the radiation wave, and $h_{e\eta}(t)$ is a non-causal impulse response function. The related frequency response function becomes:

$$H_{e\eta}(\omega) = \int_{-\infty}^{\infty} \mathrm{e}^{-i\omega t} h_{e\eta}(t)dt \tag{11}$$

For the indicated heave absorber located in the sea with water depth $h = 30$ m, it consists of a cylindrical volume with a diameter $D = 14$ m and a hemisphere with the same diameter as the cylinder. The structural mass m of the absorber is 1.84×10^6kg. The relative physical parameters of the considered point absorber have been defined in the numerical example at the end of the paper. Based on these parameters, the hydrodynamic parameters, i.e. k, m_h, $H_{rv}(\omega)$, $H_{e\eta}(\omega)$ can be calculated numerically. In the present case, the program WAMIT has been used, which is based on the boundary element method (WAMIT, 2011). Further, the impulse response functions, $h_{rv}(t)$ and $h_{e\eta}(t)$, are obtained by inverse Fourier transform of Eqs. (8) and (11) respectively.

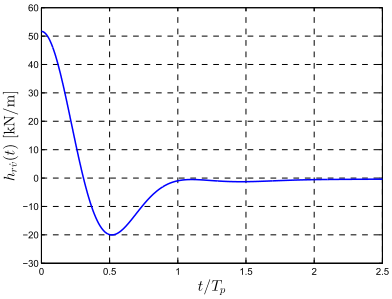

Fig. 2. Impulse response function for the radiation force, $h_{rv}(t)$.

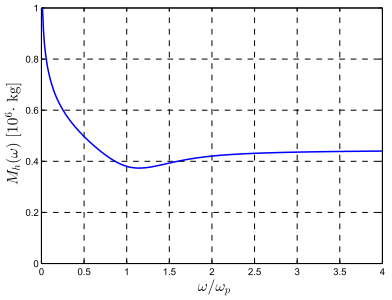

Fig. 3. Hydrodynamic added mass, $M_h(\omega)$.

Fig. 2 shows the obtained impulse response function $h_{rv}(t)$. The time has been normalized with respect to the peak period T_p. Fig. 3 shows the hydrodynamic added mass. $M_h(\omega) = M_h(-\omega)$ is an an even function of ω, cf. Eq. (9), for which reason only results for positive angular frequencies have been shown. As seen, the asymptotic value m_h is achieved for $\omega \geq 3\omega_p$. Fig. 4 shows the real and imaginary parts of the frequency response function $H_{rv}(\omega)$. The real part is a symmetric function and the imaginary part is a show-symmetric function of ω, for which reason only results for positive angular frequencies have been shown.

The impulse response function $h_{e\eta}(t)$ for the wave excitation is shown in Fig. 5. The real and imaginary parts of the related frequency response function which will be used in later section for modeling the waves are shown in Fig. 6a) and 6b).

For practical reasons the displacement $v(t)$ will be limited to a finite interval $[v_{\min}, v_{\max}]$, either in order to prevent the absorber form hitting the bottom of the sea or jumping out of the water, or because the actuator has a finite stroke. Similarly, the control force $f_c(t)$ will be constrained to

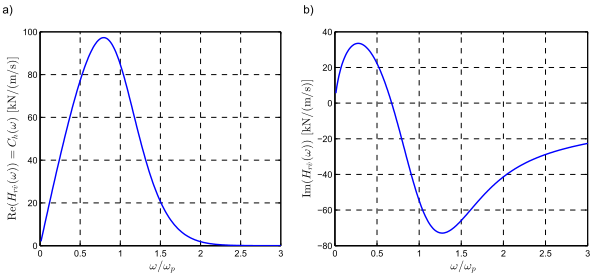

Fig. 4. Frequency response function for the radiation force. a) Re ($H_{rv}(\omega)$). b) Im ($H_{rv}(\omega)$).

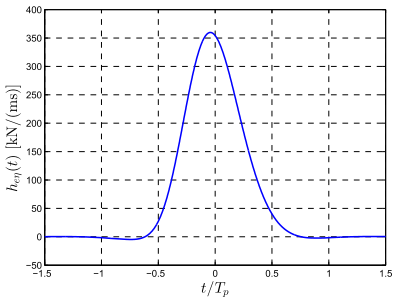

Fig. 5. Impulse response function for the wave excitation force, $h_{ef}(t)$.

a finite interval $[f_{c,\min}, f_{c,\max}]$ due to saturation in the hydraulic actuator system. Then, based on Eq. (7), the optimal control force which maximizes the absorbed energy during the control interval $[t_0, t_1]$ is obtained as the solution to the following constrained optimization problem:

$$\max J[f_c(t), \dot{v}(t)] = \int_{t_0}^{t_1} f_c(\tau)\dot{v}(\tau)d\tau$$
$$\text{s.t.} \begin{cases} (m+m_h)\dot{v}(t) + r(v(t)) + \int_{t_0}^{t} h_{rv}(t-\tau)\dot{v}(\tau)d\tau = f_e(t) - f_c(t) \\ v(t_0) = v_0, \dot{v}(t_0) = \dot{v}_0 \\ v_{\min} \le v(t) \le v_{\max} \\ f_{c,\min} \le f_c(t) \le f_{c,\max} \end{cases} \tag{12}$$

Below, merely an infinite control horizon is considered corresponding to $t_0 = -\infty$ and $t_1 = \infty$. Further, a linear buoyancy restoring force is assumed as indicated in Eq. (4).

3. . Rational approximations to the radiation force and the external wave load

For the application in time-domain simulation, control and optimization problem, the integral part of the radiation force, i.e. $f_{r,0}(t)$ in Eq. (6) is replaced by an equivalent system of coupled first-order differential equations. This is equivalent to replacing the frequency response function $H_{rv}(\omega)$ by an approximating rational function:

$$H_{rv}(\omega) \simeq \tilde{H}_{rv}(\omega) = \frac{P(z)}{Q(z)}, z = i\omega \tag{13}$$

$$\left.\begin{aligned} P(z) &= p_0 z^m + p_1 z^{m-1} + \cdots + p_{m-1} z + p_m \\ Q(z) &= z^n + q_1 z^{n-1} + \cdots + q_{n-1} z + q_n \end{aligned}\right\} \tag{14}$$

where the parameters $p_0, p_1, \cdots, p_m$ and $q_1, q_2, \cdots, q_n$ are all real. The denominator polynomial may be given on the form:

$$Q(z) = (z - z_1)(z - z_2)\cdots(z - z_n) \tag{15}$$

In order to ensure the stability and strict causality, the order of the filter given by the pair (m, n) should satisfy the condition that $m < n$ and the poles of the denominator z_j must fulfill $\mathrm{Re}(z_j) < 0$. The solution can be obtained by the MATLAB control toolbox (Mathworks, 2011). In Fig. 7 the obtained rational approximation of the order $(m, n) = (2, 3)$ to $H_{rv}(\omega)$ is compared with the target frequency response function.

Then, the relation between $f_{r,0}(t)$ and $\dot{v}(t)$ can be expressed by the differential equations:

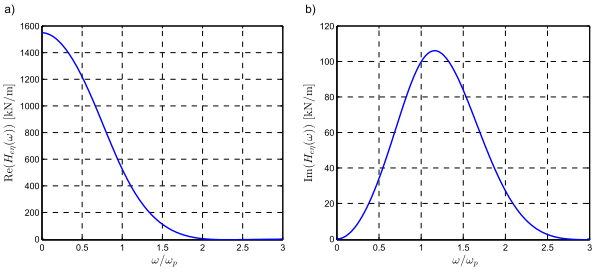

Fig. 6. Frequency response function for the wave excitation force. a) Re ($H_{ef}(\omega)$). b) Im ($H_{ef}(\omega)$).

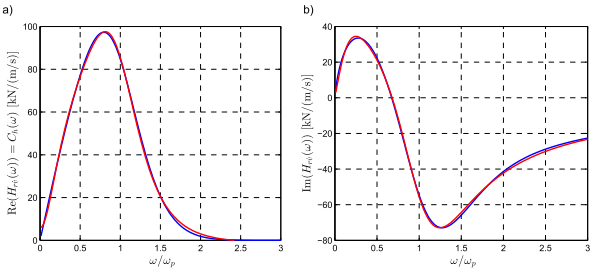

Fig. 7. The accuracy of the rational approximation to $H_{rv}(\omega)$. a) Re ($H_{rv}(\omega)$). b) Im ($H_{rv}(\omega)$). ——: Numerical determined target frequency function. ——: Rational approximation, $(m, n) = (2, 3)$.

$$\left.\begin{aligned} f_{r,0}(t) &= p_0\frac{d^m y(t)}{dt^m} + p_1\frac{d^{m-1}y(t)}{dt^{m-1}} + \cdots + p_{m-1}\frac{dy(t)}{dt} + p_m y(t) \\ &\frac{d^n y(t)}{dt^n} + q_1\frac{d^{n-1}y(t)}{dt^{n-1}} + \cdots + q_{n-1}\frac{dy(t)}{dt} + q_n y(t) = \dot{v}(t) \end{aligned}\right\} \tag{16}$$

where $y(t)$ is an auxiliary function. A harmonic varying input $\dot{v}(t) = \mathrm{Re}(\dot{V}e^{i\omega t})$ to the 2nd equation produces a harmonic varying force $f_{r,0}(t) = \mathrm{Re}(F_{r,0}\, e^{i\omega t}), F_{r,0} = \tilde{H}_{rv}(\omega)\dot{V}$, of the 1st equation, where $\tilde{H}_{rv}(\omega)$ is given by Eqs. (13) and (14). Eq. (16) can be written on the following state vector form:

$$\frac{d}{dt}\mathbf{z}_r(t) = \mathbf{A}_r\mathbf{z}_r(t) + \mathbf{b}_r\dot{v}(t) \tag{17}$$

$$f_{r,0}(t) = \mathbf{p}_r\mathbf{z}_r(t) \tag{18}$$

where $\mathbf{z}_r(t)$, $\mathbf{A}_r$, $\mathbf{b}_r$ and $\mathbf{p}_r$ can be found in detail in the reference (Nielsen et al., 2013).

In applications the stochastic wave load $f_e(t)$ can be modelled as a zero-mean, stationary Gaussian stochastic process, obtained as the output process of a unit intensity Gaussian white noise process $w_1(t)$, with the frequency response function $H_{ew_1}(\omega)$, passed through a time-invariant physically realizable rational filter. The mean value and auto-covariance function of $w_1(t)$ is given as (Nielsen and Zhang, 2017):

$$\left.\begin{aligned} E[w_1(t)] &= 0 \\ E[w_1(t_1)w_1(t_2)] &= \delta(t_2 - t_1) \end{aligned}\right\} \tag{19}$$

where $E[\cdot]$ is the expectation operator and $\delta(\cdot)$ indicates the Dirac's delta function.

Furthermore, the auto-spectral density function for wave load can be expressed as (Nielsen and Zhang, 2017):

$$S_{f_e f_e}(\omega) = |H_{e\eta}(\omega)|^2 S_{\eta\eta}(\omega) = |H_{ew_1}(\omega)|^2 S_{w_1 w_1} \tag{20}$$

where $S_{f_e f_e}(\omega)$ is double-sided auto spectral density function of wave excitation, and $S_{w_1 w_1} = \frac{1}{2\pi}$ is the double-sided auto spectral density function of unit intensity Gaussian white noise $w_1(t)$. $H_{e\eta}(\omega)$ and $H_{ew_1}(\omega)$ are impulse response functions for the wave excitation force caused by wave height and white noise, respectively. $S_{\eta\eta}(\omega)$ is the double-sided JONSWAP auto spectral density function given as (Hasselmann et al., 1973):

$$S_{\eta\eta}(\omega) = \alpha\frac{H_s^2}{\omega_p^4}\gamma^{\beta}\left(\frac{|\omega|}{\omega_p}\right)^{-5}\exp\left(-\frac{5}{4}\left(\frac{\omega}{\omega_p}\right)^{-4}\right) \tag{21}$$

where

$$\left.\begin{aligned} \alpha &= \frac{0.0312}{0.230 + 0.0336\gamma - \frac{0.185}{1.9+\gamma}} \\ \beta &= \exp\left(-\frac{1}{2}\left(\frac{|\omega| - \omega_p}{\sigma\omega_p}\right)^2\right) \\ \sigma &= \begin{cases} 0.07, |\omega| \le \omega_p \\ 0.09, |\omega| > \omega_p \end{cases} \end{aligned}\right\} \tag{22}$$

T_p is the peak period, $\omega_p = \frac{2\pi}{T_p}$ is the related angular peak frequency and H_s is the significant wave height. γ is the so-called peak enhancement parameter which controls the bandwidth of the spectrum. Small and large values of γ represents broad-and narrow-bandedness of the surface elevation spectrum.

Fig. 8 shows the one-sided auto spectral density function of the surface elevation process $S_\eta(\omega)$ and the wave excitation process $S_{f_e}(\omega)$. Both spectrums have been normalized with respect to the angular peak

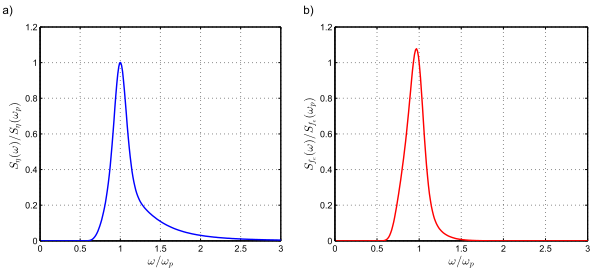

Fig. 8. One-sided normalized auto-spectral density functions. a) Surface elevation process. b) Wave excitation process.

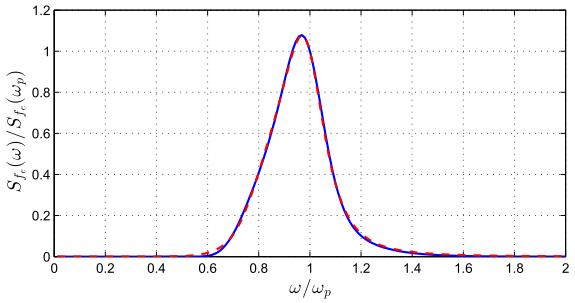

Fig. 9. Rational approximation to the one-sided auto-spectral density function of the wave load. ——: Numerical determined target auto-spectral density function. – – – –: Rational approximation, $(r,s) = (2,4)$.

frequency ω_p. As seen $S_{f_e}(\omega) \simeq 0$ for $\omega < 0.5\omega_p$ and $\omega > 1.5\omega_p$. In contrast, the surface elevation process is vanishing for $\omega \geq 3.0\omega_p$.

In analogy to Eq. (13), the frequency response function $H_{ew_1}(\omega)$ of the filter is approximated by a casual rational function:

$$H_{ew_1}(\omega) = \frac{P(z)}{Q(z)} = \frac{p_0 z^r + p_1 z^{r-1} + \cdots + p_{r-1} z + p_r}{z^s + q_1 z^{s-1} + \cdots + q_{s-1} z + q_s}, z = i\omega \tag{23}$$

The filter coefficients are obtained by solving the following optimization problem (Nielsen and Zhang, 2017):

$$\min_{\substack{p_0,\cdots,p_r \\ q_1,\cdots,q_s}} \int_{-\infty}^{\infty} \left(S_{f_e f_e}(\omega) - \frac{1}{2\pi} \frac{P(i\omega)P(-i\omega)}{Q(i\omega)Q(-i\omega)} \right)^2 d\omega \tag{24}$$

s.t.

$$\left.\begin{aligned} &\frac{1}{2\pi} \frac{P(i\omega_p)P(-i\omega_p)}{Q(i\omega_p)Q(-i\omega_p)} = S_{f_e f_e}(\omega_p) \\ &\mathrm{Re}(z_j) < 0,\ j = 1,2,\cdots,s \end{aligned}\right\} \tag{25}$$

where $z_j, j = 1,2,\cdots,s$ indicates the poles of the denominator polynomial $Q(z)$, cf. Eq. (15).

The constraint on z_j in Eq. (25) ensures that the filter becomes causal, in contrast to the underlying non-causal filter problem. Nevertheless, the obtained load process will be a zero-mean Gaussian process with the same covariance structure as the original process within the accuracy approximation of the rational auto-spectral density function to the target spectrum. Hence, these processes will be equivalent with probability 1. Fig. 9 illustrates the accuracy of the rational auto-spectral density function for $(r,s) = (2,4)$ in comparison to the target auto-spectral density function.

Next, the wave load $f_e(t)$ is obtained from the following state vector equations:

$$\frac{d}{dt}\mathbf{z}_e(t) = \mathbf{A}_e \mathbf{z}_e(t) + \mathbf{b}_e w_1(t) \tag{26}$$

$$\mathbf{z}_e(t) = \begin{bmatrix} y(t) \\ \frac{d}{dt}y(t) \\ \frac{d^2}{dt^2}y(t) \\ \vdots \\ \frac{d^{n-2}}{dt^{n-2}}y(t) \\ \frac{d^{n-1}}{dt^{n-1}}y(t) \end{bmatrix}, \mathbf{b}_e = \begin{bmatrix} 0 \\ 0 \\ 0 \\ \vdots \\ 0 \\ a_1 \end{bmatrix} \tag{27}$$

$$\mathbf{A}_e = \begin{bmatrix} 0 & 1 & 0 & \cdots & 0 & 0 \\ 0 & 0 & 1 & \cdots & 0 & 0 \\ \vdots & \vdots & \vdots & \ddots & \vdots & \vdots \\ 0 & 0 & 0 & \cdots & 0 & 1 \\ -q_s & -q_{n-1} & -q_{s-2} & \cdots & -q_2 & -q_1 \end{bmatrix} \tag{28}$$

$$f_e(t) = \mathbf{p}_e \mathbf{z}_e(t) \tag{29}$$

where:

$$\mathbf{p}_e = [p_r \quad p_{r-1} \quad \cdots \quad p_1 \quad p_0 \quad 0 \quad \cdots \quad 0] \tag{30}$$

a_1 notifies the intensity of the white noise process.

The equation for the integrated dynamic system made up of the displacement $v(t)$ and the velocity $\dot{v}(t)$ of the point absorber, and the state vector $\mathbf{z}_r(t)$ and $\mathbf{z}_e(t)$ of the rational approximations of the radiation force and the wave load may be formulated as:

$$\dot{\mathbf{z}}(t) = \mathbf{A}\mathbf{z}(t) + \mathbf{b}_{f_e} f_e(t) + \mathbf{b}_1 w_1(t) \tag{31}$$

where:

$$\mathbf{z}(t) = \begin{bmatrix} v(t) \\ \dot{v}(t) \\ z_r(t) \\ z_e(t) \end{bmatrix}, \mathbf{b}_{f_e} = \begin{bmatrix} 0 \\ \frac{1}{m_0} \\ \mathbf{0} \\ \mathbf{0} \end{bmatrix}, \mathbf{b}_1 = \begin{bmatrix} 0 \\ 0 \\ \mathbf{0} \\ \mathbf{b}_e \end{bmatrix}, \mathbf{A} = \begin{bmatrix} 0 & 1 & \mathbf{0} & \mathbf{0} \\ \frac{k}{m_0} & 0 & \frac{\mathbf{p}_r}{m_0} & \frac{\mathbf{p}_e}{m_0} \\ 0 & \mathbf{b}_r & \mathbf{A}_r & \mathbf{0} \\ \mathbf{0} & \mathbf{0} & \mathbf{0} & \mathbf{A}_e \end{bmatrix} \tag{32}$$

where $m_0 = m + m_h$. The dimension of the state vector $\mathbf{z}(t)$ is $N = 2 + n + s$.

4. Modified linear quadratic Gaussian control

In order to obtain the optimal control force, which maximizes the absorbed energy during the control interval $[t_0, t_1]$ and simultaneously reduces the variation of the displacement and control force, the following modified performance functional is applied:

$$\begin{aligned} \max J_1[f_c(t), \dot{v}(t), v(t)] &= \frac{1}{2}\int_{-\infty}^{\infty} \left(-q\dot{v}^2(t) + 2v(t)f_c(t) - rf_c^2(t) \right) dt \\ &= \frac{1}{2}\int_{-\infty}^{\infty} \left(-\mathbf{z}(t)^T \mathbf{Q}\mathbf{z}(t) + 2\mathbf{z}(t)^T \mathbf{p} f_c(t) - rf_c^2(t) \right) dt \end{aligned} \tag{33}$$

where $\mathbf{Q}$ and $\mathbf{p}$ are given as:

$$\mathbf{Q}=\begin{bmatrix} q & 0 & 0 & \cdots & 0\\ 0 & 0 & 0 & \cdots & 0\\ \vdots & \vdots & \vdots & \ddots & \vdots\\ 0 & 0 & 0 & \cdots & 0 \end{bmatrix}, \mathbf{p}=\begin{bmatrix} 0 & 1 & \cdots & 0 \end{bmatrix}^T \tag{34}$$

Traditional LQG optimization merely considers the 1st and 3rd terms in the objective functional. In the present case the 2nd term has been introduced to optimize the energy absorbtion, keeping the displacement and the control force as small as possible.

In order to solve the control problem, the variational approach will be adopted. The Hamiltonian of the control problem is defined as:

$$\mathbf{H}(\mathbf{z}(t),f_c(t),\boldsymbol{\lambda}(t),t)=\frac{1}{2}\left(-\mathbf{z}(t)^T\mathbf{Q}\mathbf{z}(t)+2\mathbf{z}(t)^T\mathbf{p}f_c(t)-rf_c^2(t)\right) +\boldsymbol{\lambda}^T(t)\mathbf{g}(\mathbf{z}(t),f_c(t),t) \tag{35}$$

where $\boldsymbol{\lambda}(t)=[\lambda_v(t),\lambda_{\dot{v}}(t),\lambda_r(t),\lambda_e(t)]^T$ is the co-state vector (Lagrange multiplier). $\mathbf{g}(\mathbf{z}(t),f_c(t),t)$ is given as:

$$\mathbf{g}(\mathbf{z}(t),f_c(t),t)=\mathbf{A}\mathbf{z}(t)+\mathbf{b}_{f_c}f_c(t)+\mathbf{b}_1w_1(t) \tag{36}$$

The Euler-Lagrange equations for optimal control become (Meirovitch, 1990): Co-state vector equation:

$$\dot{\boldsymbol{\lambda}}(t)=-\frac{\partial H}{\partial \mathbf{z}} \tag{37}$$

Stationarity condition on the control force:

$$\frac{\partial H}{\partial f_c}=0 \tag{38}$$

Due to the infinite control horizon the transversality condition $\lambda(\infty)=0$ can be ignored.

Eq. (37) yields the following differential equation for the co-state vector:

$$\dot{\boldsymbol{\lambda}}(t)=-\mathbf{A}^T\boldsymbol{\lambda}(t)+\mathbf{Q}\mathbf{z}(t)-\mathbf{p}f_c(t) \tag{39}$$

Eq. (38) provides the following solution for the optimal control force:

$$f_c(t)=\frac{1}{r}\left(\mathbf{b}_{f_c}^T\boldsymbol{\lambda}(t)+\mathbf{p}^T\mathbf{z}(t)\right) \tag{40}$$

In agreement with the conventional LQG procedure the following solution is assumed for the co-state vector at optimal control:

$$\boldsymbol{\lambda}(t)=-\mathbf{S}(t)\mathbf{z}(t) \tag{41}$$

leading to the following control law:

$$f_c(t)=-\frac{1}{r}\left(\mathbf{b}_{f_c}^T\mathbf{S}(t)-\mathbf{p}^T\right)\mathbf{z}(t)=-\mathbf{G}(t)\mathbf{z}(t) \tag{42}$$

where $\mathbf{G}(t)$ is the control gain matrix given by:

$$\mathbf{G}(t)=\frac{1}{r}\left(\mathbf{b}_{f_c}^T\mathbf{S}(t)-\mathbf{p}^T\right) \tag{43}$$

Substitution of Eqs. (41) and (42) into Eq. (39) provides the following matrix differential equation for $\mathbf{S}(t)$:

$$-\dot{\mathbf{S}}(t)\mathbf{z}(t)-\mathbf{S}(t)\left(\mathbf{A}\mathbf{z}(t)+\mathbf{b}_{f_c}f_c(t)+\mathbf{b}_1w_1(t)\right)=\mathbf{A}^T\mathbf{S}(t)\mathbf{z}(t)+\mathbf{Q}\mathbf{z}(t)-\mathbf{p}f_c(t) \tag{44}$$

$f_c(t)$ in Eq. (44) is eliminated by Eq. (42). Then, in the stationary state corresponding to infinite control horizon, the matrix $\mathbf{S}$ is obtained from the following Lyapunov equation:

$$\mathbf{S}\mathbf{A}+\mathbf{A}^T\mathbf{S}-\frac{1}{r}\left(\mathbf{S}\mathbf{b}_{f_c}-\mathbf{p}\right)\left(\mathbf{b}_{f_c}^T\mathbf{S}-\mathbf{p}^T\right)+\mathbf{Q}=0 \tag{45}$$

Eq. (45) represents a generalization to the stationary Riccati equation related to standard LQG control. Normally, the information about the future system matrices is required when the Ricatti equation is solved in order to synthesize the optimal control gain at the present time instant (Basu and Staino, 2016). In this paper, assuming the stationary state for the Riccati equation (44), corresponding to infinite control horizon, the control problem becomes causal.

5. State observation based on Kalman filtration

The control law in Eq. (42) represents that the full state vector $\mathbf{z}(t)$ can be observed. In reality merely the components $v(t)$ and $\dot{v}(t)$ are available. For this reason the control law in Eq. (42) is combined with a Kalman filter state observer. The following observer equation is assumed:

$$\mathbf{y}(t)=\mathbf{C}\mathbf{z}(t)+\mathbf{w}(t) \tag{46}$$

where:

$$\mathbf{y}(t)=\begin{bmatrix} v(t)\\ \dot{v}(t)\end{bmatrix}, \mathbf{C}=\begin{bmatrix} 1 & 0 & \mathbf{0} & \mathbf{0}\\ 0 & 1 & \mathbf{0} & \mathbf{0}\end{bmatrix}, \mathbf{w}(t)=\begin{bmatrix} a_2 & 0\\ 0 & a_3\end{bmatrix}\begin{bmatrix} w_2(t)\\ w_3(t)\end{bmatrix} \tag{47}$$

$w_2(t)$ and $w_3(t)$ are mutual independent unit intensity Gaussian white noise processes, cf, Eq. (19). a_2 and a_3 are corresponding intensities indicating the level of the noise.

Let $\mathbf{e}(t)$ be the observer error vector, defined as:

$$\mathbf{e}(t)=\mathbf{z}(t)-\hat{\mathbf{z}}(t) \tag{48}$$

The observer equation becomes (Meirovitch, 1990):

$$\dot{\hat{\mathbf{z}}}(t)=(\mathbf{A}-\mathbf{K}\mathbf{C})\hat{\mathbf{z}}(t)+\mathbf{b}_{f_c}f_c(t)+\mathbf{K}\mathbf{y}(t) \tag{49}$$

where $\hat{\mathbf{z}}(t)$ is the estimated state vector. The estimated control force $\hat{f}_c(t)$ is given as:

$$\hat{f}_c(t)=-\mathbf{G}\hat{\mathbf{z}}(t) \tag{50}$$

and the Kalman gain matrix $\mathbf{K}$ is expressed as:

$$\mathbf{K}=\mathbf{D}\mathbf{C}^T\mathbf{W}^{-1} \tag{51}$$

where $\mathbf{D}$ is the steady-state variance matrix of $\mathbf{e}(t)$ satisfying the Lyapunov equation:

$$\mathbf{A}\mathbf{D}+\mathbf{D}\mathbf{A}^T+\mathbf{V}-\mathbf{D}\mathbf{C}^T\mathbf{W}^{-1}\mathbf{C}\mathbf{D}=0 \tag{52}$$

where $\mathbf{V}$ and $\mathbf{W}$ are the intensities of the process $w_1(t)$ and $\mathbf{w}(t)$, which can be expressed as:

$$\mathbf{V}=a_1^2\mathbf{b}_1\mathbf{b}_1^T, \mathbf{W}=\begin{bmatrix} a_2^2 & 0\\ 0 & a_3^2\end{bmatrix} \tag{53}$$

6. Numerical example

A point heave wave energy converter is considered in the numerical simulation. The relevant data of the absorber and the wave excitation parameters have been indicated in Table 1.

In the following the accuracy of the theory will be tested against numerical results obtained by nonlinear programming. The nonlinear programming formulation of the optimal control problem is related to two approximations related to the state vector representation in Eqs. (17) and (18) of the convolution integral for the radiation force, and to a discretization of the performance functional iat instants of time separated by the interval $\Delta\tau$.

In order to check the accuracy in the nonlinear programming algorithm, it has been checked against the theoretical solution for optimal control of the unconstrained heave absorber due to Nielsen et al. (2013), given as:

Table 1
Heave absorber and wave excitation parameters.

Parameter	Value	Unit	Parameter	Value	Unit
H	7.00	m	v_{max}	0.50	m
D	14.00	m	v_{min}	−0.50	m
h	30.00	m	$f_{c,max}$	4.0×10^5	N
m	1.84×10^6	kg	$f_{c,min}$	-4.0×10^5	N
m_h	0.44×10^6	kg	q	9.00×10^5	N/(ms)
H_s	3.00	m	r	3.00×10^{-7}	m/(Ns)
T_p	7.42	s	a_2	0.50	$ms^{1/2}$
γ	5		a_3	0.50	$ms^{-1/2}$

$$f_c(t) = -(m+m_h)\dot{v}(t) - kv(t) + \int_t^\infty h_{r\dot{v}}(\tau - t)\dot{v}(\tau)d\tau \tag{54}$$

Fig. 10 shows the results for a time step $\Delta\tau = \frac{T_p}{150}$ in the discretization of the control interval, and a rational approximation of the order $(m,n) = (2,3)$ for the convolution integral. The nonlinear programming solution at optimal control for $v(t), \dot{v}(t)$ and $\dot{v}(t)$ were used at calculation of the theoretical solution.

Fig. 11a and 11b shows the displacement and velocity of the absorber under LQG control for full and partial state observation, corresponding to Eqs. (42) and (50), with the indicated parameters, and the comparison with nonlinear programming as formulated in appendix.

Fig. 11c indicates the corresponding control force. Fig. 11d and Table 2 indicate the instantaneous power and mean power based on LQG control. As seen, the partial observation merely reduce the mean absorbed power due to the limited state observation. In order to evaluate the effect of a_2 and a_3 on the absorbed power, two pairs (a_2, a_3) are compared.

In Table 2, the absorber power with $(a_2, a_3) = (0.50\ \mathrm{ms}^{1/2}, 0.50\ \mathrm{ms}^{-1/2})$ is larger than the absorbed power with $(a_2,\ a_3) = (1.00\ \mathrm{ms}^{1/2}, 1.00\ \mathrm{ms}^{-1/2})$. It can be known that the measurement parameters a_2 and a_3 would reduce the absorbed power generally. At the same time, the obtained sub-optimal solution base on LQG, full state observation is compared to the optimal solution obtained by nonlinear programming. The details of the nonlinear programming algorithm has been given in an appendix.

In order to investigate the broad-banded wave, the wave condition with $H_s = 3\mathrm{m}, T_p = 7.42\mathrm{s}$ and $\gamma = 1$ has also been considered. Fig. 12 shows the trajectories of $v(t)$ and $\dot{v}(t)$, control force $f_c(t)$ and instantaneous absorbed power $P(t)$ at optimal control. The mean absorbed power is also shown in Table 2. As seen, The same analysis results are applied to the extreme broad-banded wave.

Given a sea-state defined by the parameters H_s, T_p, and γ a sufficient long realization of $f_e(t)$ is generated from Eqs. (26) and (29) using a so-called broken line equivalent white noise process for $w_1(t)$ (Nielsen and

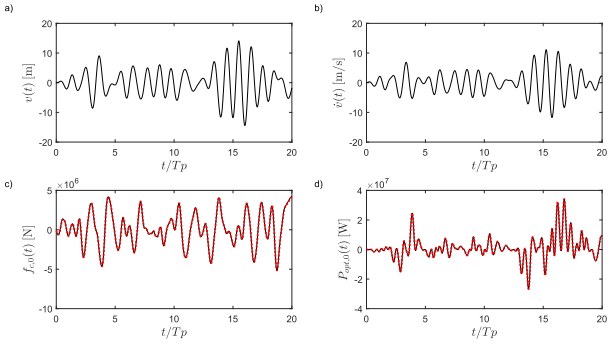

Fig. 10. Unconstrained case. The trajectories, control force and instantaneous absorbed power at optimal control. a) $v(t)$. b) $\dot{v}(t)$. c) $f_{c,0}(t)$. d) $P_{opt,0}(t)$. ——:Nonlinear programming solution. ·····:Unconstrained analytical solution (Nielsen et al., 2013).

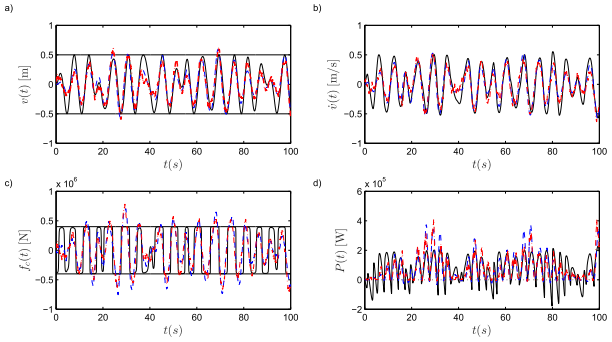

Fig. 11. The trajectories of $v(t)$ and $\dot{v}(t)$, control force $f_c(t)$ and instantaneous absorbed power $P(t)$ at optimal control. $H_s = 3\mathrm{m}$, $T_p = 7.42\mathrm{s}$ and $\gamma = 5$. $f_{c,max} = -f_{c,min} = 4\times10^5\mathrm{N}$ and $v_{max} = -v_{min} = 0.5\mathrm{m}$. a) $v(t)$. b) $\dot{v}(t)$. c) $f_c(t)$. d) $P(t)$. ——:Nonlinear programming solution. - - -:LQG, full state observation. ·····:LQG, partial state observation.

Table 2
Mean absorbed power under different wave conditions.

	$\gamma = 5$	$\gamma = 1$
Nonlinear programming	78.1005 kW	84.3520 kW
LQG, full state observation	77.0597 kW	83.3994 kW
LQG, partial state observation with (a_2, a_3)=(0.50ms$^{1/2}$, 0.50ms$^{-1/2}$)	73.4893 kW	80.4685 kW
LQG, partial state observation with (a_2, a_3)=(1.00ms$^{1/2}$, 1.00ms$^{-1/2}$)	61.3112 kW	76.2606 kW

negative correlated to the magnitude of the constraints on the displacement and control force.

In Fig. 11d, at optimal control $P(t)$ may have negative loops. Actually, an imposed constrain $f_c(t) \equiv 0$, corresponding to $P(t) \equiv 0$ during a time interval with negative power absorption in the optimal control, will produce a non-optimal velocity trajectory $\dot{v}(t)$ out-side the said time interval via the impact on the equation motion Eq. (12), resulting in a reduced average absorbed power during a longer control horizon. The same observation was made by Falnes (2002).

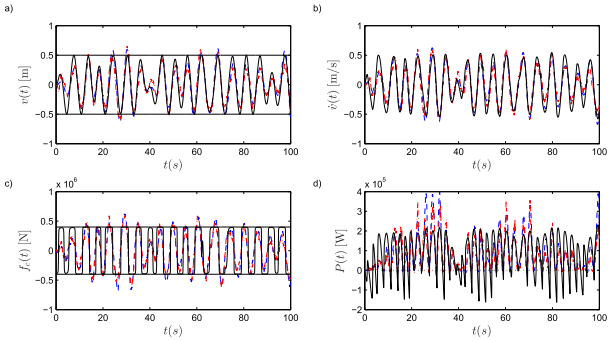

Fig. 12. The trajectories of $v(t)$ and $\dot{v}(t)$, control force $f_c(t)$ and instantaneous absorbed power $P(t)$ at optimal control. $H_s = 3$m, $T_p = 7.42s$ and $\gamma = 1$. $f_{c,\max} = -f_{c,\min} = 4 \times 10^5$N and $v_{\max} = -v_{\min} = 0.5$m. a) $v(t)$. b) $\dot{v}(t)$. c) $f_c(t)$. d) $P(t)$. ——:Nonlinear programming solution. - - -:LQG, full state observation. -----:LQG, partial state observation.

Zhang, 2017). Next, the load realization applied in LQG control is used for the nonlinear programming solution for the optimal solution. Finally, q and r are determined so the standard deviations σ_v and σ_{f_c} are identical for the nonlinear programming solution and the LQG solution with full state observation. When nonlinear programming is applied, the computational cost grows exponentially with the length of the control horizon. For this reason stable solutions for the parameters q and r can't be achieved by merely using a single realization of the wave stationary load process $f_e(t)$ of limited length. Instead a finite number N of independent time series of the wave load of limited length should be generated, which from samples of q and r are generated based on nonlinear programming. Next, stable estimates of q and r may be obtained as ensemble averages of the indicated sample values. Then, the calculation time of the approach merely growth linearly with N. Assuming that all involved stochastic processes are ergodic it doesn't matter which realization of $w_1(t)$ (and hence of $f_e(t)$) is used. The indicated standard deviations are determined by time-averages of $N = 6$ independent time series of $v(t)$ and $f_c(t)$ in the interval [0, 100s] where the time step $\Delta\tau$ is $\frac{T_p}{150}$. Further, according to the Pontryagin's maximum principle (Pontryagin et al., 1962), the optimal control is obtained for the maximum value of the Hamiltonian as given by Eq. (35). Then, an increase or decrease of the weights q and r implies a decrease or increase of $v(t)$ and $f_c(t)$ at optimal control. In the present model it follows that q and r are

7. Conclusions

In this paper, a control law based on the LQG approach is used to maximize the absorbed energy of a wave energy point absorber system. As a result of rational approximations to the radiation force and the wave load, the integrated dynamic system is reformulated as a linear stochastic differential equation which is driven by a unit intensity Gaussian white noise. Further, the Kalman filter technique is employed to estimate the combined state vector based on noise observation of $v(t)$ and $\dot{v}(t)$. The proposed LQG control successfully demonstrated the ability to extract and maximize the absorbed power while keeping the absorber motion and control force small. Based on a specific calibration technique of the parameters q and r entering the performance functional of the LQG solution close to optimal control force solutions are generated in cased of low signal to noise ratios of the observed state variables. For higher noise level a certain reduction appears in the absorbed power.

Acknowledgements

The authors gratefully acknowledge the financial support from project 675659-ICONN-H2020-MSCA-ITN-2015.

Appendix. Nonlinear programming algorithm

The optimal control problem in Eq. (12) is reformulated as a nonlinear programming problem by discretizing the objective functional and the state vector in time:

$$\begin{aligned}
&\max J(\mathbf{X}(\tau_M)) = x_{n+3}(\tau_M)\\
&\text{subject to the path and inequality constraints :}\\
&\left.\begin{aligned}
&\mathbf{c}(\mathbf{X}(\tau_j)) = 0\\
&\mathbf{h}(\mathbf{X}(\tau_j)) = \begin{bmatrix} v(\tau_j) & -v_{\max} \\ -v(\tau_j) & +v_{\min} \\ f_c(\tau_j) & -f_{c,\max} \\ -f_c(\tau_j) & +f_{c,\min} \end{bmatrix} - \mathbf{s}(\tau_j) = 0\\
&\mathbf{s}(\tau_j) \geq 0
\end{aligned}\right\}
\end{aligned} \tag{55}$$

where $\tau_j = t_0 + j\,\Delta\tau\,, j = 0, 1, \ldots, M$.

$\mathbf{s}(t)$ indicates a vector function of slack variables. The time step in the discretization of the interval $]t_0, t_1]$ is given as $\Delta\tau = \frac{t_1 - t_0}{M}$. The vector $\mathbf{X}(t)$ of dimension $2n + 6$ and the path constrain vector $\mathbf{c}(\mathbf{X}(t))$ of dimension $n + 3$ are defined as:

$$\mathbf{X}(t) = \left[v(t), \dot{v}(t), \mathbf{z}_r^T(t), x_{n+3}(t), \frac{d}{dt}v(t), \frac{d}{dt}\dot{v}(t), \frac{d}{dt}\mathbf{z}_r^T(t), \frac{d}{dt}x_{n+3}(t)\right]^T \tag{56}$$

$$\mathbf{c}(\mathbf{X}(t)) = \begin{bmatrix} \frac{d}{dt}v(t) - \dot{v}(t) \\ M\frac{d}{dt}\dot{v}(t) + \mathbf{p}_r\mathbf{z}_r(t) + r(v(t)) - f_e(t) + f_c(t) \\ \frac{d}{dt}\mathbf{z}_r(t) - \mathbf{A}_r\mathbf{z}_r(t) - \mathbf{b}_r\dot{v}(t) \\ \frac{d}{dt}x_{n+3}(t) - f_c(t)\dot{v}(t) \end{bmatrix} \tag{57}$$

The inherent approximation in the indicated nonlinear programming formulation concerns the discretization of the time continuous problem into $M + 1$ discrete instants of time for optimization, and the use of the rational approximation in Eq. (18) for the force $f_{r,0}(t)$.

The formulation applies to both displacement constraints and control force constraints. In case, merely control force constraints are prescribed the algorithm is applied by using large values of $v_{\max}$ and small values of $v_{\min}$.

The applied algorithm for solving the indicated nonlinear programming problem is described in (El-Bakry et al., 1996).

References

Archimedes Wave Swing, 2004. Archimedes Wave Swing. http://www.awsocean.com/.

Basu, B., Staino, A., 2016. Control of a linear TimeVarying system with a forward Riccati formulation in wavelet domain. J. Dyn. Syst. Meas. Contr. 138 (10), 104502. ASME.

Cretel, J.A., Lightbody, G., Thomas, G.P., Lewis, A.W., 2011. Maximisation of energy capture by a wave-energy point absorber using model predictive control. IFAC Proceedings Volumes 44 (1), 3714–3721.

Cummins, W., 1962. The impulse response functions and ship motions. Schiff-stechnik 9, 101109.

El-Bakry, A.S., Tapia, R.A., Tsuchiya, T., Zhang, Y., 1996. On the formulation and theory of the Newton interior-point method for nonlinear programming. J. Optim. Theor. Appl. 89 (3), 507–541.

Falnes, J., 2002. Ocean Waves and Oscillating Systems: Linear Interactions Including Wave-Energy Extraction. Cambridge University Press.

Faltinsen, O., 1990. Sea Loads on Ships and Offshore Structures. Cambridge University Press.

Hartl, R.F., Sethi, S.P., Vickson, R.G., 1995. A survey of the maximum principles for optimal control problems with state constraints. SIAM Rev. 37 (2), 181–218.

Hasselmann, K., Barnett, T.P., Bouws, E., et al., 1973. Measurements of Wind Wave Growth and Swell Decay During the Joint North Sea Project (JONSWAP). Deutches hydrographisches institut.

Kassem, A.M., Besheer, A.H., Abdelaziz, A.Y., 2015. A linear quadratic Gaussian approach for power transfer maximization of a point absorber wave energy converter. Elec. Power Compon. Syst. 43 (8–10), 1173–1181.

Lattanzio, S.M., Scruggs, J.T., 2011. Maximum power generation of a wave energy converter in a stochastic environment. In: Control Applications (CCA), 2011 IEEE International Conference on, pp. 1125–1130 (IEEE).

Li, G., Weiss, G., Mueller, M., Townley, S., Belmont, M.R., 2012. Wave energy converter control by wave prediction and dynamic programming. Renew. Energy 48, 392–403.

Mathworks, 2011. Control System Toolbox 9.1. Mathworks, Inc.

Meirovitch, L., 1990. Dynamics and Control of Structures. John Wiley & Sons.

Newman, J., 1977. Marine Hydrodynamics. The MIT Press.

Nielsen, S.R.K., Zhang, Z., 2017. Stochastic Dynamics. Aarhus Unversity Press.

Nielsen, S.R.K., Zhou, Q., Kramer, M.M., Basu, B., Zhang, Z., 2013. Optimal control of nonlinear wave energy point converters. Ocean Engineering 72, 176–187.

Ozkop, E., Altas, I.H., 2017. Control, power and electrical components in wave energy conversion systems: a review of the technologies. Renew. Sustain. Energy Rev. 67, 106–115.

Pelamis Wave, 2012. Pelamis Wave Power. http://www.pelamiswave.com/.

Pontryagin, L.S., Boltyanskii, V.G., Gamkrelitze, R.V., Mishenko, E.F., 1962. The Mathematical Theory of Optimal Processes. John Wiley and Sons, New York. Interscience Publishers.

Ringwood, J.V., Bacelli, G., Fusco, F., 2014. Energy-maximizing control of wave-energy converters: the development of control system technology to optimize their operation. IEEE Contr. Syst. Mag. 34 (5), 30–55.

Scruggs, J.T., Lattanzio, S.M., Taflanidis, A.A., Cassidy, I.L., 2013. Optimal causal control of a wave energy converter in a random sea. Appl. Ocean Res. 42, 1–15.

Sichani, M.T., Chen, J.B., Kramer, M.M., Nielsen, S.R.K., 2014. Constrained optimal stochastic control of non-linear wave energy point absorbers. Appl. Ocean Res. 47, 255–269.

WAMIT, 2011. WAMIT User Manual version 7.0. Technical Report.

Wang, L., Engström, J., Göteman, M., Isberg, J., 2015. Constrained optimal control of a point absorber wave energy converter with linear generator. J. Renew. Sustain. Energy 7 (4), 043127.

Wave Star Energy, 2003. Wave Star Energy. http://wavestarenergy.com/.

Wavedragon, 2005. Wave Dragon. http://www.wavedragon.net/.

Zou, S., Abdelkhalik, O., Robinett, R., Bacelli, G., Wilson, D., 2017. Optimal control of wave energy converters. Renew. Energy 103, 217–225.

Paper D

Semi-Active Feedforward Control of a Floating OWC Point Absorber for Optimal Power Take-Off

Tao Sun, Søren R.K. Nielsen

The paper has been published in the
IEEE transactions on Sustainable Energy Early Access

D.1 Author's Right

Copyright - It is the policy of the IEEE to own the copyright to the technical contributions it publishes on behalf of the interests of the IEEE, its authors, and their employers, and to facilitate the appropriate reuse of this material by others. To comply with United States copyright law, authors are required to sign and submit a completed IEEE Copyright Form. This form returns to authors and their employers full rights to reuse their material for their own purposes.

https://ieeexplore.ieee.org/stamp/stamp.jsp?arnumber=8207795

This article has been accepted for publication in a future issue of this journal, but has not been fully edited. Content may change prior to final publication. Citation information: DOI 10.1109/TSTE.2019.2923279, IEEE Transactions on Sustainable Energy

Semi-active feedforward control of a floating OWC point absorber for optimal power take-off

Tao Sun and Søren R.K. Nielsen

***Abstract*—The performance of a floating oscillating water column wave energy converter is depending on the variation of the pressure above atmospheric pressure in the pressure chamber above the water column. The pressure can be semi-actively controlled by the opening and closure of a valve between the pressure chamber and the generator. In the paper a control is suggested, where the closure time intervals of the valve are taken as a fixed fraction of the peak period of a given sea-state. The control relies on an estimation of the external wave loads, which in turn depend on the prediction of the future surface elevation in a given prediction interval, for which reason it is classified as a feedforward (open loop) control strategy. A Kalman-Bucy filter has been devised for the indicated prediction. The optimal fraction of time of the sub-optimal controller with a closed valve is determined by comparison with the performance of the optimal control obtained by nonlinear programming. For a given sea-state it is demonstrated that the reduced performance of the sub-optimal controller is primarily related to the estimation error of the wave loads.**

***Index Terms*—wave energy, oscillating water column, heave absorber, semi-active control, feedforward control**

I. Introduction

An Oscillating Water Column (OWC) wave energy converter (WEC) extracts energy by driving an oscillating water column which compresses or expands the air in a chamber not connected to the sea. The change of the internal energy of the air in the pressure chamber can next be transformed to electric energy via the generated air flow through a valve to the turbine. OWCs have been deployed as fixed structures at the shoreline or nearshore, or integrated in breakwaters and floating structures [1]. For the floating OWC device, the relative motion between the float and the internal free surface provides the air flow. One of the main advantages of floating OWC devices is that it is possible to widen the bandwidth of frequencies where the system performs well if the resonance peaks from the floater and water column are tuned to or close to the dominant wave frequency of the incoming wave [2]. In any case, in order to improve wave energy conversion an effective control strategy of the relative motion between the float and the surface of water column for a floating OWC devices or the motion of the surface of the water column for a fixed OWC device should be devised.

Reference [3] applied latching control for control of fixed OWC wave energy converter including the air turbine numerically. A valve, which switches rapidly between a closed and an open state, was applied to further improve the performance of the device. The closing of the valve causes a rapid increase of the pressure, which causes an increased power absorption at the succeeding reopening. The optimal control problem was derived by a variational approach with Hamiltonian formalism [4], and solved by the conditional gradient method [5]. It shows that phase-control of the oscillating water column is feasible for irregular waves and that energy-capture can be significantly increased by applying a flow-control in the power-conversion system. Reference [6] performed a numerical analysis of latching control of an OWC spar-buoy wave energy converter considering for regular waves. The compressibility of the air in the chamber plays an important role because it allows a relative motion between the floater and the internal free surface.

Further, in order to increase wave energy conversion, some studies for turbogenerator control of the OWC device have been performed. The aerodynamic design of the Wells turbine to the OWC performance was investigated by Brito-Melo et al., [7]. Garrido et al. presented a sliding-mode-control-based vector control scheme to improve the lacks of accuracy and robustness of parameters for PI controller [8]. A control scheme including a rotational speed control and an airflow control has been introduced to improve the wave energy conversion [9]. Flow behaviour between the air chamber and the turbine was investigated through CFD simulation by El Marjani et al., [10]. In the present paper, merely a Wells turbine is considered.

Generally, in order to analyze the interaction between the floater and the OWC, there are two different approaches, known as the piston model [11] and the uniform pressure distribution model [12], respectively. The piston model presumes that the vertical particle motion of the water column is constrained to move with the same displacement under the assumption of limited pressure chamber dimensions compared to the incident wavelengths [2], [13]. In the uniform pressure distribution model, the governing equations are expressed in terms of the dynamic air pressure on the OWC internal free surface and flow rate displace by the OWC surface motion, rather than forces and velocities as in the modelling of oscillating body converters. Further, for the piston model the interaction between waves and the WEC can be analysed by using the wave-structure interaction theory [11], [14] for a two-body coupling system. Therefore, the piston model is introduced to calculate the hydrodynamic parameters for the floating OWC system.

The paper presents a sub-optimal solution for the control of a floating OWC heave point absorber. Given the closure intervals of the valve are taken as a fixed fraction of the peak period of a given sea-state, the semi-active control of the opening and closure of a valve will be considered. Then,

The authors Tao Sun and Søren R.K. Nielsen are with the Department of Civil Engineering (e-mail: tsu@civil.aau.dk; srkn@civil.aau.dk).

Manuscript received XX XX, 2019; revised XX XX, 2019.

This article has been accepted for publication in a future issue of this journal, but has not been fully edited. Content may change prior to final publication. Citation information: DOI 10.1109/TSTE.2019.2923279, IEEE Transactions on Sustainable Energy

the wave load vector, the input to the system, needs to be estimated. Finally, a numerical example is provided to investigate the performance of the suggested control algorithm.

II. Methodology

A. Equation of motion of the floating OWC device

When the internal water surface moves up, or the device structure moves down, the volume of the pressure chamber becomes smaller, which creates an increased pressure in the pressure chamber. The increased chamber pressure drives the air out of the pressure chamber, and at the same time pushes the device structure upward and the internal water surface downward, so that the air volume is enlarged.

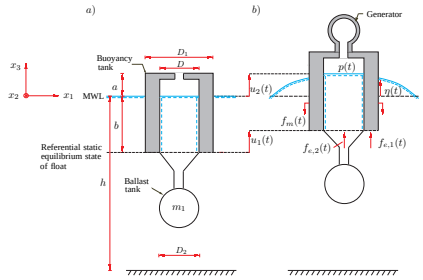

Fig. 1: Loads on floating OWC device. a) Static equilibrium state. b) Dynamic state.

Fig. 1a shows the floating OWC device in the static equilibrium state, where a and b indicates the parts of the float above and below the mean water level MWL. a is the height of the pressure chamber, and b is the submerged part of the pressure chamber. h specifies the water depth. The outer diameters of the buoyancy tank and ballast tank are D_1 and D_2, and D is the diameter of the water column. m_1 is the structural mass including the ballast.

The motion of the point absorber is referred to an inertial (x_1, x_2, x_3)-coordinate system with the (x_1, x_2)-plane positioned in the MWL-plane, and the x_3-axis orientated in the upwards direction. The origin of the coordinate system is placed at the centerline of the point absorber. The surface elevation $\eta(x_\beta, t)$ is considered positive in the x_3-direction. Index notation of two-dimensional vectorial quantities is applied with Greek indices ranging over $\alpha, \beta = 1, 2$ and Latin indices ranging over $k = 1, 2, 3$, respectively. The summation convention is abandoned by means of parentheses around dummy indices, i.e. $a_\alpha\, b_\alpha = a_1 b_1 + a_2 b_2$, whereas $a_{(\alpha)} b_{(\alpha)}$ merely indicates the product of a_α and b_α.

The water flow is considered incompressible, irrotational and non-viscous, and linear (Airy) wave theory is assumed. ρ_w signifies the mass density of the water. $p(x_k, t)$ signifies the thermodynamic pressure of the air in the pressure chamber above the atmospheric pressure p_0. The pressure is assumed to be constant throughout the pressure chamber, so $p(x_k, t) \simeq p(t)$.

The surface elevation $\eta(x_\beta, t)$ inside the pressure chamber is dominated by the mean surface elevation $u_2(t)$ of the water column from the MWL. Hence, the following approximation applies:

$$\eta(x_\beta, t) \simeq u_2(t) \tag{1}$$

Equation (1) is known as the piston approximation. Since the water column is assumed to be infinite rigid, the constraint can be imposed at any position along the length b at the water column, if the mass of the water column above the constraint is added as a point mass m_2.

Let $u_1(t)$ be the vertical displacement of the float in the x_3-direction. For the float, the pressure produces a force $p(t)A$ on the system in the direction of the degree of freedom $u_1(t)$, and a force $-p(t)A$ on the water column in the direction of the degree of freedom $u_2(t)$, where $A = \frac{\pi}{4} D^2$ indicates the surface area of the water column. Further, the vertical components of the dynamic restoring force from the mooring system are given by the linear stiffness relation $f_m(t) = k_m\, u_1(t)$, where km is the combined stiffness coefficient from all cables. Due to the piston model, the following vectorial Cummings equation applies:

$$\left.\begin{aligned} &\mathbf{M}\,\ddot{\mathbf{u}}(t) + \mathbf{f}_r(t) + \mathbf{r}\big(\mathbf{u}(t)\big) = \mathbf{f}_e(t) - \mathbf{f}_c(t)\ ,\ t \in]t_0, t_1] \\ &\mathbf{u}(t_0) = \mathbf{u}_0\ ,\ \dot{\mathbf{u}}(t_0) = \dot{\mathbf{u}}_0 \end{aligned}\right\} \tag{2}$$

where

$$\left.\begin{aligned} \mathbf{u}_0 &= \begin{bmatrix} u_{1,0}(t) \\ u_{2,0}(t) \end{bmatrix} \quad , \quad \dot{\mathbf{u}}_0 = \begin{bmatrix} \dot{u}_{1,0}(t) \\ \dot{u}_{2,0}(t) \end{bmatrix} \\ \mathbf{u}(t) &= \begin{bmatrix} u_1(t) \\ u_2(t) \end{bmatrix} \quad , \quad \mathbf{f}_c(t) = \mathbf{a}\, p(t) \quad , \quad \mathbf{a} = \begin{bmatrix} -1 \\ 1 \end{bmatrix} A \\ \mathbf{f}_e(t) &= \begin{bmatrix} f_{e,1}(t) \\ f_{e,2}(t) \end{bmatrix} \quad , \quad \mathbf{r}\big(\mathbf{u}(t)\big) = \begin{bmatrix} (k_m + \rho_w\, g\, A_1)\, u_1(t) \\ \rho_w\, g\, A\, u_2(t) \end{bmatrix} \\ \mathbf{M} &= \begin{bmatrix} m_1 + m_{11}(\infty) & m_{12}(\infty) \\ m_{21}(\infty) & m_2 + m_{22}(\infty) \end{bmatrix} \end{aligned}\right\} \tag{3}$$

t_0 is the initial time, and t_1 the terminal time of the control horizon. $\mathbf{u}_0$ and $\dot{\mathbf{u}}_0$ signify the initial value vectors of the system at the initial time t_0. $A_1 = \frac{\pi}{4}(D_1^2 - D^2)$ is the sectional area of the float surrounding the pressure chamber.

$\mathbf{f}_e(t)$ is a vector storing the external wave load vector and $\mathbf{r}\big(\mathbf{u}(t)\big)$ specifies the restoring force from buoyancy and the mooring system. ρ_w indicates the mass density of the water and g is the acceleration of gravity. $\mathbf{M}$ signifies the mass matrix. The components $m_{\alpha\beta}(\infty)$ indicate the added mass matrix of the water outside the float and below the piston at infinite frequency. $\mathbf{f}_r(t)$ represents the radiation damping of the system given as:

$$\mathbf{f}_r(t) = \int_{t_0}^{t} \mathbf{h}_r(t - \tau)\, \dot{\mathbf{u}}(\tau)\, d\tau \tag{4}$$

The related frequency response matrix is given by the Fourier transform:

$$\mathbf{H}_r(\omega) = \int_{-\infty}^{\infty} \mathrm{e}^{-i\omega t}\, \mathbf{h}_r(t)\, dt = \int_{0}^{\infty} \mathrm{e}^{-i\omega t}\, \mathbf{h}_r(t)\, dt \tag{5}$$

where i indicates the complex unit. In the last statement it has been used that $\mathbf{h}_r(t)$ is causal, i.e. $\mathbf{h}_r(t) = \mathbf{0}$, $t < 0$, which makes a rational approximation to $\mathbf{f}_r(t)$ possible.

This article has been accepted for publication in a future issue of this journal, but has not been fully edited. Content may change prior to final publication. Citation information: DOI 10.1109/TSTE.2019.2923279, IEEE Transactions on Sustainable Energy

The external wave load vector may be represented by the following convolution integral of the surface elevation $\eta(t)$:

$$\mathbf{f}_e(t) = \int_{-\infty}^{\infty} \mathbf{h}_e(t-\tau)\,\eta(\tau)\,d\tau \qquad (6)$$

where $\mathbf{h}_e(t)$ indicates a non-causal impulse response vector because $\mathbf{h}_e(t) \neq \mathbf{0}, t < 0$. Due to the non-causality of $\mathbf{h}_e(t)$, the prediction of the surface elevation $\eta(\tau), \tau > t$ is necessary in order to calculate the wave loads at the time t.

The hydrodynamic parameters $m_{\alpha\beta}$, $\mathbf{h}_r(t)$, $\mathbf{h}_e(t)$ are computed based on the boundary element program WAMIT [15]. Fig. 2 shows the submerged geometry discretization for the floating OWC device. The kinematic constraint has been specified at the bottom of the water column as marked in blue. Correspondingly, $m_2 = \rho_w\, A\, b$.

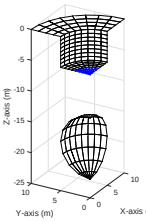

Fig. 2: The submerged geometry discretization for the floating OWC device.

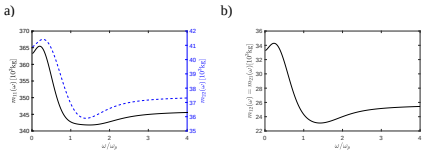

Fig. 3: Hydrodynamic added mass matrix. ——: The float. - - -: The OWC.

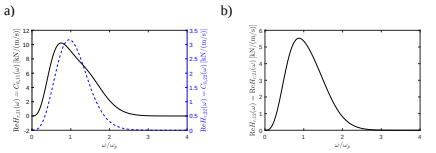

Fig. 4: Imaginary part of the frequency response matrix for the radiation force vector. ——: The float. - - -: The OWC.

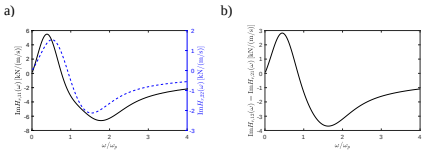

Fig. 5: Real part of the frequency response matrix for the radiation force vector. ——: The float. - - -: The OWC.

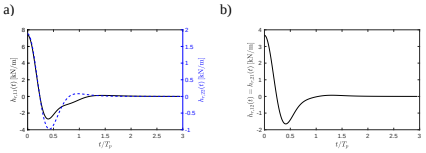

Fig. 6: Impulse response matrix for the radiation force vector. ——: The float. - - -: The OWC.

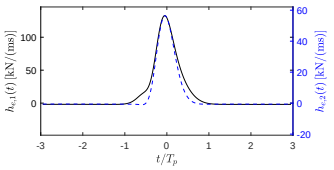

Fig. 7: Impulse response vector for the excitation force vector. ——: The float. - - -: The OWC.

Fig. 3 shows the hydrodynamic added mass for the float and the OWC. Figs. 3-7 refer to the absorber shown in Fig. 1 with the parameter values given in Table I in the numerical example. The angular frequency ω has been normalized with respect to the peak angular frequency $\omega_p = \frac{2\pi}{T_p}$, where T_p is the peak period of the considered sea-state.

The real and imaginary parts of the related frequency response matrix for the radiation force are shown in Figs. 4 and 5. Merely the function values for positive angular frequency, given that $\mathrm{Re}\big(H_{r,\alpha\beta}(\omega)\big)$ is an even function and $\mathrm{Im}\big(H_{r,\alpha\beta}(\omega)\big)$ is an odd function of ω.

The impulse response matrices for the radiation force and wave load vectors are shown in Figs. 6 and 7. The impulse response matrix $\mathbf{h}_r(t)$ is symmetric, i.e., $\mathbf{h}_r(t) = \mathbf{h}_r^T(t)$ as indicated in Fig. 6b. In turn this means that the frequency response matrix $\mathbf{H}_r(\omega)$ and the related added mass matrix $\mathbf{m} = \frac{1}{\omega}\mathrm{Im}(\mathbf{H}_r(\omega))$ become symmetric as well. As seen, $h_{e\eta,\alpha}(t) \simeq 0$ for $|t| > T_p$. Hence, surface elevations beyond one peak wave period ahead will not affect the present wave load vector $\mathbf{f}_e(t)$.

B. Thermodynamics of the air

The air is considered an adiabatic, isentropic ideal gas. Then, the pressure is given by the constitutive equation [16]:

$$\frac{p(t)+p_0}{p_0} = \left(\frac{\rho(t)}{\rho_0}\right)^{\gamma} \quad , \quad \gamma = \frac{c_p}{c_v} \simeq 1.4 \qquad (7)$$

where $\rho(t)$ indicates the time-varying mass density of air, ρ_0 is the referential value at atmospheric pressure, and c_p and c_v indicate the specific heat at constant pressure and constant volume.

p_0 turns out to be significantly larger than even extreme values of $p(t)$ in a practical OWC device. Hence, equation (7)

This article has been accepted for publication in a future issue of this journal, but has not been fully edited. Content may change prior to final publication. Citation information: DOI 10.1109/TSTE.2019.2923279, IEEE Transactions on Sustainable Energy

can be linearised to provide the following approximation for $\rho(t)$:

$$\rho(t) \simeq \rho_0 \left(1 + \frac{p(t)}{\gamma\, p_0}\right) \tag{8}$$

The pressure variation $p(t)$ in the air chamber is related to the volume flow rate of air through the turbine (positive for outward flow). The pressurized air is driven out in exhalation, while in inhalation, the atmosphere air with the density ρ_0 is inhaled. Thus, the air volume flow rate during exhalation and inhalation should be considered different due to the different mass densities corresponding to:

$$Q(t) = \begin{cases} -\dfrac{1}{\rho(t)} \dfrac{d\big(\rho(t)\, V(t)\big)}{dt} & , \quad p(t) \geq 0 \\ -\dfrac{1}{\rho_0} \dfrac{d\big(\rho(t)\, V(t)\big)}{dt} & , \quad p(t) < 0 \end{cases} \tag{9}$$

where $V(t) = V_0 + A\left(u_1(t) - u_2(t)\right)$ is the volume of the air chamber. $V_0 = A\, a$ is the initial volume of the air chamber. Then, $\dot{V}(t)$ can be written as:

$$\dot{V}(t) = A\left(\dot{u}_1(t) - \dot{u}_2(t)\right) \tag{10}$$

Differentiation of (8) provides:

$$\dot{\rho}(t) = \frac{\rho_0}{\gamma\, p_0}\, \dot{p}(t) \tag{11}$$

In the following a Wells turbine is considered, for which the mass flow is given as [7]:

$$Q(t) = k\, \beta(t)\, p(t) \tag{12}$$

where k is a constant which represents the damping of the turbine. $\beta(t)$ represents the proportional opening of the valve and is constrained to satisfy $0 \leq \beta(t) \leq 1$.

Further, in order to avoid the stalling behavior of the Wells turbine when the airflow exceeds a certain value, greatly decreasing its efficiency, the airflow speed through the turbine must be limited, which can be carried out by the air-valve control, which is widely used in OWC systems [17], [18]. Alternatively, control of the rational speed can be applied to avoid the stalling behavior [19].

Combining Eqs. (9), (10), (11) and (12), the following differential equation is obtained, which relates the air pressure variation $p(t)$ to the relative velocity of the inner free surface and the float.

$$\begin{cases} \dot{p}(t) V(t) + (\gamma p_0 + p(t))\left(\dot{V}(t) + k\, \beta(t)\, p(t)\right) = 0, \; p(t) \geq 0 \\ \dfrac{V(t)}{\gamma p_0} \dot{p}(t) + \left(1 + \dfrac{p(t)}{\gamma p_0}\right) \dot{V}(t) + k\, \beta(t)\, p(t) = 0, \; p(t) < 0 \end{cases} \tag{13}$$

For the turbine, the instantaneous absorbed power can be expressed as [20]:

$$P(t) = Q(t)\, p(t) \tag{14}$$

Insertion of (12) in (14) provides the following relation for the instantaneous power take-off:

$$P(t) = k\, \beta(t)\, p^2(t) \tag{15}$$

The dynamic of the system is given by (2) in combination to (13), corresponding to:

$$\left.\begin{array}{l} \mathbf{M}\, \ddot{\mathbf{u}}(t) + \mathbf{f}_r(t) + \mathbf{r}\big(\mathbf{u}(t)\big) = \mathbf{f}_e(t) - \mathbf{f}_c(t) \;,\; t \in]t_0, t_1] \\ \left.\begin{array}{l} \dot{p}(t) + \dfrac{\gamma p_0 + p(t)}{V(t)} \left(\dot{V}(t) + k\, \beta(t)\, p(t)\right) = 0, \; p(t) \geq 0 \\ \dot{p}(t) + \big(\gamma p_0 + p(t)\big) \dfrac{\dot{V}(t)}{V(t)} + \dfrac{\gamma\, p_0\, k\, \beta(t)\, p(t)}{V(t)} = 0, \; p(t) < 0 \end{array}\right\} \\ \mathbf{u}(t_0) = \mathbf{u}_0 \;,\; \dot{\mathbf{u}}(t_0) = \dot{\mathbf{u}}_0 \;,\; p(t_0) = 0 \end{array}\right\} \tag{16}$$

The semi-active control of the system is related to the time variation of the function $\beta(t)$. The optimal control is the trajectory of $\beta(t)$, which optimizes the absorbed energy in the interval $[t_0, t_1]$ given as:

$$E = \int_{t_0}^{t_1} P(\tau)\, d\tau = \int_{t_0}^{t_1} k\, \beta(\tau)\, p^2(\tau)\, d\tau \tag{17}$$

C. Rational approximation to radiation force vector

In the following, an approximate finite dimensional state vector representation of $\mathbf{f}_r(t)$ will be introduced. It should be noticed that the indicated state vector representation will be used in the numerical time integration of (16), and the nonlinear programming solution for the optimal power take-off.

Then, each component $H_{r,\alpha\beta}(\omega) = H_{r,\beta\alpha}(\omega)$ of the frequency response matrix $\mathbf{H}_r(\omega)$ defined by (5) are replaced by a rational approximation $\tilde{H}_{r,\alpha\beta}(s)$ of the order (l, m) given as [21]:

$$\tilde{H}_{r,\alpha\beta}(s) = \frac{P_{(\alpha)(\beta)}(s)}{Q_{(\alpha)(\beta)}(s)} \quad , \quad s = i\omega \tag{18}$$

where

$$\left.\begin{array}{l} P_{\alpha\beta}(s) = p_{0,\alpha\beta} s^l + p_{1,\alpha\beta} s^{l-1} + \cdots + p_{l-1,\alpha\beta} s + p_{l,\alpha\beta} \\ Q_{\alpha\beta}(s) = s^m + q_{1,\alpha\beta} s^{m-1} + \cdots + q_{m-1,\alpha\beta} s + q_{m,\alpha\beta} \end{array}\right\} \tag{19}$$

The parameters $p_{0,\alpha\beta}, p_{1,\alpha\beta}, \ldots, p_{l-1,\alpha\beta}, p_{l,\alpha\beta}$ and $q_{1,\alpha\beta}, \ldots, q_{m-1,\alpha\beta}, q_{m,\alpha\beta}$ are all real. The order (l, m) of the filters may be chosen freely with the only restrictions that $l < m$, and that all poles of $Q_{\alpha\beta}(s)$ must have negative real parts in order to ensure stability and causality.

The component $f_{r,\alpha\beta}(t)$ indicates the contribution to the component $f_{r,\alpha}(t)$ of $\mathbf{f}_r(t)$, when the system is driven by component $\dot{u}_\beta(t)$ of $\dot{\mathbf{u}}(t)$ alone. Further, the relationship between $\mathbf{f}_r(t), f_{r,\alpha}(t), f_{r,\alpha\beta}(t)$ can be expressed as:

$$\mathbf{f}_r(t) = \begin{bmatrix} f_{r,1}(t) \\ f_{r,2}(t) \end{bmatrix} = \begin{bmatrix} f_{r,11}(t) + f_{r,12}(t) \\ f_{r,21}(t) + f_{r,22}(t) \end{bmatrix} \tag{20}$$

Then, $f_{r,\alpha\beta}(t)$ can be obtained as output of the following filter equations, given on the matrix form:

$$\left.\begin{array}{l} f_{r,\alpha\beta}(t) = \mathbf{p}_{r,(\alpha)(\beta)}\, \mathbf{z}_{r,(\alpha)(\beta)}(t) \\ \dfrac{d}{dt}\mathbf{z}_{r,\alpha\beta}(t) = \mathbf{A}_{r,(\alpha)(\beta)}\, \mathbf{z}_{r,(\alpha)(\beta)}(t) + \mathbf{b}_{r,(\alpha)(\beta)} \dot{u}_{(\beta)}(t), \; t \in [t_0, \infty[\end{array}\right\} \tag{21}$$

This article has been accepted for publication in a future issue of this journal, but has not been fully edited. Content may change prior to final publication. Citation information: DOI 10.1109/TSTE.2019.2923279, IEEE Transactions on Sustainable Energy

where

$$\mathbf{z}_{r,\alpha\beta}(t) = \begin{bmatrix} y_{\alpha\beta}(t) \\ \frac{d}{dt}y_{\alpha\beta}(t) \\ \frac{d^2}{dt^2}y_{\alpha\beta}(t) \\ \vdots \\ \frac{d^{m-1}}{dt^{m-1}}y_{\alpha\beta}(t) \end{bmatrix}, \quad \mathbf{b}_{r,\alpha\beta} = \begin{bmatrix} 0 \\ 0 \\ 0 \\ \vdots \\ 1 \end{bmatrix} \tag{22}$$

$$\mathbf{A}_{r,\alpha\beta} = \begin{bmatrix} 0 & 1 & 0 & \cdots & 0 & 0 \\ 0 & 0 & 1 & \cdots & 0 & 0 \\ \vdots & \vdots & \vdots & \ddots & \vdots & \vdots \\ 0 & 0 & 0 & \cdots & 0 & 1 \\ -q_{m,\alpha\beta} & -q_{m-1,\alpha\beta} & -q_{m-2,\alpha\beta} & \cdots & -q_{2,\alpha\beta} & -q_{1,\alpha\beta} \end{bmatrix} \tag{23}$$

$$\mathbf{p}_{r,\alpha\beta} = \begin{bmatrix} p_{l,\alpha\beta} & p_{l-1,\alpha\beta} & \cdots & p_{1,\alpha\beta} & p_{0,\alpha\beta} & 0 & \cdots & 0 \end{bmatrix} \tag{24}$$

Finally, equation (21) can be written on the matrix form:

$$\left.\begin{aligned} \frac{d}{dt}\mathbf{z}_r(t) &= \mathbf{A}_r\,\mathbf{z}_r(t) + \mathbf{B}_r\,\dot{\mathbf{u}}(t) \\ \mathbf{f}_r(t) &= \mathbf{P}_r\,\mathbf{z}_r(t) \end{aligned}\right\} \tag{25}$$

where

$$\left.\begin{aligned} \mathbf{A}_r &= \begin{bmatrix} \mathbf{A}_{r,11} & \mathbf{0} & \mathbf{0} & \mathbf{0} \\ \mathbf{0} & \mathbf{A}_{r,12} & \mathbf{0} & \mathbf{0} \\ \mathbf{0} & \mathbf{0} & \mathbf{A}_{r,21} & \mathbf{0} \\ \mathbf{0} & \mathbf{0} & \mathbf{0} & \mathbf{A}_{r,22} \end{bmatrix}, \mathbf{B}_r = \begin{bmatrix} \mathbf{b}_{r,11} & \mathbf{0} \\ \mathbf{0} & \mathbf{b}_{r,12} \\ \mathbf{b}_{r,21} & \mathbf{0} \\ \mathbf{0} & \mathbf{b}_{r,22} \end{bmatrix} \\ \mathbf{P}_r &= \begin{bmatrix} \mathbf{p}_{r,11}\,\mathbf{p}_{r,12} & \mathbf{0} & \mathbf{0} \\ \mathbf{0} & \mathbf{0} & \mathbf{p}_{r,21}\,\mathbf{p}_{r,22} \end{bmatrix}, \mathbf{z}_r(t) = \begin{bmatrix} \mathbf{z}_{r,11}(t) \\ \mathbf{z}_{r,12}(t) \\ \mathbf{z}_{r,21}(t) \\ \mathbf{z}_{r,22}(t) \end{bmatrix} \end{aligned}\right\} \tag{26}$$

Further, the differential equation (25) should be solved with the initial value $\mathbf{z}_r(t_0) = \mathbf{0}$. Notice that $\mathbf{A}_{r,12} = \mathbf{A}_{r,21}$, $\mathbf{b}_{r,12} = \mathbf{b}_{r,21}$ and $\mathbf{p}_{r,12} = \mathbf{p}_{r,21}$ due to the symmetry of $\tilde{\mathbf{H}}_r(\omega)$.

Figs. 8 - 10 show the rational approximation $\tilde{H}_{r,\alpha\beta}(\omega)$ of order $(l,m) = (3,4)$. As seen, a good agreement is obtained to the target frequency response functions $H_{r,\alpha\beta}(\omega)$. Further, time has been normalized with respect to the peak period T_p in the auto-spectrum density function for the surface elevation $\eta(t)$ given by (29), and the angular frequency with respect to $\omega_p = \frac{2\pi}{T_p}$. $T_p = 6.77$s was used, cf. Table I.

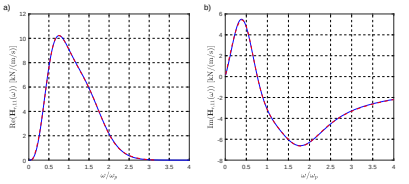

Fig. 8: Rational approximation of order $(m,n) = (3,4)$ to $H_{r,11}(\omega)$. a) $\mathrm{Re}(H_{r,11}(\omega))$. c) $\mathrm{Im}(H_{r,11}(\omega))$. ——: Numerical determined target. - - - : Rational approximation.

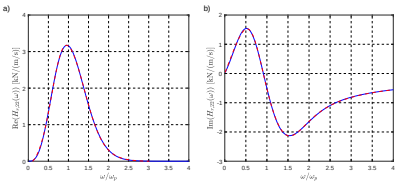

Fig. 9: Rational approximation of order $(m,n) = (3,4)$ to $H_{r,22}(\omega)$. a) $\mathrm{Re}(H_{r,22}(\omega))$. c) $\mathrm{Im}(H_{r,22}(\omega))$. ——: Numerical determined target. - - - : Rational approximation.

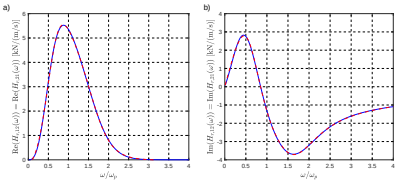

Fig. 10: Rational approximation of order $(m,n) = (3,4)$ to $H_{r,12}(\omega)$. a) $\mathrm{Re}(H_{r,12}(\omega))$. c) $\mathrm{Im}(H_{r,11}(\omega))$. ——: Numerical determined target. - - - : Rational approximation .

III. Nonlinear Programming Solution of the Optimal Control Problem

Based on Eqs. (15), (16) and (25), the optimal control problem subject to the following state equation can be expressed as:

$$\left.\begin{aligned} &\max J[p,\beta] = \int_{t_0}^{t_1} k\,\beta(\tau)\,p^2(\tau)d\tau \\ &\text{s.t.} \\ &\dot{\mathbf{z}}(t) = \begin{bmatrix} \dot{\mathbf{u}}(t) \\ \mathbf{M}^{-1}\left(-\mathbf{P}_r\,\mathbf{z}_r(t) - \mathbf{r}\big(\mathbf{u}(t)\big) + \big(\mathbf{f}_c(t) - \mathbf{a}\,p(t)\big)\right) \\ \mathbf{A}_r\,\mathbf{z}_r(t) + \mathbf{B}_r\,\dot{\mathbf{u}}(t) \\ \left.\begin{aligned} -\frac{\gamma p_0 + p(t)}{V(t)}\left(\dot{V}(t) + k\,\beta(t)\,p(t)\right),\ p(t) \geq 0 \\ -\big(\gamma p_0 + p(t)\big)\frac{\dot{V}(t)}{V(t)} - \frac{\gamma\,p_0\,k\,\beta(t)\,p(t)}{V(t)},\ p(t) < 0 \end{aligned}\right\} \end{bmatrix} \\ &0 \leq \beta(t) \leq 1 \end{aligned}\right\} \tag{27}$$

where

$$\mathbf{z}(t) = \begin{bmatrix} \mathbf{u}(t)^T & \dot{\mathbf{u}}(t)^T & \mathbf{z}_r(t)^T & p(t) \end{bmatrix}^T \tag{28}$$

The surface elevation $\eta(t)$ can be generated from the double-sided JONSWAP spectrum defined by [22]:

$$S_{\eta\eta}(\omega) = \delta\,\frac{H_s^2}{\omega_p}\,\psi^{\,\varepsilon}\left(\frac{|\omega|}{\omega_p}\right)^{-5}\exp\left(-\frac{5}{4}\left(\frac{\omega}{\omega_p}\right)^{-4}\right) \tag{29}$$

This article has been accepted for publication in a future issue of this journal, but has not been fully edited. Content may change prior to final publication. Citation information: DOI 10.1109/TSTE.2019.2923279, IEEE Transactions on Sustainable Energy

where

$$\left.\begin{aligned} \delta &= \frac{0.0312}{0.230 + 0.0336\,\psi - \frac{0.185}{1.9+\psi}} \\ \varepsilon &= \exp\left(-\frac{1}{2}\left(\frac{|\omega| - \omega_p}{\sigma\,\omega_p}\right)^2\right) \\ \sigma &= \begin{cases} 0.07 & , \quad |\omega| \le \omega_p \\ 0.09 & , \quad |\omega| > \omega_p \end{cases} \end{aligned}\right\} \tag{30}$$

H_s is the significant wave height, and ψ is the peak enhancement parameter, which controls the bandwidth of the spectrum.

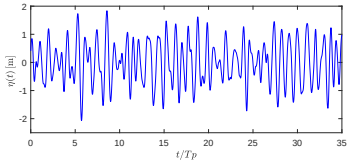

Fig. 11: Surface elevation process.

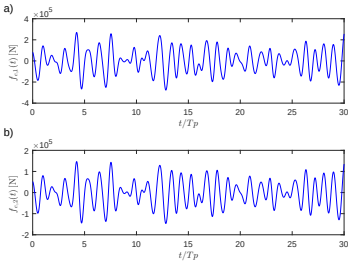

Fig. 12: Components of the wave load vector. a) The float. b) The OWC.

Fig. 11 shows a time series of $\eta(t)$ generated from the double-sided auto spectral density function in (29) with the parameters $T_p = 6.77\text{s}, \text{H}_\text{s} = 2.5\text{m}, \gamma = 3.3$. This and equivalent time series will be used in the bench-marking of the below suggested sub-optimal control strategy. Fig. 12 shows the time series of the related wave load components $f_{e,1}(t)$ and $f_{e,2}(t)$ on the float and the OWC as calculated by (6). The indicated time series will be used as a reference in the validation of the estimation problem described in Section 4.

The optimization problem in (27) can be solved by nonlinear programming [23], as a benchmark for the validation of the subsequent suggested control. Fig. 13 shows the trajectories of $\mathbf{u}(t)$, $\dot{\mathbf{u}}(t)$ and $\ddot{\mathbf{u}}(t)$ for the float and the OWC at optimal control, using the time series for the wave load given in Fig. 12. Further, the relative displacement $u_2(t) - u_1(t)$ is shown in Fig. 13a, which is determining the pressure in the pressure chamber.

Fig. 14 shows the related time series of $p(t)$ and $\beta(t)$ at optimal control indicated with a blue signature. $[t_1, t_3]$ and

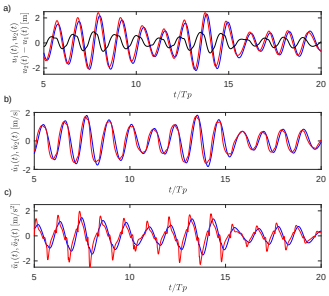

Fig. 13: Time series of trajectories at optimal control. ——: $u_1(t), \dot{u}_1(t), \ddot{u}_1(t)$. ——: $u_2(t), \dot{u}_2(t), \ddot{u}_2(t)$. ——: $u_2(t) - u_1(t)$.

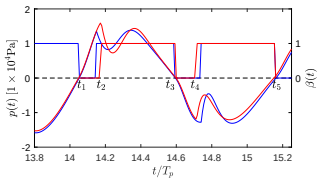

Fig. 14: $p(t)$ and $\beta(t)$ at optimal control and sub-optimal control, $\alpha = 0.12$. ——: $p(t)$ at optimal control. ——: $p(t)$ at sub-optimal control. ——: $\beta(t)$ at optimal control. ——: $\beta(t)$ at sub-optimal control.

$[t_3, t_5]$ denote the intervals with $p > 0$ and $p < 0$. Further, $[t_1, t_2]$ and $[t_3, t_4]$ indicate the subintervals with the valve closed corresponding to $\beta(t) = 0$, which causes the pressure to increase and decrease rapidly in these intervals. The valve is opened at the times t_2 and t_4 corresponding to $\beta(t) = 1$, which brings forward a temporarily decrease and increase of $p(t)$, as indicated by local extremes of the pressure.

At the optimal control, the length of the time interval with a closed valve varies somewhat due to the random sea-state. The idea of the considered sub-optimal control is to use a constant time interval with a closed valve of the length $\alpha T_p = t_2 - t_1 = t_4 - t_3$ at both positive and negative dynamic pressure. Then, the sub-optimal semi-active control of the valve can be written as

$$\begin{aligned} \beta(t) \;=\; & H\big(p(t)\big)\,H\big(t - t_1 - \alpha T_p\big) \\ & + H\big(-p(t)\big)\,H\big(t - t_3 - \alpha T_p\big) \end{aligned} \tag{31}$$

where $H(t)$ is the unit step function, defined as:

$$H(t) = \begin{cases} 1\,, & t \ge 0 \\ 0\,, & t < 0 \end{cases} \tag{32}$$

The optimal control value of α for a given sea-state is obtained by maximizing the absorbed energy of the sub-optimal controller in a given control interval relative to the absorbed energy at optimal control using the same sufficiently long realization of the surface elevation and the same wave load vector $\mathbf{f}_e(t)$. In Fig. 14, the performance of the sub-

This article has been accepted for publication in a future issue of this journal, but has not been fully edited. Content may change prior to final publication. Citation information: DOI 10.1109/TSTE.2019.2923279, IEEE Transactions on Sustainable Energy

optimal controller has been indicated with a red signature, using the exact wave load vector and $\alpha = 0.12$.

The computational cost of the nonlinear programming calculation grows exponentially with the length of the control interval. For this reason the statistical stable optimal solution for α can hardly be achieved by merely using a single realization of the wave load process $\mathbf{f}_e(t)$. Instead a finite number N of independent realizations of the wave load vector processes of limited length is generated, each of which provides a sample of α based on nonlinear programming. Next, the final estimate of α is obtained by an ensemble average of these sample values. In this case, the calculation time merely grows linearly with N. Assuming that all involved stochastic processes are ergodic both of these approaches are equivalent.

With $\beta(t)$ given by (31), the state variables $\mathbf{u}(t)$ and $p(t)$ can be obtained by numerical time integration if the wave load vector $\mathbf{f}_e(t)$ can be estimated. $\mathbf{f}_e(t)$ depends on future surface elevations, which needs to be predicted at least one peak period T_p ahead, cf. the discussion related to Fig. 7. The prediction will be performed by a suitable Kalman-Bucy filter.

IV. Estimation of wave load vector

At first a rational approximation to $S_{\eta\eta}(\omega)$ driven by unit intensity Gaussian white noise is devised, given as

$$S_{\eta\eta}(\omega) \simeq \frac{P(s)\,P(-s)}{Q(s)\,Q(-s)}\,\frac{1}{2\pi} \quad , \quad s = i\omega \tag{33}$$

Fig. 15 shows the rational approximation of order $(r, s) = (3, 6)$ to the double-side JONSWAP auto-spectral density function $S_{\eta\eta}(\omega)$ for the surface elevation given by (29).

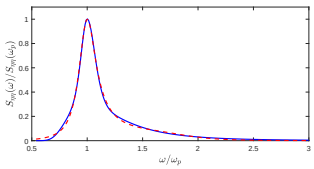

Fig. 15: Rational approximation to JONSWAP $S_{\eta\eta}(\omega)$ of order $(3, 6)$. ——: $S_{\eta\eta}(\omega)$. - - -: Rational approximation.

Then, the state equations for the surface elevation can be expressed as, [24]:

$$\left\{\begin{array}{l} \dfrac{d\mathbf{Y}(t)}{dt} = \mathbf{A}_c\mathbf{Y}(t) + \mathbf{b}_c\,w_1(t) \\ \eta(t) = \mathbf{p}_c\,\mathbf{Y}(t) + c\,w_2(t) \end{array}\right. \tag{34}$$

where $c\,w_2(t)$ is the measurement noise, c is a constant indicating the noise level. $w_1(t)$ and $w_2(t)$ are the unit intensity Gaussian white noises defined by the following mean value function and auto-covariance function:

$$\left.\begin{array}{l} E[w_\alpha(t)] = 0 \\ E[w_\alpha(t)\,w_\beta(t+\tau)] = \delta_{\alpha\beta}\,\delta(\tau) \end{array}\right\} \quad , \quad \alpha\,,\,\beta = 1, 2. \tag{35}$$

where $\delta(\cdot)$ is the Dirac function and $\delta_{\alpha\beta}$ is the Kronecker's delta. The column vectors $\mathbf{Y}(t)$, $\mathbf{b}_c$, the row vector $\mathbf{p}_c$ and the system matrix $\mathbf{A}_c$ has the similar expressions as shown in Eqs. (22), (23) and (24). Hence the optimal Kalman-Bucy observer equation reads, [25]:

$$\frac{d\hat{\mathbf{Y}}(t)}{dt} = \mathbf{A}_c\hat{\mathbf{Y}}(t) + \mathbf{K}(t)\big(\eta(t) - \mathbf{p}_c\,\hat{\mathbf{Y}}(t)\big) \tag{36}$$

where $\hat{\mathbf{Y}}(t)$ is the estimated state vector. $\mathbf{K}(t)$ indicates the time dependent Kalman gain vector, expressed as:

$$\mathbf{K}(t) = \mathbf{P}(t)\mathbf{p}_c^T\,\frac{1}{c^2} \tag{37}$$

where $\mathbf{P}(t) = E[\mathbf{e}(t)\,\mathbf{e}(t)^T]$ is the covariance matrix of the error vector $\mathbf{e}(t) = \mathbf{Y}(t) - \hat{\mathbf{Y}}(t)$. The stationary value of $\mathbf{P}(t)$ as $t \to \infty$ is given by the following algebraic Riccati equation, [25]:

$$\mathbf{A}_c\mathbf{P} + \mathbf{P}\,\mathbf{A}_c^T - \mathbf{P}\mathbf{p}_c^T\,\frac{1}{c^2}\mathbf{p}_c\,\mathbf{P} + \mathbf{b}_c\,\mathbf{b}_c^T = \mathbf{0} \tag{38}$$

Then, the prediction equation is expressed as:

$$\frac{d\bar{\mathbf{Y}}(\tau)}{d\tau} = \mathbf{A}_c\,\bar{\mathbf{Y}}(\tau) \quad , \quad \tau \in [t, t + T_\eta] \tag{39}$$

where $\bar{\mathbf{Y}}(\tau)$ is the predicted state vector at the time τ, t the present time and T_η the prediction horizon.

Hence, the predicted surface elevation $\bar{\eta}(\tau)$ can be obtained:

$$\bar{\eta}(\tau) = \mathbf{p}_c\,\bar{\mathbf{Y}}(\tau) = \mathbf{p}_c\,e^{\mathbf{A}_c\,(\tau - t)}\,\hat{\mathbf{Y}}(t)\;,\; \tau \in [t, t + T_f] \tag{40}$$

where $e^{\mathbf{A}_c\,\tau}$ signifies the exponential matrix function, and the initial vector $\bar{\mathbf{Y}}(t)$ is the smoothed estimate from (36).

V. Numerical Example

The following parameter values have been applied. As seen, the stiffness of the mooring system is ignored in the example.

TABLE I: Heave absorber and wave excitation parameters

Parameter	Value	Unit	Parameter	Value	Unit
a	2.00	m	m_1	8.3695×10^5	kg
b	5.00	m	$m_{11}(\infty)$	3.4515×10^5	kg
h	100.00	m	$m_{12} = m_{21}$	2.5644×10^4	kg
D	5.00	m	$m_{22}(\infty)$	0.3736×10^5	kg
D_1	10.00	m	H_s	2.50	m
D_2	10.00	m	T_p	6.77	s
ρ_0	1.225	kg/m^3	γ	3.3	
ρ_w	1025	kg/m^3	k	1×10^{-3}	m·s
p_0	101325	Pa	c	0.1	m
k_m	0	N/m			

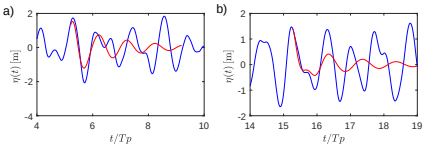

Fig. 16: Prediction of $\bar{\eta}(t)$ of the surface elevation for different start times with noise level $c = 0.1$m. $T_p = 6.77$s, $\mathrm{H_s} = 2.5$m, $\gamma = 3.3$. a) Start at $\tau = 5.2T_p$. b) Start at $\tau = 15.3T_p$. ——: Reference $\eta(t)$. ——: Predicted $\bar{\eta}(\tau)$.

This article has been accepted for publication in a future issue of this journal, but has not been fully edited. Content may change prior to final publication. Citation information: DOI 10.1109/TSTE.2019.2923279, IEEE Transactions on Sustainable Energy

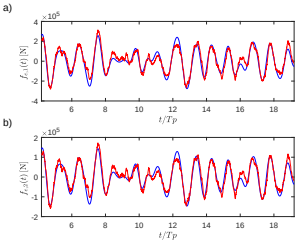

Fig. 17: Estimate of wave load vector $\mathbf{f}_e(\tau)$ with noise level $c = 0.1\text{m}$ corresponding to continuous predicted surface elevations. a) Predicted wave load component $\bar{f}_{e,1}(\tau)$. b) Predicted wave load component $\bar{f}_{e,2}(\tau)$. ——: Reference $\mathbf{f}_e(t)$. ——: Estimated $\bar{\mathbf{f}}_e(\tau)$.

Fig. 16 shows the prediction of surface elevation compared to the reference time series given in Fig. 11. As seen, predictions beyond T_p becomes inaccurate.

Fig. 17 shows the related estimate of $\mathbf{f}_e(t)$. At each instant of time, the surface elevation has been predicted one wave peak period ahead. Then, in combination with the previous surface elevations of the time series, the estimate of $\mathbf{f}_e(t)$ has been obtained from (6). At practical applications of the control, the previous surface elevations are assumed to be available from continuous measurements. The deviation from the reference value is a consequence of the prediction error of the surface elevation and the measurement noise.

Next, based on the average of $N = 4$ independent realizations of the length $30T_p$ of the surface elevation for a given sea state, the optimal value of the control parameter α can be obtained by maximizing the absorbed energy as indicated by (17). The red curve in Fig. 20 shows the variation of the absorbed energy as a function of α, where the exact wave loads related to the time series of surface elevations have been applied. As seen, a maximum is obtained approximately at $\alpha = 0.12$, where the reduction compared with the optimal absorbed energy as indicated by the blue line is 5.95%. For $\alpha = 0$, corresponding to a constantly open valve, the reduction is 10.24%.

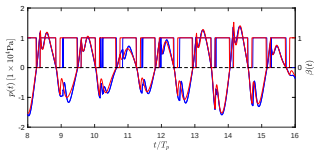

Fig. 18: $p(t)$ and $\beta(t)$ at optimal control and sub-optimal control with estimated wave load vector, $\alpha = 0.12$. ——: $p(t)$ at optimal control. ——: $p(t)$ at sub-optimal control. ——: $\beta(t)$ at optimal control. ——: $\beta(t)$ at sub-optimal control.

Fig. 18 shows the comparison of the variation of $\beta(t)$ and $p(t)$ at optimal control and sub-optimal control with $\alpha = 0.12$ and the estimated $\mathbf{f}_e(t)$ indicated in Fig. 17. A small deviation is obtained between the pressure variation at optimal and suggested sub-optimal control.

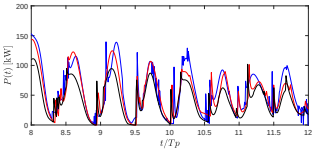

Fig. 19: Instantaneous Power take-off for different controls. ——: Power take-off at optimal control. ——: Power take-off at sub-optimal control with exact wave loads, $\alpha = 0.12$. ——: Power take-off at sub-optimal control with estimated wave loads, $\alpha = 0.12$.

Fig. 19 shows the instantaneous power take-off for the optimal control, the sub-optimal control using exact wave loads, and the sub-optimal control with estimated wave loads. All curves have been obtained as the average of the results from the previously mentioned $N = 4$ independent realizations of the surface elevation. $\alpha = 0.12$ is used in both sub-optimal controls.

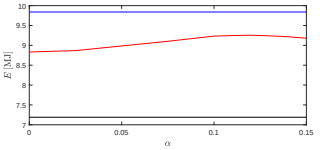

Fig. 20: Absorbed energy of sub-optimal controller as a function of α.

The black line in Fig. 20 indicates the average absorbed energy of the sub-optimal controller with $\alpha = 0.12$ and estimated wave loads for the $N = 4$ considered realizations of the surface elevation. The performance of the controller is 26.93% below that of the optimal controller and 22.31% below that of the sub-optimal controller with $\alpha = 0.12$ and exact wave loads. Hence, the primary reason of the indicated reduction is related to the estimation error of the wave loads.

VI. Conclusion

The paper focuses on the optimal control of a floating oscillating water column wave energy point absorber for power take-off. The piston model has been used for simulating the motion of the water column, and a linear model was used for the mass flow to the turbine. A semi-active control algorithm was suggested, where the opening and closing of the valve between the pressure chamber and the turbine is given as a fixed fraction of the peak period of the considered sea-state. The optimal value of the said fraction was determined by comparison to the optimal solution obtained by nonlinear programming. The devised control strategy relies on the estimation of the wave loads on the float and the wave column, which were obtained by a Kalman-Bucy filter prediction of the future sea surface elevation. The performance of the devised controller has been compared to that of the optimal control obtained by nonlinear programming. It is demonstrated that

This article has been accepted for publication in a future issue of this journal, but has not been fully edited. Content may change prior to final publication. Citation information: DOI 10.1109/TSTE.2019.2923279, IEEE Transactions on Sustainable Energy

the reduced performance primarily is related to the errors of the wave load estimation.

ACKNOWLEDGMENT

The authors gratefully acknowledge the financial support from project 675659-ICONN-H2020-MSCA-ITN-2015.

REFERENCES

[1] A.F. Falcao, J.C. Henriques, "Oscillating-water-column wave energy converters and air turbines: a review", *Renew. Energy*, vol. 85, pp. 1391-1424, 2015.
[2] J. Falnes,"Wave-energy conversion through relative motion between two single-mode oscillating bodies", *Journal of Offshore Mechanics and Arctic Engineering*, vol. 121, no. 1, pp. 32-38, 1999.
[3] R.E. Hoskin, B.M. Count, N.K. Nichols, D.A.C. Nicol, " Phase control for the oscillating water column.", *In Hydrodynamics of Ocean Wave-Energy Utilization*, pp. 257-268, 1986. Springer, Berlin, Heidelberg.
[4] R.V. Gamkrelidze, L.S. Pontrjagin, V.G.E. Boltjanskij, "The mathematical theory of optimal processes", Macmillan Company, 1964.
[5] W.A. Gruver, E. Sachs, "Algorithmic Methods in Optimal Control", Pitman, 1980.
[6] J.C.C. Henriques, A.F.O. Falcao, R.P.F. Gomes, L.M.C. Gato, "Latching control of an OWC spar-buoy wave energy converter in regular waves", *In ASME 2012 31st International Conference on Ocean, Offshore and Arctic Engineering*, pp. 641-650, 2012, American Society of Mechanical Engineers.
[7] A. Brito-Melo, L.M.C. Gato, A.J.N.A Sarmento, "Analysis of Wells turbine design parameters by numerical simulation of the OWC performance", *Ocean Engineering*, vol. 29, no. 12, pp. 1463-1477, 2002.
[8] A.J. Garrido, I. Garrido, M. Amundarain, M. Alberdi, M. De la Sen, "Sliding-mode control of wave power generation plants", *IEEE Transactions on Industry Applications*, vol. 48, no. 6, pp. 2372-2381, 2012.
[9] M. Alberdi, et al., "Complementary control of oscillating water column-based wave energy conversion plants to improve the instantaneous power output", *IEEE Transactions on Energy Conversion*, vol. 26, no. 4, pp. 1021-1032, 2011.
[10] A. El Marjani, F.C. Ruiz, M.A. Rodriguez, M.P. Santos, "Numerical modelling in wave energy conversion Systems", *Energy*, vol. 33, no. 8, pp. 1246-1253, 2008.
[11] D.V. Evans, "The oscillating water column wave-energy device", *IMA Journal of Applied Mathematics*, vol. 22, no. 4, pp. 423-433, 1978.
[12] D.V. Evans, " Wave-power absorption by systems of oscillating surface pressure distributions", *Journal of Fluid Mechanics*, vol. 114, pp. 481-499, 1982.
[13] R.W. Robinson," The effects of geometric-wavefield interactions on the performance of oscillating water column wave energy converters". Queen's University of Belfast, 1982.
[14] J. Falnes,"Ocean waves and oscillating systems: linear interactions including wave-energy extraction", Cambridge university press, 2002.
[15] C.H. Lee, J.N. Newman, WAMIT User manual. WAMIT, Inc, 2016
[16] A.J. Sarmento and A.D.O. Falcão, " Wave generation by an oscillating surface-pressure and its application in wave-energy extraction " , *Journal of Fluid Mechanics*, 150, pp. 467-485, 1985.
[17] A.F.D.O. Falcao, L.C. Vieira, P.A.P. Justino, and J.M.C.S. Andre, "Bypass air-valve control of an OWC wave power plant.", *Journal of Offshore Mechanics and Arctic Engineering*, vol. 125, no. 3, pp. 205210, 2003.
[18] A.J. Garrido, et al., "Mathematical modeling of oscillating water columns wave-structure interaction in ocean energy plants.", *Mathematical Problems in Engineering*, 2015.
[19] J. Lekube, A.J. Garrido, I. Garrido, "Rotational Speed Optimization in Oscillating Water Column Wave Power Plants Based on Maximum Power Point Tracking," in IEEE Transactions on Automation Science and Engineering, vol. 14, no. 2, pp. 681-691, 2017.
[20] A.J.N.A. Sarmento, L.M.C. Gato, A.D.O. Falco, "Turbine-controlled wave energy absorption by oscillating water column devices", *Ocean engineering*, vol. 17, no. 5, pp. 481-497, 1990.
[21] T. Perez, T.I. Fossen, "A matlab toolbox for parametric identification of radiation-force models of ships and offshore structures".
[22] K., Hasselmann, T.P. Barnett, E. Bouws, et al., "Measurements of wind wave growth and swell decay during the Joint North Sea Project (JONSWAP)", Deutches Hydrographisches Institut, 1973.
[23] T. Sun, S.R.K. Nielsen, "Stochastic optimal control of a heave point wave energy converter based on a modified LQG approach", *Ocean Engineering*, 154, 357-366, 2018.
[24] S.R.K. Nielsen, Z. Zhang, "Stochastic Dynamics". Aarhus University Press, 2017.
[25] L. Meirovitch, "Dynamics and Control of Structures", John Wiley & Sons, 1990.

Tao Sun is a currently PhD student at the Department of Civil Engineering, Aalborg University, Denmark. His major research area is vibration control of offshore structures.

Søren R.K. Nielsen is a professor at the Department of Civil Engineering, Aalborg University, Denmark. His research areas include stochastic and nonlinear dynamics, elastodynamics, structural reliability theory and vibration control.

ISSN (online): 2446-1636
ISBN (online): 978-87-7210-479-9

AALBORG UNIVERSITY PRESS